Master of Science Thesis

# Application of C/PEKK UD Tape for Welded Aircraft Movables

## A trade study for a single aisle aircraft rudder

Salwan al Jaberi

Faculty of Aerospace Engineering · Delft University of Technology

TU Delft Delft University of Technology

# Application of C/PEKK UD Tape for Welded Aircraft Movables

## A trade study for a single aisle aircraft rudder

Master of Science Thesis

For obtaining the degree of Master of Science in Aerospace Engineering
at Delft University of Technology

Salwan al Jaberi

29 January 2018

Faculty of Aerospace Engineering · Delft University of Technology

The work in this thesis was conducted in collaboration with GKN Fokker Aerostructures. Their support is gratefully acknowledged.


Delft University of Technology
Faculty of Aerospace Engineering
Department of Aerospace Structures and Materials

**GRADUATION COMMITTEE**

Dated: 29 January 2018

Chair holder:

Dr.ir. Roeland de Breuker

Committee members:

Dr.ir. Julien F.M. van Campen

Dr.ir. Irene Fernandez Villegras

ir. Ad Bastiaansen

# Abstract

Fokker Aerostructures has extensive knowledge on welded Thermoplastic (TP) composite aircraft movables and has developed several components using Carbon fibre PolyPhenylene Sulfide (C/PPS) fabric. In a strive to further improve the products offered by Fokker Aerostructures the performance of Carbon fibre PolyEtherKetoneKetone (C/PEKK) on component level was assessed in this study. In this study 3 concepts were designed for a fictitious Next Signle Aisle aircraft (NSA) rudder to perform a trade-off between the two composite materials and the two stiffening concepts.

An existing C/PPS multi-rib rudder concept, designed earlier at Fokker Aerostructures, is used as a reference. Specified requirements were elaborated to create a C/PEKK based multi-rib rudder redesign. Two multi-rib concepts, each with a different minimum skin thickness, were made and compared. The weight and cost of these two concepts was found to be nearly equal. Alternative stiffening concepts for the multi-rib were generated in collaboration with experts at Fokker Aerostructures. Grid-stiffening (GS) of the skin using a short fibre reinforced composite was selected. The GS skin allowed most of the ribs to be omitted so that part count and assembly effort could be reduced.

The C/PEKK rudder showed to have a near equal weight to the C/PPS reference. The higher stiffness allowed less ribs to be used, but the weight gain was undone by the 3% higher density of the C/PEKK composite compared to C/PPS. The improved Buy-to-Fly ratio (BtF) and automated layup of the skins using Automated Fiber Placement (AFP) allowed a cost reduction of 10% with respect to the C/PPS reference. The weight of the Grid-Stiffened (GS) rudder is less than 3% higher than than the C/PPS reference rudder. The cost of the GS rudder is however 21% less than the C/PPS reference rudder.

The multi-rib concept proved to be the lightest, regardless of the used material. The Technology Readiness Level (TRL) of some manufacturing processes for C/PEKK is low and required more development. The C/PEKK rudder shall be a viable option in the near future when all envisioned manufacturing concepts and welding of C/PEKK tape become available. The GS rudder requires more research and development. The short fibre material and manufacturing process of the grid have a low TRLand are not yet qualified. A discrete model of the GS skin is also required to better understand the behaviour of the rudder. Thus the GS rudder is expected to be a viable solution in the long term future.

# Table of Contents

# List of Figures

# List of Tables

# Preface

This thesis report is the result of a 1.5 year combined internship and thesis project at GKN Fokker Aerostructures. The project was still in the definition phase when I called Remco, my future supervisor, to enquire about another internship assignment which had already been given when I called. Remco then tolled me that he had another project in the works, which turned out to be exactly what I was looking for. After a meeting we decided to jointly write a proposal and the project was fixed.

The goal of the project was to perform a thorough trade-off using data derived from structural analysis. The designs would be made following top level requirements and considerations relevant for the 'business case'. This made the project multidisciplinary and required inputs from several departments and specialists at Fokker Aerostructures. The support of R&D, Weight & Balance, Cost Estimating, Tools & Methods and the Industrialization department was crucial for the completion of this project. I am thankful for the help provided by the colleagues at Fokker Aerostructures who are too many to name. Special thanks go out to the Productgroup Movables & Fuselages, it was a privilege to perform my assignment at this department and to get an insight into the Aerospace Engineering industry.

I am grateful for the supervision that Remco Gijseman, Ad Bastiaansen and Matthijs Kettenis provided throughout the project. With their help I developed both technical and professional skills that I will cherish for the rest of my career. I would also like to thank my supervisors from the TU Delft; Sonell Shroff and Julien van Campen. Their guidance helped me develop a critical view on the academic goals of the project and to better understand the smeared-stiffness approach for the alternative concept development.

This project not only marks the end of my studies, but also my time as a student. In my time studying in Delft I have made friends for life during experiences that have shaped me. This all would not have been possible without the support of my family and friends. I am thankful and owe much to all, in particular to my parent for their unconditional love and patience.

Salwan al Jaberi
Delft, 22 January 2018

# List of Abbreviations

**5H** Five Harness weave fabric

**AFP** Automated Fiber Placement
**ATL** Automatic Tape Laying

**BtF** Buy-to-Fly ratio

**C/PEEK** Carbon fibre PolyEther Ether Ketone
**C/PEKK** Carbon fibre PolyEtherKetoneKetone
**C/PPS** Carbon fibre PolyPhenylene Sulfide
**CAD** Computer Aided Design
**CAI** Compression After Impact
**CCM** Continous Compression Moulding
**CER** Cost Estimating Relationships

**F&DT** Fatigue & Damage Tolerance
**FE** Finite Element
**FEM** Finte Element Model

**GS** Grid-Stiffened

**HM** Hinge Moment

**KBE** Knowledge Based Engineering
**KDF** Knock-Down Factor

**LE** Leading Edge
**LL** Limit Load

**MPC** Multi-Point Constraint

**NDI** Non-Destructive Inspection
**NSA** Next Signle Aisle aircraft

**OEM** Original Equipment Manufacturer
**OHT** Open Hole Tension
**OML** Outer Mould Line
**OoA** Out of Autclave

**PBS** Product Breakdown Structure

**RBE** Ridged Body Element
**RF** Reserve Factor
**RiaM** Rudder in a Month
**RTM** Resin Transfer Molding

**SF** Short Fibre

**TE** Trailing Edge
**TP** Thermoplastic
**TPRC** ThermoPlastic Research Company
**TRL** Technology Readiness Level

**UD** Uni-Directional
**UL** Ultimate Load
**Us** UltraSonic

**VTP** Vertical Tail Plane

**WIBOMOD** WIng BOx MODeller

"Im very good at integral and differential calculus; I know the scientific names of being animalculous: In short, in matters vegetable, animal and mineral, I am the very model of a modern Major-General."

— *Major-General Stanley, in The Pirates of Penzance*

# Chapter 1

# Introduction

## 1.1 Background and Motivation

Fokker Aerostructures has developed welded Thermoplastic (TP) Carbon fibre PolyPhenylene Sulfide (C/PPS) movables that have been successfully used on several business jets. Preliminary feasibility studies have shown that the current movables are suitable for up-scaling to the size used on commercial transport aircraft. Such components may have a high production rate of up to 60 aircraft per month. Combined with the large dimension automation of the manufacturing process is considered to be necessary to be commercially viable. Several Original Equipment Manufacturer (OEM) however are unwilling to accept PPS as a matrix material due to its susceptibility to micro-cracking. Fokker Aerostructures has developed an Automated Fiber Placement (AFP) system for manufacturing TP composites using UltraSonic (Us) tacking and Carbon fibre PolyEtherKetoneKetone (C/PEKK) Uni-Directional (UD) tape.

Till date not much work has been done at Fokker Aerostructures to size C/PEKK components manufactured with AFP. It remains unclear if a commercial aircraft size movable would be more cost effective or light weight when manufactured with C/PEKK compared to C/PPS. The material price of C/PEKK is higher than that of C/PPS, the current material used for business jet movables, but this may be offset by the higher mechanical properties of the first material. A study into the manufacturing cost of skin panels has shown that a C/PEKK skin can be produced using AFP at nearly the cost of the current C/PPS fabric hand-layup process. Thus C/PEKK has a more sustainable outlook as it is accepted by more OEM's.

In the skin panel cost study the effect of the higher material properties was neglected. A comparison for cost can thus only be accurately performed on component level where part count, weight and assembly cost are considered. Fokker Aerostructures strives to further develop TP composite technology for movables and other aircraft structures to offer cost- and weight-effective solutions to OEM's. Based on this global objective and the discussion in this Section the following problem statement is formulated:

"Fokker Aerostructures currently lacks a mature thermoplastic composite solution for large movables produced in high volumes and for OEM's that do not accept C/PPS."

## 1.2 Objective and Research Question

Fokker Aerostructures needs to quantify the impact on cost and weight of utilizing C/PEKK combined with AFP for a commercial aircraft size movable. To allow a comparison between different materials and manufacturing methods on component level a fictional rudder model dubbed the Next Signle Aisle aircraft (NSA) rudder was created by Fokker Aerostructures. A C/PPS based multi-rib concept for the NSA rudder has already been created at Fokker Aerostructures. By performing a trade-off between multiple NSA rudder concepts the feasibility of offering C/PEKK based movables to a wider range OEM's can be determined. The objective can be reached by answering the following research question and sub-question:

*What is the change in cost and weight performance of an NSA multi-rib rudder designed in C/PEKK combined wih AFP manufacturing compared to the C/PPS design and how can the C/PEKK design be further improved by exploiting the opportunities of AFP and C/PEKK?*

- What is the cost and weight of a C/PEKK redesign of the C/PPS reference rudder?
- Do other stiffening or manufacturing concepts, more suitable for C/PEKK and AFP, exist that can improve on the baseline multi-rib design?
- How do the C/PEKK multi-rib and alternative concepts compare to the C/PPS reference?

## 1.3 NSA Rudder Inputs

The NSA rudder definition consists of an Outer Mould Line (OML), hinge- and actuators-interface and 6 representative load cases. Additional requirements have been defined for the multi-rib rudder by Fokker Aerostructures which are used for the design and are explained in Chapter 2. The NSA rudder definition however is set-up such that any material and manufacturing system can be applied to generate a concept as long as the design can be certified according to airworthiness regulations. This flexibility will allow many design philosophies to be compared. For this reason the NSA rudder definition is presented in this Section, separete from the requirements and design principals explained in Chapter 2.

The OML of the NSA rudder is shown in Figure 1.1 where some of the dimensions are also given. The position of the actuators and bracket is shown in Figure 2.1. The hinge line is fixed, but the interface with the brackets connecting to the Vertical Tail Plane (VTP) is not defined.

The rudder is a relatively lightly loaded structure and much of the applied loads are induced by the displacement of the VTP. Deflection of the rudder induces lift which yaws the aircraft as shown in Figure 1.2. The rudder must not generate any lift during level flight and thus the rudder is symmetric. The rudder is free to rotate around the hinge line and span-wise

**Table 1.1:** Load cases (LC) for the NSA rudder.

| no. | Description | Condition | Deflection [°] | HM [Nm] | **SF** | Remark |
|---|---|---|---|---|---|---|
| 1 | Max. Hinge Moment | Intact | -25 | 10732 | 1.5 | |
| 2 | Min. Hinge Moment | Intact | +25 | -10732 | 1.5 | |
| 3 | Actuator 3 Jam | Failed | 0 | -3656 | 1.0 | Act. 3 force is 72345 N |
| 4 | Ground Gust | Failed | +34 | 8611 | 1.0 | Act. 1 & 2 disconnected |
| 5 | In-plane Bending | Intact | -24 | 10190 | 1.5 | |
| 6 | Act. 3 overpressure | Failed | -30 | 9101 | 1.0 | Act. 1 & 2 disconnected |

forces are very low, so the rudder is only constrained in span-wise direction at a single hinge. A cross-section of the loaded rudder is sketched in Figure 1.3.

The rudder hinges about the hinge line and the rotation is constrained by the actuators. The rudder is loaded by hinge displacements, which are not sketched, and aerodynamic load which is assumed to vary linearly. The NSA rudder has 3 actuators and 7 hinge brackets. The aerodynamic load induces a torsion in the wing box which is countered by the actuators. The load cases on the NSA rudder are shown in Table 1.1. The aerodynamic force is indicated by a total Hinge Moment (HM).

Two types of load cases are defined; 'intact' and 'failed' which represent the state of the rudder. In an 'intact' load case the rudder and its interface to the VTP are assumed to be undamaged and the load is derived from the operational flight envelope, which is also called Limit Load (LL). Thus the load case is subjected to a safety factor of 1.5 as indicated by the column '**SF**' in Table 1.1, which is also known as Ultimate Load (UL). The most left column in Table 1.1 described the failure of the rudder. For load case 4 and 6 this is disconnection of actuators 1 and 2, while for load case 3 this is a jamming of actuator 3. The probability of occurrence of such failure is low and thus the rudder may only meet LL.

## 1.4 Structure of the Report

The presented objective and research question shall be answered in the following Chapters. Chapter 2 contains a discussion of the requirements, design and analysis method and tools, and the manufacturing processes using C/PEKK. Chapter 3 described the alternative concept development and selection process. A total of three rudder concepts were designed in this study, two multi-rib and one Grid-Stiffened (GS) rudder. In Chapters 4 and 5 the design of the C/PEKK multi-rib rudders and GS rudder are presented respectively. The results and trade-off are presented in Chapter 6 and the conclusion and recommendations are presented in Chapter 7.

The requirements are given in Section 2.1 and it is recommended to read at least this section before chapters 4 and 5. The decision to develop the GS rudder is explained in Chapter 3. Some elements that apply to all rudder concepts are discussed in Chapter 4. Common manufacturing related aspects are treated in Section 2.4.

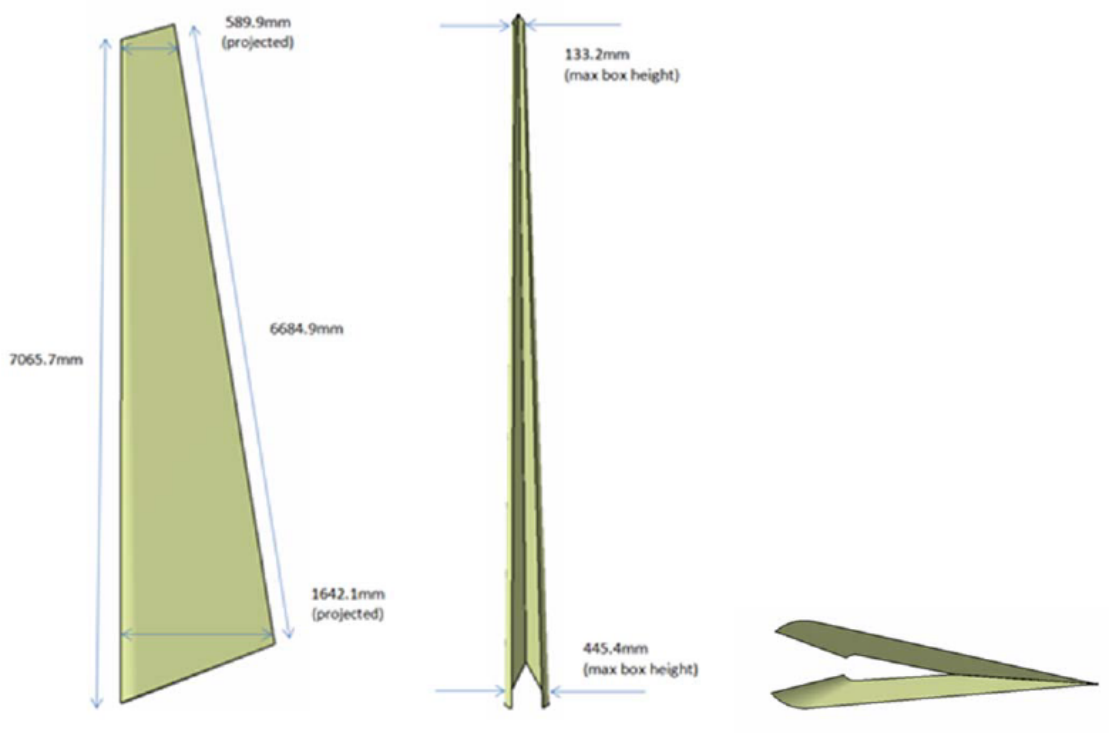


**Figure 1.1:** Sketch of the outer mould line of the NSA rudder.

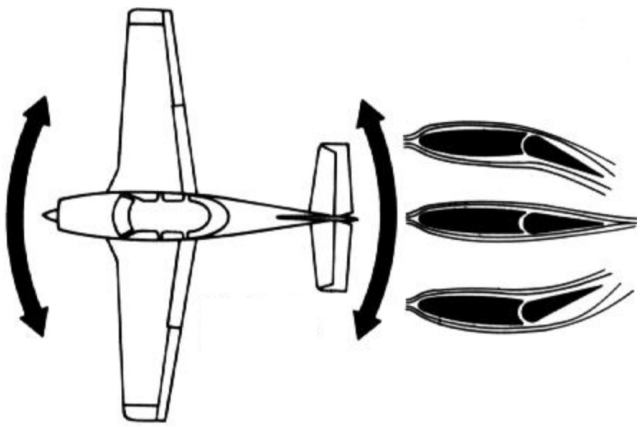

**Figure 1.2:** Sketch of aircraft motion due to rudder deflection. (Courtesy of avstop.com)

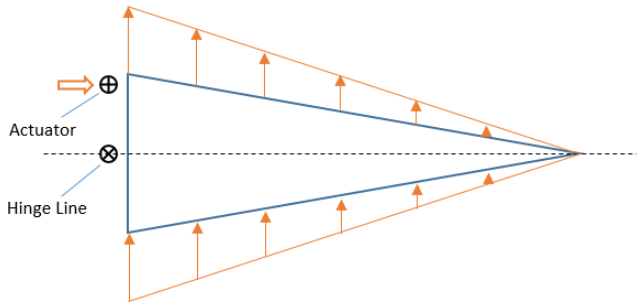


**Figure 1.3:** Cross-sectional sketch of loads on the rudder.

# Chapter 2

# Rudder Design Principals

## 2.1 Requirements Overview

A set of requirements for the Next Signle Aisle aircraft (NSA) rudder were defined to facilitate the trade-off and are listed in an internal Fokker document [3]. The full set of requirements is proprietary and shall not be presented in this report. An important requirement that is not defined in the requirements document is the allowed deformation of the skin due to aerodynamic load, the consequences of the absence of such requirements shall be discussed in Chapters 4 and 5. The most important requirements that do not stem from strength and stiffness considerations are discussed in this Section to improve understanding of the final design.

**Interchangeability** The NSA rudder concepts shall be interchangeable and thus have the same interface geometry with the Vertical Tail Plane (VTP) as the Carbon fibre PolyPhenylene Sulfide (C/PPS) reference rudder. The interface loads of the rudder shall not vary significantly from that of the reference rudder. The hinge and actuator bracket positions relative to the skin are shown as blocks in Figure 2.1.

**Lightening strike damage resistance** To ensure sufficient damage resistance in case of lightening strike the Trailing Edge (TE) and the section above the hinge closest to the tip (Hinge 7), marked in green in Figure 2.1, require a minimum thickness of 1.8 mm. The tip shall also be covered with copper wire mesh to improve the conductivity of the surface.

**Leading edge stiffness** The deformation of the Leading Edge (LE) must be limited so that a minimum clearance with the VTP is maintained. The cord-wise bending stiffness ($EI_{yy}$) of the LE shall be not less than $4.53 * 10^4\ Nmm^2$.

**Flush skin repair** Following the current repair philosophy the skin must have minimum thickness of 1.24 mm to allow a countersunk fastened patch repair of lightly loaded monolithic skin sections. This area is indicated in yellow in Figure 2.1.

**Skin-rib weld-interface repair** To ensure proper repairability of the weld joining the skins to the rib flange the minimum thickness of the skin at the interface shall be 1.8 mm. This will allow the use of countersunk fasteners for repair of the joint so that aerodynamic flushness is maintained.

**Load introduction at hinge and actuator brackets** In a multi-rib rudder design a rib shall be placed behind every hinge and actuator to improve load introduction into the box structure.

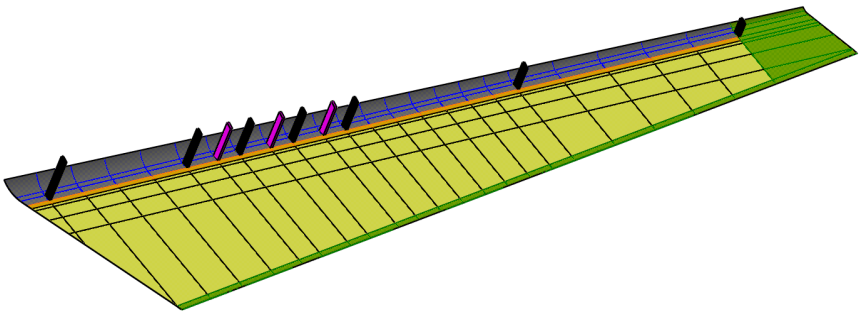

**Figure 2.1:** Skin zones with minimum thickness requirements and Actuator (black) and Hinge bracket (purple) positions.

## 2.2 Materials

The Three Thermoplastic (TP) materials used in the rudder concepts in this study are discussed in this section. The TenCate Cetex TC1100[1] (C/PPS) material is used in the reference rudder and is the current standard at Fokker Aerostructures. The other two materials are the Cytec APC PEKK-FC[2] (Carbon fibre PolyEtherKetoneKetone (C/PEKK)) and the Victrex PEEK 90HMF40[3] (Carbon fibre PolyEther Ether Ketone (C/PEEK)). The Cytec material is a continuous fibre Uni-Directional (UD) tape, that is increasingly used over fabric, for aerospace structures and will be the standard TP tape material at Fokker Aerostructures. The third material is a Short Fibre (SF) reinforced compound used as a reference for the overmolded grid of the Grid-Stiffened (GS) rudder discussed in Chapter 5. There is currently no C/PEKK SF compound commercially available with the desired properties. Due to the similarity of PEKK and PEEK polymer and the large influence of the fibres on stiffness and strength it is assumed that a C/PEKK compound can be designed easily with similar properties as the Victrex material.

The relevant material properties of the three materials are listed in table 2.1. It is noted that these properties are derived from public data sheets and in case of C/PPS and C/PEKK vary

[1] www.tencatecomposites.com/product-explorer/products/u0I7/TenCate-Cetex-TC1100
[2] www.cytec.com/sites/default/files/datasheets/APC-PEKK-FC_CM_EN.pdf
[3] www.victrex.com/~/media/datasheets/victrex_tds_90hmf40.pdf

slightly from the qualification data that was used in this study. A B-basis correction and appropriate knock-downs have been applied on the relevant material properties, but these values cannot be presented in this document. The most significant difference between the C/PPS and C/PEKK composites is that the first is a fabric, where a Five Harness weave fabric (5H) was used for the reference rudder, while the latter is a UD tape. This is evident in the stiffness values $E_{11}$ and $E_{22}$ of the materials, where it is noted that the C/PEEK compound is assumed to be isotropic. The C/PEKK composite has a higher fibre volume fraction $v_f$.

**Table 2.1:** Properties of used materials using average values without B-basis correction.

| **Property** | **C/PPS** | **C/PEKK** | **C/PEEK** |
|---|---|---|---|
| $E_{11}$ [GPa] | 53.75 | 133 | 43 |
| $E_{22}$ [GPa] | 52.75 | 1.2 | 43 |
| $G_{12}$ [GPa] | 2.65 | 5.2 | N/A |
| OHT [$\mu\epsilon$] | 4991 (HW80) | 6397 (HW120) | - |
| CAI [$\mu\epsilon$] | -4030 (HW80) | -4689 (HW120) | - |
| $\epsilon_u$ [$\mu\epsilon$] | - | - | 5116 (H120) |
| $T_m$ [°C] | 280 | 337 | 343 |
| $T_g$ [°C] | 90 | 159 | 143 |
| $v_f$ [%] | 50 | 60 | 40 |
| $t_{ply}$ [mm] | 0.3 | 0.138 | - |
| $\rho$ [$m/cm^3$] | 1.55 | 1.6 | 1.45 |

The stiffness values are computed averages of compressive and tensile values at dry room temperature conditions. No shear stiffness was provided for the Victrex material, but it was not needed for the smeared stiffness approach used to model the GS skin. Due to the better polymer mechanical properties and higher $v_f$ of C/PEKK the allowable strains are higher. To be conservative, a strain limit based on notched allowables are imposed on the design. Under tension the most severe case is Open Hole Tension (OHT) while under compression loading this Compression After Impact (CAI). Values are computed for hot and wet conditions (HW) to simulate the most severe operating temperature of the aircraft from a material allowable point of view. While the maximum operating temperature is 80 °C and used to compute the C/PPS allowable (HW80) there was only a hot wet allowable available for 120 °C for C/PEKK (HW120).

The C/PEKK composite allowables are better than the C/PPS composite despite the more severe environmental knock-down. For the C/PEEK compound a strain allowable was computed based on the data sheet and is less accurate than the values used for the other materials. The use a strain allowable is Fokker Aerostructures practice and stems from the observation that the failure strain of laminates with different layups is more similar than the failure stress. It is noted that the difference in material properties is not a guarantee for a better performance on component level.

## 2.3 Modelling and Sizing Approach

The three NSA rudder concepts were developed with the use of WIng BOx MODeller (WIBOMOD) and CAD2FEM, two software extensions developed in-house at Fokker Aerostructures, to create a Computer Aided Design (CAD) model and Finte Element Model (FEM) respectively. These extensions are for CATIA® and PATRAN® respectively and are part of a Knowledge Based Engineering (KBE) project called Rudder in a Month (RiaM) currently running at Fokker Aerostructures [4]. In this section WIBOMOD and CAD2FEM will be discussed followed by a description of the sizing flow used to develop the concepts, a more elaborate discussion of the modelling and sizing approach is given in the literature study preceding this thesis project [5].

### 2.3.1 Wing Box Modeller (WIBOMOD)

WIBOMOD is also a KBE tool used to parametrically define a wing-like structure such as a rudder. The tool is aimed for use in conceptual studies with limited level of detail in exchange for simplicity by integration into CATIA®. Only an Outer Mould Line (OML) required as an input for WIBOMOD, but interface points are required to make a practical model. WIBOMOD also automatically computes relevant quantities of the model such as weight and part dimension. The data can be exported as EXCEL or XML files for coupling with CAD2FEM or other activities such as cost and weight estimation. An example of a multi-rib rudder generated in WIBOMOD is shown in Figure 2.2.

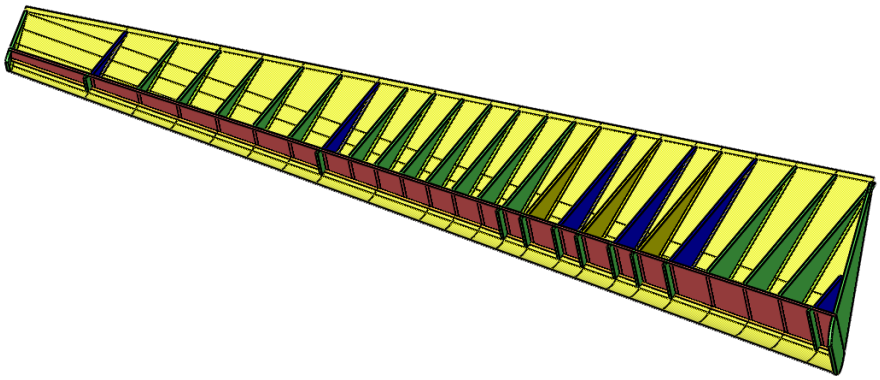

**Figure 2.2:** An example of a multi-rib rudder designed in WIBOMOD, the left hand skin is removed to expose the substructure.

### 2.3.2 CAD2FEM

CAD2FEM is a Fokker Aerostructures in house developed tool that can generate a FEM automatically in PATRAN®. Unlike WIBOMOD this model is not parametric, but generates a complete new model (database) from scratch in a matter of minutes. The brackets are modelled using a Multi-Point Constraint (MPC) of Ridged Body Element (RBE) (RBE2) resulting in load introduction through a single line of nodes representing a bracket. An

example of a FEM constructed with CAD2FEM is shown in Figure 2.3 where each MPC is coloured purple.

The FEM is constructed using the geometry definition from WIBOMOD exported as IGS files. The properties of the parts, loads and boundary conditions, connections and interfaces are provided in XML format. CAD2FEM is a program written in the PATRAN native PATRAN Command Language (PCL) and reads the model definition in the XML files to construct the model.

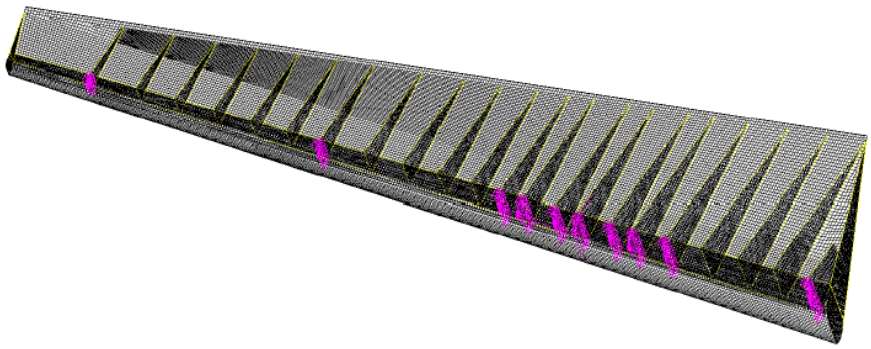

**Figure 2.3:** An example of a FEM of a multi-rib rudder constructed using CAD2FEM, the left hand skin is removed to expose the substructure.

The default element used to model the parts of the rudder are four noded quadrilateral (QUAD4) elements to which a composite material card (PCOMP) is assigned. When the taper ratio of QUAD4 elements becomes more than 0.2, three noded triangular (TRIA3) elements are used locally. Flanges are modelled as 1 dimensional beam (CBEAM) elements to which the cross-sectional properties of the corresponding rib or spar laminate are assigned. The interface is modelled by a mesh tie between the various parts and the beam elements representing the flanges.

### 2.3.3 Sizing Flow

A typical sizing flow using a CAD and FEM are shown in Figure 2.4. First a CAD model is made to define the geometry of each part and this may be done based on simple analytical calculations or engineering judgement. Then a FEM is constructed using the geometry of the CAD model to perform analysis on the structure. If a structure doesn't meet strength, stiffness or any other criteria the design must be changed. When only a material change is required, like the lay-up of a certain region, the FEM doesn't need re-meshing and the element properties can be changed directly. If geometrical changes like repositioning of a rib are required the CAD model must be updated followed by an update of the FEM.

In the current study the skin layup of the mutli-rib concepts was changed in the XML files defining the FEM to automatically update the NASTRAN® Bulk Data File (BDF). This was not possible for the GS skin due to the automatic element selection procedure of CAD2FEM, requiring the BDF to be changed manually instead as is explained in Section 5.3.1.

Changing the geometry of the FEM proved labour intensive due to the lack of a direct link between WIBOMOD and CAD2FEM. Exporting a model to IGS and XML files also took

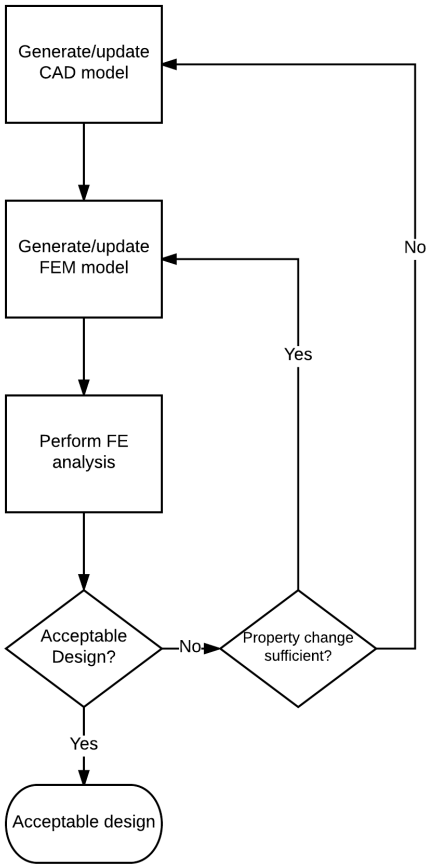


**Figure 2.4:** Typical sizing flow using a CAD and FEM model.

almost 30 minutes reducing the number of changes that could be implemented. The post processing of the NASTRAN results was performed in PATRAN or using an EXCEL based tool to locate the critical region in a SOL105 linear buckling analysis. The latter allowed changes to the skin layup to be performed quickly without inspecting each Eigenmode for each load case manually. The EXCEL tool was available at Fokker Aerostructures and a second EXCEL tool was made to write the XML code.

## 2.4 Part Manufacturing

The NSA is envisioned to be an aircraft produced in high rate. The manufacturing process must accommodate the high move rates of current single aisle aircraft such as the Airbus A320 and Boeing 737 each manufactured at a rate of approximately 50 aircraft per month. Simultaneously the manufacturing process must be robust to prevent any disruption of the aircraft final assembly. When possible Out of Autclave (OoA) manufacturing concepts are presented along with autoclave based processes. However the high part quality and ability to smooth-out small defects created during layup are solid reasons to use autoclave based manufacturing processes. In this section the envisioned part manufacturing processes for the

monolithic skins, ribs and spar are presented and discussed. Assembly and Overmolding are discussed separately for each concept. The manufacturing concepts presented in this section were used to assess process times and modify the cost estimation model.

### 2.4.1 Rib manufacturing

The ribs are to be manufactured by press-forming, a proven process that can facilitate high move rates due to the short cycle time associated with the forming step. The basic principle is to use a two sided mould mounted on a press to shape a 2D blank heated above its material $T_g$ into a 3D part. An example of a glass fibre PPS press-formed rib is shown in Figure 2.5 where both the blank and final part are shown. One half of the two sided mould is also visible on the right image of Figure 2.5.

Rib manufacturing can be split into two independent processes; the first is the manufacturing of the blanks and the second is the press-forming and subsequent finishing steps. The blanks can be manufactured using an autoclave by layup of a large laminate (slab) out of which the blanks are cut. Due to the simple flat shape of the preforms Automatic Tape Laying (ATL) using wide tapes can be used to efficiently manufacture the laminate. It is also possible to cut the blanks out of an unconsolidated laminate and to consolidate the blanks individually in a heated press. The main steps for an autoclave based process are listed below.

1. Layup of a single blank slab for 1 shipset using wide tape ATL.
2. Autoclave consolidation of the blank slab.
3. Water-jet cutting of the blank slab to produce the rib blanks.
4. Press-forming of the blanks to produce the ribs.
5. Drying to prepare for welding.

To omit the expensive autoclave step, press consolidation of the blanks is also considered. Step 2 in the list above would be omitted and a press consolidation step is added between steps 3 and 4. A schematic of the flow starting from the press consolidation step is shown in Figure 2.6. While both consolidation strategies appear to be viable more studies are required to determine the exact cost and quality difference. It is also noted that while an autoclave is available, investment in the development of a new process could be difficult to justify.

### 2.4.2 Skin manufacturing

The skin is the most costly, heaviest and largest part of the rudder as is shown in Chapter 6. It is to be manufactured by Automated Fiber Placement (AFP) and autoclave consolidation using an in-house developed AFP set-up shown in Figure 2.7 that utilizes UltraSonic (Us) tacking to layup the skin. The C/PEKK skin manufacturing process is more mature compared to the other part manufacturing processes with a relatively high Technology Readiness Level (TRL). Design guidelines derived from the capabilities of the AFP end-effector were imposed on the sizing to obtain a feasible design and are also discussed.

**Figure 2.5:** Images of A380 J-nose LE rib blank (Left) and press-formed rib (Right). (Courtesy of Composites World magazine)

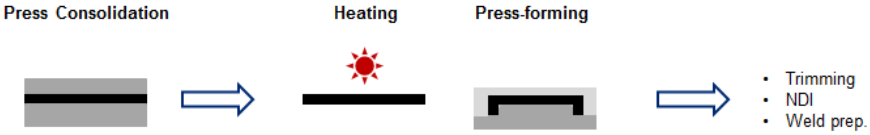


**Figure 2.6:** Process flow of OoA press-forming.

The skins can be manufactured by the use of AFP on an OML mould. After layup the skin can be manufactured by using the same process steps as the current thermoplastic components manufactured at Fokker Aerostructures. The manufacturing steps are listed below.

1. AFP of skin.
2. Bagging of skin.
3. Autoclave consolidation of skin.
4. Trimming and Non-Destructive Inspection (NDI) of skin.
5. Drying to prepare for welding.

The skin can be laid in the final shape and no additional shaping is required. The use of an OML mould reduces tooling cost and allows thickness changes to be made without modification to the tooling. Trimming can be done by water-jet cutting for improved accuracy and speed. In a high rate environment cheap aluminium moulds can be used for layup and invar moulds can be used for consolidation, reducing the number of invar moulds. Invar is the material of choice for consolidation of TP composites due to the high consolidation temperatures going up to 400 °C resulting in large thermal expansion in regular steel moulds.

The skin cost is mainly driven by weight, due to the material price, and layup time. Minimizing these two parameters results in the most cost effective design and will also reduce overall component cost. Three design guidelines were identified to have the highest impact for the level of detail of a conceptual design. The first is the 100 mm minimum tow length of the AFP end-effector, which limits the length and geometry of a patch. Second is the fixed

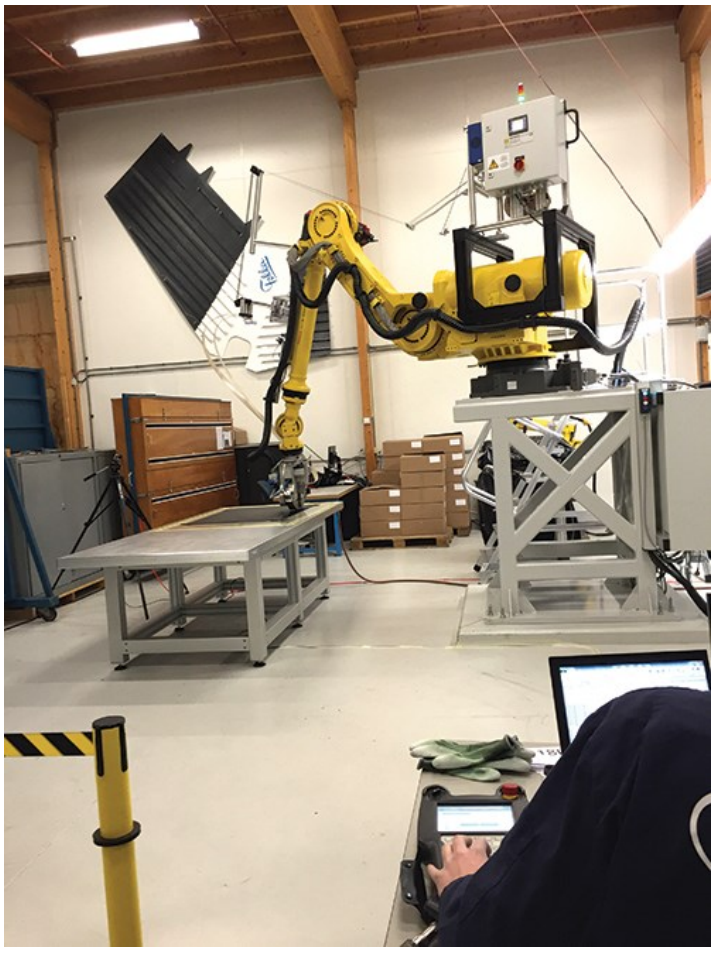

**Figure 2.7:** Thermoplastic fibre placement set-up developed at Fokker Aerostructures. (Courtesy of Composites World magazine)

tow width of 10 mm that governs the width of a pocket and becomes predominant in design of ply drop regions. The third is related to the kinematics of the robot arm and the average layup speed. The robot arm requires some distance to accelerate and reach its top speed and thus highest layup rate. Designing the skin such that the number of long tows is relatively high improves the layup speed.

### 2.4.3 Spar Manufacturing

Manufacturing a spar using TP UD material is very different from the current fabric based process used at Fokker. Spar preforms are made by hand layup of C/PPS fabric where the plies are tacked at a few spots using an Us torch. The preform is then draped over the consolidation mould and shaped by the vacuum bag. A tacked tape preform would be too stiff to shape using a vacuum bag alone. Three manufacturing processes are proposed and one is chosen as a baseline and discussed in more detail.

The spar can be laid flat to create a preform and then formed or directly laid into its final shape. When a preform is made two options are available; Press-forming can be applied in

a similar manner as rib press-forming or a hot-forming step is introduced to shape the spar followed by autoclave consolidation. The third option is to use AFP to lay the spar into its final shape, followed by autoclave consolidation. The main drawback of press-forming is the limited number of allowed thickness steps in the spar. This shall result in a heavier and thus more expensive product. Within Fokker Aerostructures limited knowledge is available on hot-forming and shaping tacked plies may induce defects in the final product. AFP is taken as a baseline to retain design freedom and reduce the risk of the manufacturing concept.

A major limitation of Us tacking AFP is the inability to place tows over strongly curved surfaces. This is intrinsic to the design of the end-effector shown in Figure 2.8 where the tows are placed and tacked on the surface by pressure exerted by the Us torch. The head of the Us torch is specifically shaped and must be within a narrow range of angles to properly tack the tows. To manufacture the spar AFP with laser tacking must be used as an alternative as demonstrated by the NLR and shown in Figure 2.9. This method requires more expensive equipment compared to Us tacking and will result in longer layup times. This is considered in the recurring cost of the spar, but further studies are required to investigate the impact on non-recurring cost. The process steps for the manufacturing of the spar are equal to that of the skin described in section 2.4.2 with the exception of the tacking method of the AFP robot.

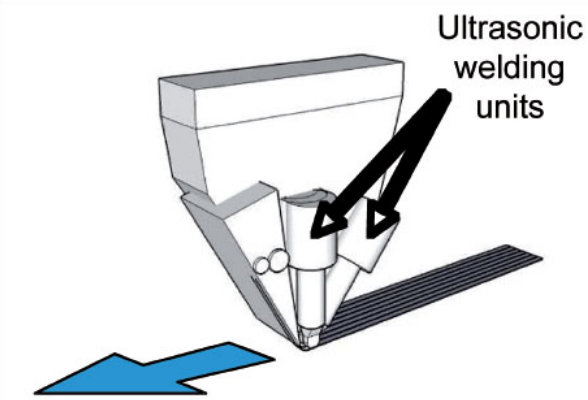


**Figure 2.8:** Schematic drawing of an Us tacking AFP end-effector. (Courtesy of Composites World Magazine)

## 2.5 Cost and Weight Estimation

The cost and weight estimation methods used are described in the literature study [5] and a summery is given in this section. The weight estimation is mostly done automatically using WIBOMOD and is straight forward. Cost estimation is done by the Cost Estimating department of Fokker Aerostructures using proprietary tools that shall not be discussed in detail. Part cost is highly driven by material price, thus an accurate weight estimation shall also improve the cost estimation.

**Figure 2.9:** AFP of C/PEKK wing pylon spar using laser tacking at the NLR. (Courtesy of the NLR)

### 2.5.1 Weight Estimation

The rudder weight is obtained by a bottom-up estimation of the parts, fasteners and accessories. The individual weights are estimated using several methods and are discussed in this section. The used approach was checked by the Weight & Balance department of Fokker Aerostructures.

The weight of the composite parts, as modelled, is computed by WIBOMOD using the provided laminate information. Details such as copper wire mesh, primer, brackets, etc. are estimated by the Weight & Balance department and used as is. The fastener- and weld interface patch -weight are computed manually using the joint lengths and selected joining method. Ramp-down regions in the skin are not modelled and the weight of these regions is estimated to be 3% of the total skin weight as advised by the Weight & Balance department.

A smeared weight approach is used to compute the weight of the GS skin. There is no discrete definition of the modelled grids, as is explained in Chapter 5, preventing an exact weight calculation. For each used grid type the volume of the stiffeners was computed and multiplied with the density shown in Table 2.1. The weight was then divided by the area of a unit cell, which was chosen to be fixed to 250 by 250 mm as discussed in Chapter 5. The skin areas to which certain grids were assigned in the FEM are extracted and multiplied with the corresponding smeared weight to obtain the total weight. It is assumed that areas where a part of a unit cell must be used shall have a weight proportional to its area.

### 2.5.2 Cost Estimation

Tools from the Cost Estimation department of Fokker Aerostructures based on the parametric cost estimation method are used for this study. The parametric method is described and

compared to other cost estimations methods by Curran et al. [6]. The method is based on the creation of a Cost Estimating Relationships (CER) for each cost driver based on historic data. The cost can then be estimated using a limited number of quantities of a part. It is noted that this only concerns the recurring cost of the rudder. Non-recurring cost, profit, risks and other tariffs related to the business case are not considered in this study.

A CER is generated by correlation of cost data from accounting (actual cost) to the description of activities of the manufacturing process (planned cost). This will provide regression curves that can be used to estimate the cost of similar parts. In the case of composite parts the weight is related to cost for each manufacturing process. For this study the CER for certain processes, such as laser tacking AFP, was modified to estimate the cost of manufacturing processes that are currently not applied at Fokker Aerostructures.

For the cost estimation a Product Breakdown Structure (PBS) is created containing all parts and sub assemblies of the rudder. The brackets and accessories, such as the tin cap, are equal for all concepts and were assumed to be equal to the C/PPS reference and directly copied. The composite parts and fasteners were modified for each concept.

# Chapter 3

# Alternative Concept Development

## 3.1 State-of-Art Rudder Design

Almost all current large transport aircraft rudders consist of a monocoque honeycomb sandwich skin with composite face sheets e.g. the Airbus A320 rudder shown in Figure 3.1. Fokker Aerostructures developed a Thermoplastic (TP) multi-rib rudder for the Gulfstream G650 aircraft shown in Figure 3.2. The thin monolithic skins between the ribs are allowed to post-buckle resulting in a more weight efficient design. These two rudders are representative for the two stiffening concepts currently applied for large aircraft rudders.

The use of sandwich structures for rudder skins started in the 1983 at Airbus as explained by Hermann [7]. The simple assembly, low part count and number of fasteners combined with surface smoothness and high specific stiffness make a sandwich skin rudder an efficient design. However moisture ingression, low damage tolerance and the difficult repair of sandwich structures are significant drawbacks that have driven Airbus to adapt a multi-rib blade-stiffened skin design for the A350 XWB aircraft.

The advantages of a TP post-buckling multi-rib rudder are well understood and are judged to be most efficient in combination with press-forming and welding, resulting in the Carbon fibre PolyEtherKetoneKetone (C/PEKK) concept development presented in Chapter 4. Limitations of the multi-rib rudder are the large number of ribs which have a low stability when the box height becomes large. This section discusses the activities performed to develop and select an alternative stiffening concept to the honeycomb sandwich and multi-rib rudder compatible with the TP composite technology of Fokker Aerostructures. The C/PEKK multi-rib shall serve as a benchmark for the performance of C/PEKK while the alternative concept shall serve as a benchmark for the multi-rib concept.

## 3.2 Alternative Concept Generation

Two methods were used to generate alternative rudder concepts for this study. The first was a literature search into structural concepts that could be applied to the Next Signle Aisle aircraft

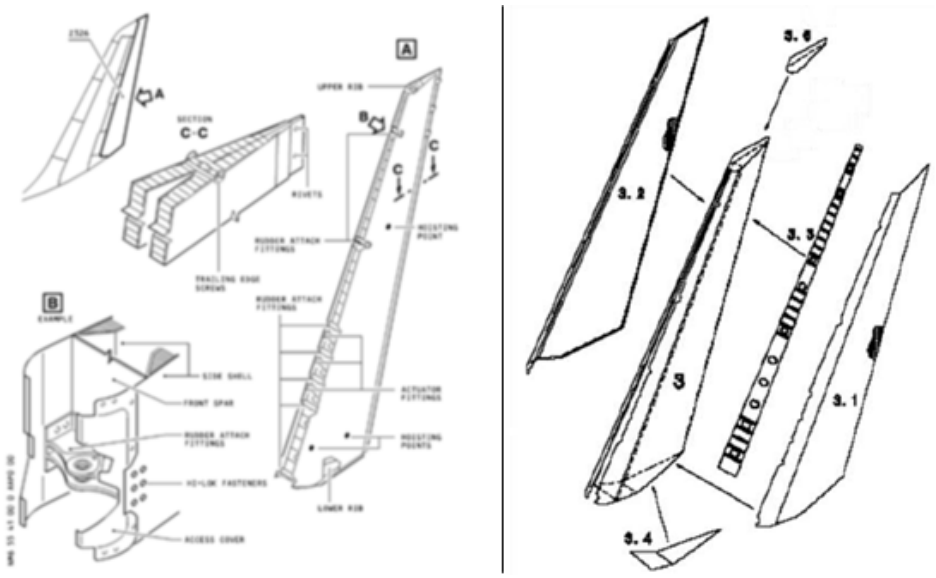

**Figure 3.1:** Airbus A320 rudder details (left) and exploded view (right). (Courtesy of Airbus Industry)

**Figure 3.2:** Image of the C/PPS rudder for the Gulfstream G650 business jet. (Courtesy of Fokker Aerostructures)

(NSA) rudder. The second method was a brainstorm session with a multi-disciplinary group of experts from Fokker Aerostructures. These activities were performed after the C/PEKK multi-rib rudder concepts described in Chapter 4 were finalized so that the cost and weight data could be used as a benchmark. It is acknowledged that in the current single aisle market an Original Equipment Manufacturer (OEM) values low component cost to the extent that a (slight) weight penalty compared to a weight optimized concept is deemed acceptable. Thus

the concept generation phase was focused not only on weight reduction, but also on cost reduction alone.

The alternative concepts are sketched and described while also stating the envisioned advantages and expected disadvantages. Depending on the nature of the concept either a chord-wise cross-sectional or plan-form sketch are made. A sketch of the multi-rib concept, used as a reference is shown in Figure 3.3.

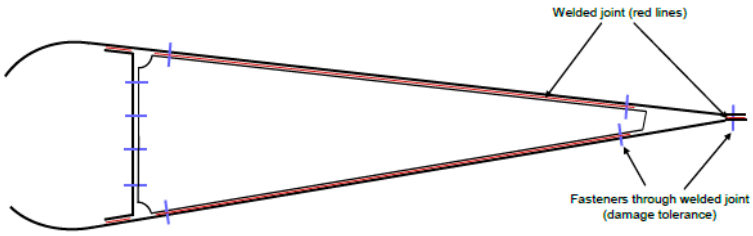


**Figure 3.3:** Cross-sectional view of the welded multi-rib rudder concept at a rib position without a hinge bracket.

### 3.2.1 Concept 1: Half Ribs

Concept 1 strives to integrate the composite wing box parts by co-consolidating the ribs directly to the skin as shown in Figure 3.4. Each rib shall be split into two parts (coloured blue and orange in Figure 3.4) and welded in the middle of the wing box as shown in the side view. The Fokker Aerostructures butt-joint technology is used to join the ribs to the skin using a filler consisting of a Short Fibre (SF) compound. A cross-sectional view of a But-joint is shown as an insert in Figure 3.4. The spar and hinge brackets shall remain unchanged from the multi-rib reference and additional brackets shall be used to fasten the ribs to the spar web. The halve ribs consist of flat blanks and are co-consolidated with the skin using tooling blocks.

The advantages of this concept is the simplicity of the ribs and joint. The halve ribs are flat and do not need to be press-formed. Welding can be done over a straight line without the need for complicated folding welding tools as shown in Figure 4.26 for the current multi-rib rudders. Lack of repairability of the butt-joint is the biggest threat for this concept. If a butt-joint fails, the rudder could fail completely as it is not possible to install fasteners at the ends of the joint. The tooling blocks required to co-consolidate the halve ribs with the skins will be heavy and expensive. It is also unlikely that post-buckling of the skin may be allowed because of the presence of a Butt-joint.

### 3.2.2 Concept 2: Front Spar - Leading Edge (FSLE) assembly

Concept 2 tries to integrate the area containing the most parts to reduce assembly cost. A sketch of the concept is shown in Figure 3.5 where the spar and leading edge are an integral Resin Transfer Molding (RTM) manufactured part. The hinge and actuator brackets are envisioned to be inserted in the mould and fixed with additional fasteners after curing. The skins and ribs are manufactured in a similar way as the multi-rib reference and the

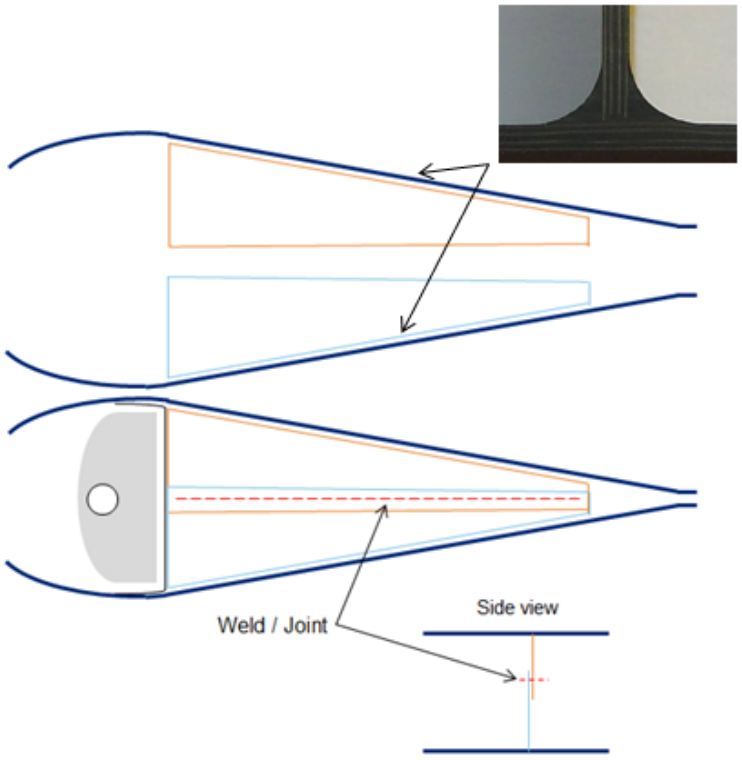


**Figure 3.4:** Cross-sectional view of concept 1: "Halve Ribs". The two skins with co-consolidated halve ribs are (top) and assembled box.

thermoplastics parts are welded. As the RTM FSLE assembly consists of a thermoset material the skins cannot be welded to it and are mechanically fastened.

The advantage of this concept is that the areas requiring high dimensional accuracy and show strong curvatures are made using RTM, a method better suitable for such parts. By inserting the brackets in the mould the hinge line can be controlled accurately allowing the brackets to be drilled beforehand. Manufacturing the FSLE assembly successfully however is expected to be a challenge. The thermal expansion of the aluminium brackets may result in defects in the composite. The skin-spar joint is also expected to be a weak point in the design due to the torsion moment that the box may induce and require relatively more material compared to the multi-rib baseline. Combined with the relatively low stiffness of RTM composites due to the low fibre volume fraction and lower bearing strength the overall weight of this concept is expected to be high.

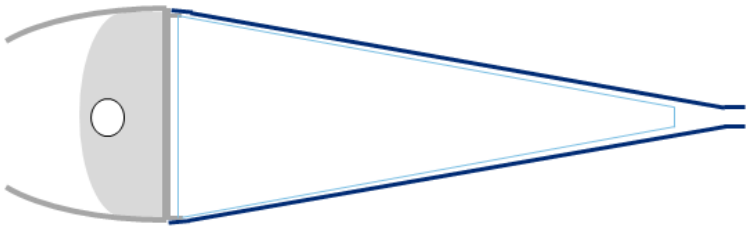

**Figure 3.5:** Cross-sectional view of concept 2: Integrated RTM leading edge, spar and brackets.

### 3.2.3 Concept 3a: Conventional Stiffened Skin Multi-rib

Concept 3a strives to reduce the number of ribs and simplify the welding process. Hat stiffeners or open section stiffeners are used to stiffen the skin instead of ribs. The orientation of the stiffeners shall be used as an optimization parameter and is not yet defined. Ribs shall still be used but the number of ribs shall be minimized as shown on the left side of Figure 3.6. The skins, spar and ribs shall be manufactured in the same way as the multi-rib reference.

By minimizing the number of ribs tooling cost shall be reduced, at the expense of optimization freedom. The design shall use a limited number of stiffeners made of C/PEKK that are press-formed. Thus only several moulds shall be required instead of unique mould for each rib. The stiffeners are welded on the skins before the rudder is assembled simplifying the closed box welding operation. A big disadvantage is that the number of weld lines shall increase significantly. The stiffeners might become heavier than ribs to act as panel breakers and result in higher cost. It is noted that this concept only works for a rudder with a straight wedge cross-section so that straight stiffeners can be used.

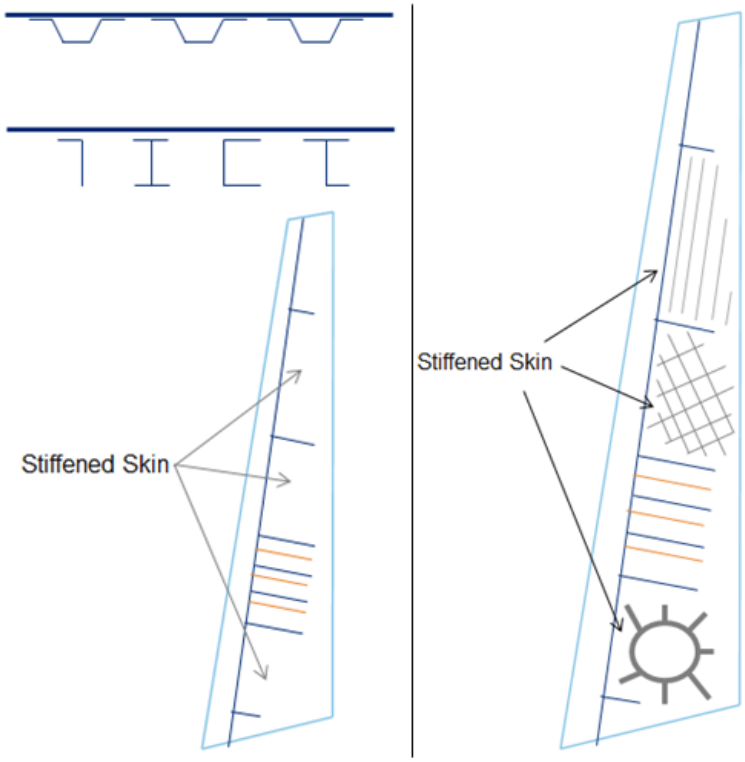


**Figure 3.6:** Plan-form view of concept 3a/b: Conventional tp stiffener stiffened skin (left / 3a) and 3D printed SF stiffener stiffened skin (right / 3b).

### 3.2.4 Concept 3b: 3D Printed Stiffened Skin Multi-rib

Concept 3b was developed by tackling the two disadvantages of concept 3a, namely weight and thus cost of the continuous fibre composite and the increased number of joints. By using a 3D printed SF compound to build the stiffeners directly on the skin there will be no need

for welding or fasteners. The substructure is equal to that of concept 3a, so that the geometry and material of the stiffeners is the only difference as shown on the right side of 3.6.

The material price of SF compound is lower than that of a continuous fibre composite. A weight increase due to the lower stiffness shall not directly result in a cost increase. Overmolding can be used to manufacture the stiffeners at high rate and potentially at lower recurring cost. Topology optimization can be used to create an efficient design, as the manufacturing process can accommodate many geometries. The Technology Readiness Level (TRL) of the manufacturing methods is however very low and the strength properties of overmolded or 3D printed stiffeners is unknown. It remains to be determined if SF stiffeners can be effective by compensating the reduced modulus with an increased moment of inertia.

### 3.2.5 Concept 4: Topology Optimized Substructure

Concept 4 strives to further reduce cost and potentially weight by optimizing the substructure. The topology optimized substructure, as for example the wing concept by J.S. Rao[1] shown in Figure 3.7, shall be 3D printed on one skin using SF C/PEKK and the second skin can be welded or bonded to the rudder. The skins may also be stiffened like in concept 3b to further optimize the design. A continues fibre insert may be used for the spar web if necessary.

Design freedom and integration of parts are the biggest advantages of this concept. By employing topology optimization the weight may be reduced compared to other concepts. With exception of the skin, the concept is fully Out of Autclave (OoA). The low TRL and difficult repair and inspection are the biggest limitations for this concept.

### 3.2.6 Concept 5: Corrugated Core Sandwich

Concept 5 is inspired by steel bridge design where sandwich constructions with a corrugated core welded to the face sheets, as shown in Figure 3.8, are used. The weld-ability of TP composites combined with roll-forming can be used to manufacture the skins out of a corrugated core sandwich. The front spar, Leading Edge (LE) region and brackets shall remain equal to the multi-rib reference.

The proven efficiency of sandwich skin rudder is utilized but without the disadvantages associated with the honeycomb core such as poor repair-ability and moisture ingression. The core geometry can be tailored and made variable to optimize the design. It is noted that the core webs should be oriented in chord-wise direction rather than span-wise as sketched in Figure 3.8. A major disadvantage is the weight of this concept when minimum thickness requirements are imposed for repairability. When the weight of the skins and ribs of the C/PEKK multi-rib rudder of Chapter 4 is smeared over the projected area of the skin a smeared thickness can be computed. It was found that the average thickness of the skin must be 16.93 layers while the minimum thickness for a symmetric and balanced laminate is 7 layers. Thus the face sheets alone would weigh as much as the minimum for an equal weight to the C/PEKK multi-rib without any provisions for load introduction or thickening patches to allow a fastened repair.

[1] http://www.altairatc.com/india/previous-events/2008/06_OS_Aircraft_Wing_Design_by_Topology_Optimisation_Using_OptiStruct_NAL_ADA.pdf

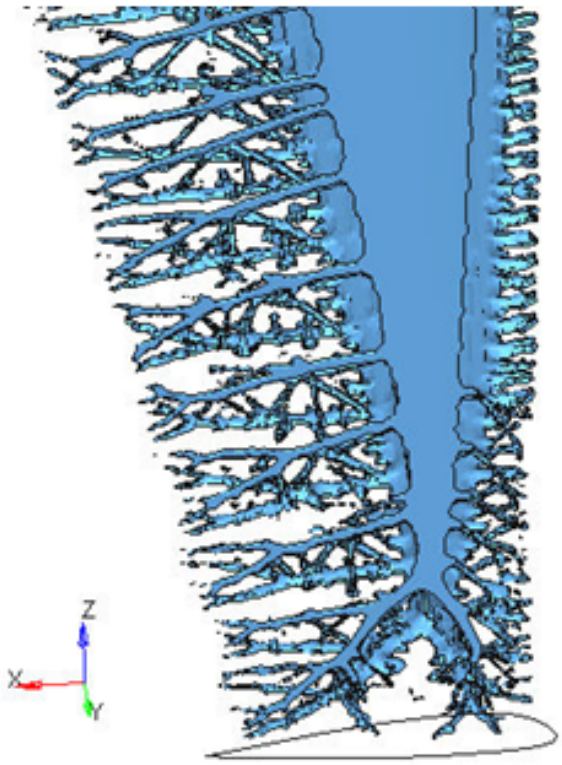


**Figure 3.7:** Topology optimized wing sub-structure designed by J.S. Rao et al. using Altair OptiStruct®.

### 3.2.7 Concept 6: Pin Reinforced Core Sandwich

In the same philosophy as concept 5 an alternative sandwich construction is proposed to improve the honeycomb core based sandwich. The pin reinforced foam core sandwich is described by Marasco et al. [8]. In this concept carbon fibre pins are inserted into the foam core to improve its mechanical properties. The stiffened core can be adhesively bonded to the face sheets (called K-Cor) or the face sheets can be mechanically pressed onto the core so that the pins penetrate the face sheets to create a mechanical lock (called X-Cor) as shown in 3.9.

The pin density and orientation can be controlled to tailor the core properties locally. It is also possible to remove the core after the sandwich is manufactured to reduce weight. Marasco et al. showed that an X-Cor sandwich can be 15% stiffer than a honeycomb sandwich offering the potential for weight reduction. The biggest disadvantage is the absence of a feasible manufacturing concept as the pins and foam cannot be co-consolidated with the TP face sheets.

### 3.2.8 Concept 7: Grid-stiffened Skin

A grid stiffened skin consisting of continuous fibre stiffeners is the $7^{\text{th}}$ concept and based on the expectation that a grid stiffened skin can be sufficiently effective compared to a monocoque

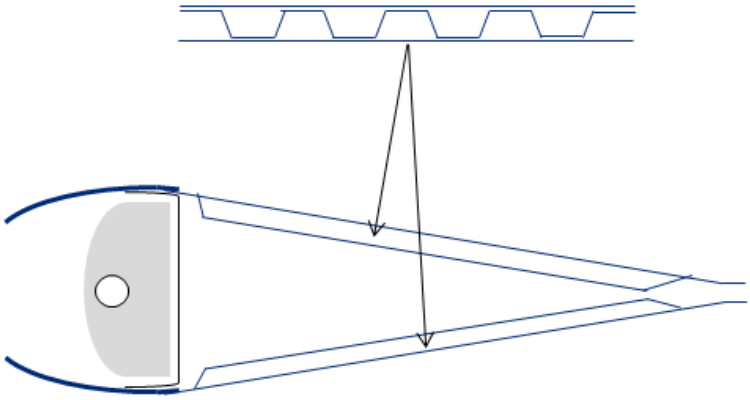

**Figure 3.8:** Cross-sectional view of concept 5: Corrugated core sandwich.

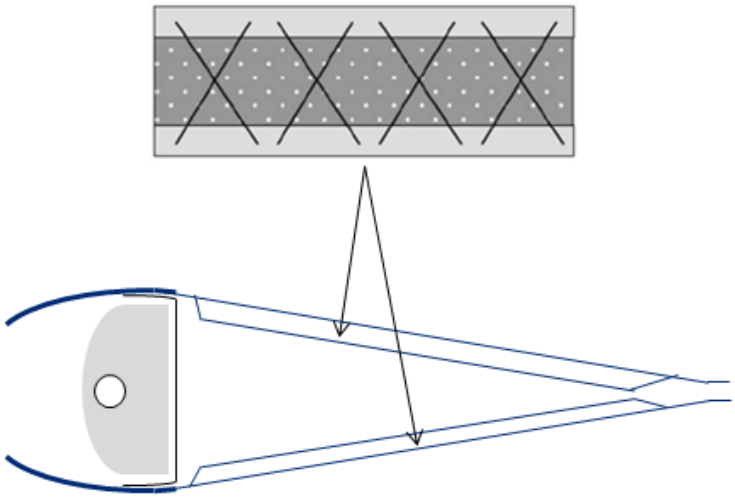

**Figure 3.9:** Cross-sectional view of concept 5: Pin stiffened core sandwich.

sandwich construction. The spar and brackets shall be made in the same manner as the multi-rib reference but the skin and grid shall be manufactured by Automated Fiber Placement (AFP) of C/PEKK.

The skin and grid shall be made of the same stiff material and potentially yield a lower weight design compared to the multi-rib concept. The grid can be optimized and designed to be damage tolerant. A disadvantage of this concept is the required tooling to consolidate the grid. Unlike thermosetting composite based grids it is not possible to use cheap silicone tooling blocks[2] (which may be used up to 350 °C) and Invar is probably required. No repair concept for a Grid-Stiffened (GS) skin is yet available, which is also a disadvantage.

[2] https://www.compositesworld.com/articles/new-options-for-trapped-tooling

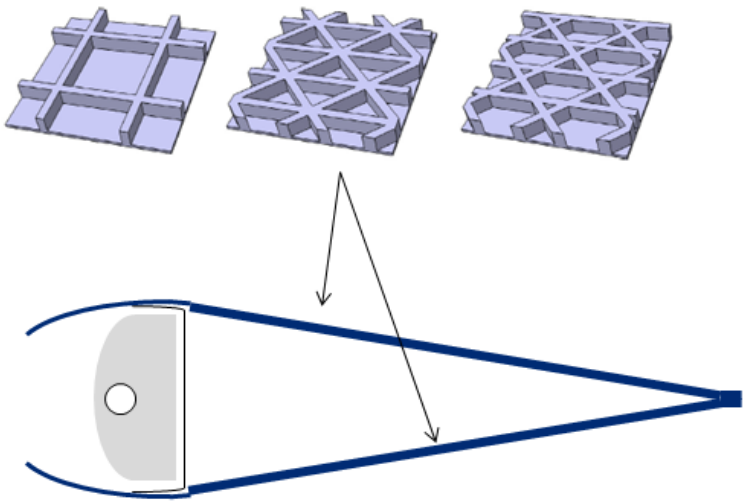

**Figure 3.10:** Cross-section of concept 7: Grid-stiffened skin.

## 3.3 Alternative Concept Selection

Following the concept generation phase trade-off criteria were developed to assess the concepts. A second session with experts was held to assess the performance of each concept for the given criteria. Based on the scores concept 3b was selected and developed into the SF compound GS skin concept presented in Chapter 5.

### 3.3.1 Trade-off Criteria

The trade-off criteria were derived from the problem statement given in Section 1.1 and sorted in five categories. These are weight, cost, "required effort to TRL 6", "high rate capability" and operational performance. Weight and cost are logical parameters to assess the feasibility of the concepts. The other three criteria are relevant to assess the development time frame of the concepts, the possibility to produce the quantities associated with a NSA and the operational aspects on which must be improved compared to the sandwich skin concept.

The categories and sub-criteria are shown in the table in Figure 3.11. Cost is split into recurring and non-recurring cost, only the first is considered in the cost estimation and in this way non-recurring cost can also be assessed. Industrialization and certification cost of certain concepts can be high and is captured in this way. Operational performance is split into three sub-criteria; Fatigue & Damage Tolerance (F&DT) the main drawback of sandwich structures, Repairability which is the second drawback of sandwich structures and Inspectability because this appears to be critical for certain concepts. The C/PEKK multi-rib was taken to be the baseline in the trade-off and performance was measured relative to this concept. The assessment was done qualitatively with experts and performance was measured in 5 levels described on the bottom of Figure 3.11.

| Category | Mark | Remark |
|---|---|---|
| **Weight** | | |
| **COST** | | |
| Recurring Cost (Part manufacturing & Assembly)<br><br>Non-Recurring Cost (Engineering & Tooling) | | |
| **Required effort to TRL 6** (Industrialization & Certification) | | |
| **High Rate Capability** | | |
| **Operational Performance** | | |
| Fatigue & Damage Tolerance<br>Reparability<br>Inspectability | | |

Mark w.r.t. baseline: -- poor, - less, 0 equal, + better, ++ best

**Figure 3.11:** Trade-off table used to assess the alternative concepts.

### 3.3.2 Concept Assessment

The trade-off table of Figure 3.11 was filled in with a group of experts and the results are shown in Figure 3.12 and discussed in this section. Considering that none of the concepts is expected to be more weight efficient than the multi-rib reference a concept was selected that would yield a reduction of recurring cost. Inspection of the table in Figure 3.12 shows that this would only be viable for concepts 3b and 5. Concept 3b was selected for further development after analysis of the results.

**Cost** Most concepts are judged to have a neutral recurring cost due to automated production or the use of more integrated parts. Concept 3a, sketched on the left side of Figure 3.6, is the only concept that is expected to have higher recurring cost compared to the baseline. This emphasizes te need to reduce the number of parts and joints, which is characteristic to this concept, in order to reduce recurring cost.

The non-recurring cost show a correlation with the process speed and required equipment. Concepts 1 and 6 are judged to require less moulds and have shorter process times for assembly. Concept 4 doesn't require any moulds and it is judged that the cost of 3D printing shall be sufficiently low to compensate for the long process times. Concept 3 is judged to have a higher non-recurring cost due to the addition of new process steps above the existing manufacturing steps of a multi-rib such as 3D printing or stiffener welding.

**Effort to TRL 6** The multi-rib rudder is the most mature concept due to previous work at Fokker Aerostructures, but certain building blocks have not reached TRL 6 so that the concept

cannot be offered readily to customers. The other concepts were compared the multi-rib rudder and concepts 1, 3a and 7 were judged to require comparable development effort as the multi-rib. Concepts 2 and 5 are expected to require more development time due to the large RTM part and new sandwich construction respectively. The other concepts are expected to require much more development effort due to the new materials and manufacturing processes that must be introduced.

**Manufacturing rate** While all concepts are judged suitable for a high manufacturing rate concept 5 stands out significantly. Due to the simple and mostly thin skins it is expected that Continous Compression Moulding (CCM) can be employed to efficiently manufacture the skins. Concepts 4 and 6 are expected to also be more suitable for high manufacturing rates due to the limited number of process steps, level of part integration, low part count and potential OoA processing.

**Fatigue & Damage Tolerance** F&DT is expected to be good for concepts 3b, 4 and 7 due to the redundancy that can be designed into the stiffening elements. Concept 2 scores lowest due to the critical joint between the RTM front spar and TP torsion box. The performance of the pin core reinforced concept could not be assessed because there is no clear concept to join the pins to the face sheets. The other concepts are expected to perform equal to the multi-rib.

**Repairability & Inspectability** The repairability of concepts 1 and 4 is poor due to the butt-joint and irregular substructure respectively. Sandwich constructions and densely stiffened skins are also more difficult to repair, all other concepts have comparable repairability. Inspectability is also very poor for concept 4 and is caused by the difficult accessibility. Inspection of the butt-joint inside a closed box and a complicated 3D printed stiffening geometry such as concepts 1 and 3b are also more difficult to inspect. All others score more of less comparable to the multi-rib.

While no clear winning concept can be appointed, when the requirement for a lower recurring cost is imposed only concepts 3b and 5 remain. While concept 5 scores slightly better on most other criteria it is expected that the concept is not suitable for the low loads observed in a rudder. This will result in the use of minimum dimensions for the skins, leaving little to no room for sizing and probably resulting in a too heavy design. Concept 3b utilizes SF material which has a better outlook on cost reduction and 3D printing is considered to be a key technology by GKN, the mother company of Fokker Aerostructures. Lastly, overmolding is also expected to be viable for this concept with the potential to further reduce cost. Thus concept 3b was selected as a baseline for further development.

| Category | C1: Halve ribs | C2: FSLE assy | C3a: conv. Stiff. | C3b: 3D print. stiff | C4: Topology opt. | C5: Corrugated core | C6: Pin core | C7: GS |
|---|---|---|---|---|---|---|---|---|
| **Weight** | - | - | - | - | - | - | 0 | - |
| **Cost** | | | | | | | | |
| Recurring Cost (Part manufacturing & Assembly) | 0 | 0 | - | + | 0 | + | 0 | 0 |
| Non-Recurring Cost (Engineering & Tooling) | + | -\0 | - | - | + | 0\+ | + | 0 |
| **Required effort to TRL 6** (Industrialization & Certification) | 0 | - | 0 | -- | -- | - | -- | 0 |
| **High Rate Capability** | 0 | 0 | -\0 | 0 | + | ++ | + | 0 |
| **Operational Performance** | | | | | | | | |
| Fatigue & Damage Tolerance | 0 | - | 0 | + | + | -\0 | ? | + |
| Reparability | -- | 0 | 0 | - | -- | -\0 | - | - |
| Inspectability | - | 0 | 0 | - | -- | 0 | -\0 | 0\+ |

**Figure 3.12:** Assessment of all the concepts, performance is w.r.t. the C/PEKK multi-rib concept.

# Chapter 4

# The Multi-rib Rudder

Much effort was put into the development of the Carbon fibre PolyEtherKetoneKetone (C/PEKK) multi-rib rudder to understand the difference with the Carbon fibre PolyPhenylene Sulfide (C/PPS) concept. The difference between a tape and fabric material was felt in the design of a ply library with the Automated Fiber Placement (AFP) rules in mind. Two ply libraries, one with a base laminate of 1.24 mm (9 tape layers) and the other with a 1.52 mm (11 tape layers) base, were used to size the skin resulting in two concepts for the C/PEKK Multi-rib rudder. These were dubbed MR9 and MR11 respectively.

A ply library consists of a family of laminates where layers are added consecutively to maximize continuity of the layers of the skin. The base laminate is the starting point from which other laminates are designed according to the lamination rules such as explained by Kassapoglou [9]. The 9 layer laminate has the same thickness as the C/PPS reference rudder minimum skin thickness. The 11 layer base laminate results in a more efficient ply library for the applied loads and allows effective placement of patches at the weld interface. A thickness of 1.52 mm is also the minimum requirement of a general, more strict, Fokker Aerostructures design guideline for a fastened repair.

## 4.1 Final Designs

The final designs for concepts MR9 and MR11 are presented in this section to provide a visualization of the two concepts. This will improve understanding of the sizing and structural analysis that shall be discussed in the next sections.

### 4.1.1 9 layer base concept (MR9)

Concept MR9 with hidden left hand skin is shown in Figure 4.1. The front spar is coloured red, brackets placed behind an actuator bracket or hinge bracket are shown in yellow and blue respectively while additional ribs are shown in green. The Next Signle Aisle aircraft (NSA)

rudder has 7 hinge brackets and 3 actuator brackets, where the ribs have been named to their respective bracket. Concept MR9 has 24 ribs in total, where the top rib shown in 4.1 models the metal tip cap of the rib and is not counted as a rib. The root rib, used to close the box, is also counted as a rib. The brackets are modelled by the green blocks as explained in Section 2.1.

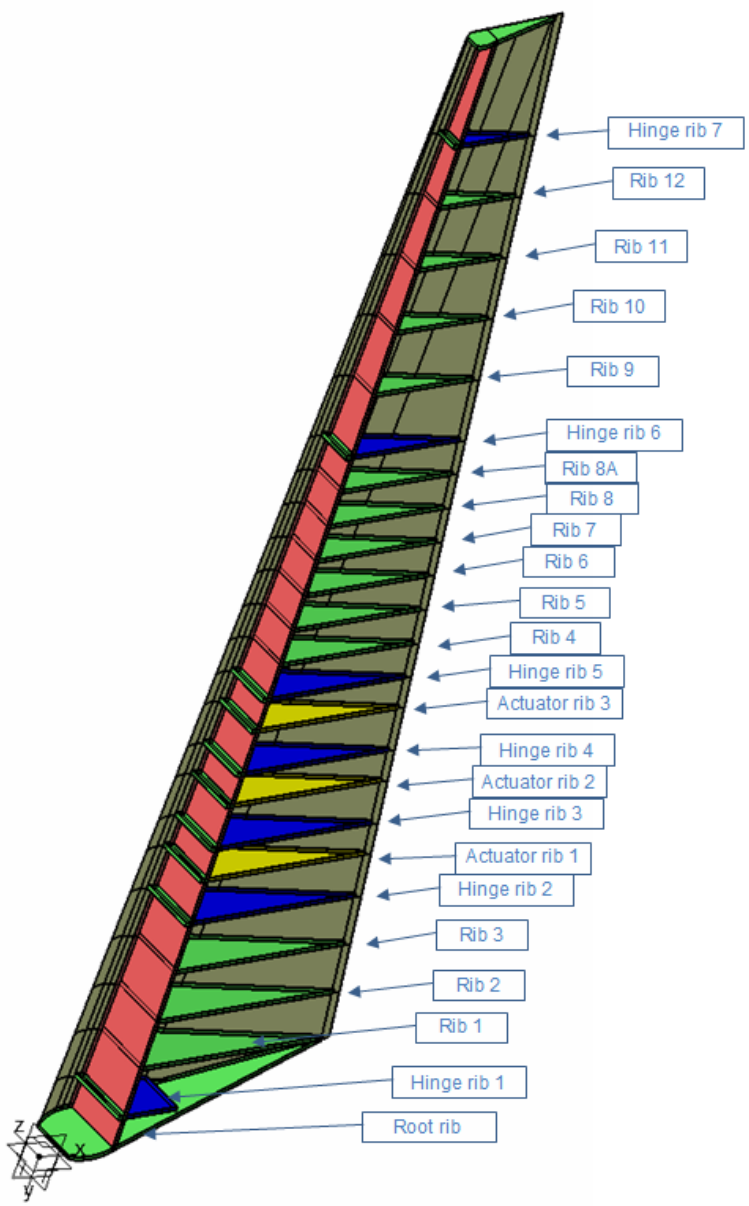


**Figure 4.1:** CATIA model of MR9 with the left hand skin hidden to show the substructure.

### 4.1.2 11 layer base concept (MR11)

The configuration of concept MR11 is shown in Figure 4.2 in a similar way as MR9. The ribs behind the hinge and actuator brackets are at the same position as in MR9 and only the

additional ribs above hinge 5 have varied pitch resulting in a total of 22 ribs including the root rib.

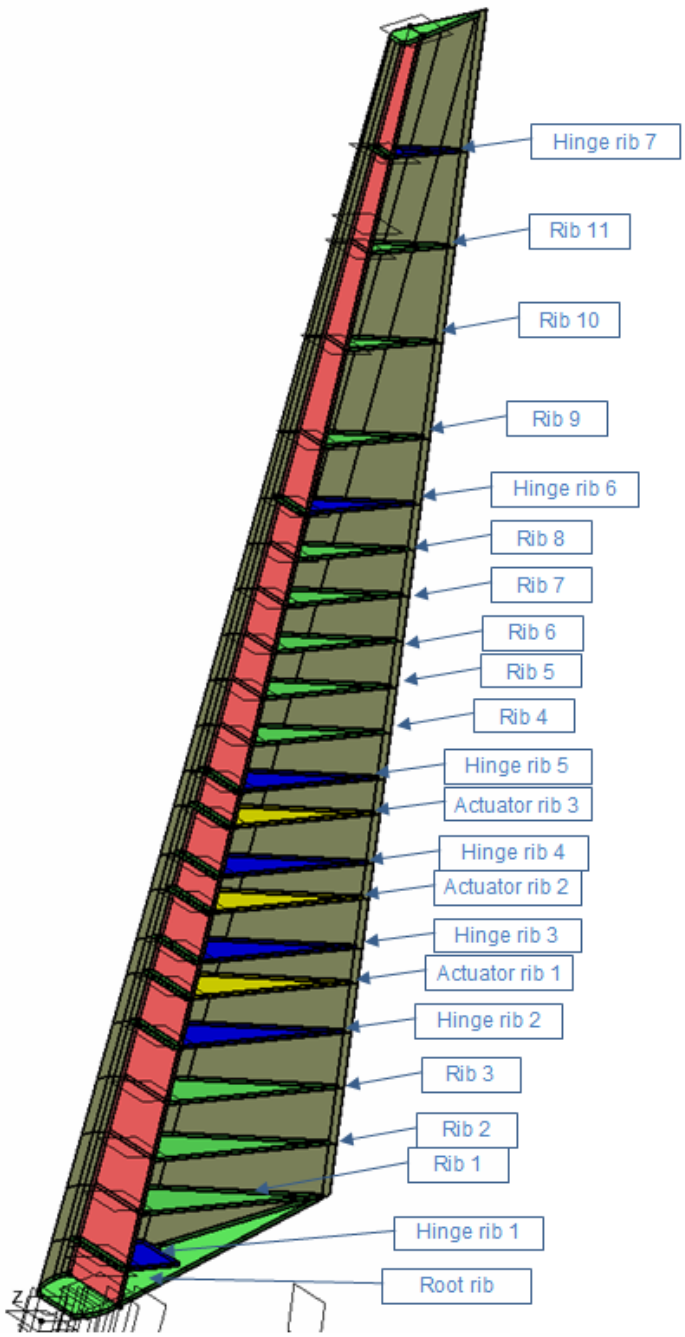


**Figure 4.2:** CATIA model of MR11 with the left hand skin hidden to show the substructure.

## 4.2 Sizing Methods

The rudder sizing is globally driven by stability rather than strength resulting in a trade-off between adding ribs to the substructure or increasing skin thickness to stabilize the bays. It is observed that for an optimum design the minimum number of ribs must be found for a given skin thickness. In some bays, such as the root of the rudder, the box height results in large ribs and thickening of the skins is a more suitable option. The skin also needed to be thickened in the area aft of the actuator brackets because of the high loads in that region.

### 4.2.1 Post-Buckling Skin Philosophy

The skins are allowed to post-buckle under certain conditions described in the stress (structural analysis) guidelines of previous rudder designs made by Fokker Aerostructures [10]. The allowed post-buckling envelope is dependant on the load case and skin thickness of the buckled region. The buckling point expressed as a percentage of Limit Load (LL) is shown in Figure 4.3. Skin laminates up to 1.52 mm (or 11 layers) are allowed to buckle at 70% LL in load cases where the rudder is undamaged. Laminates with a thickness larger than 1.52 and below 2 mm are allowed to buckle at 100% LL, beyond this thickness no buckling is allowed up to Ultimate Load (UL). The thickness dependant buckling point is imposed to limit the energy stored in the posed-buckled skin and avoid damage during unloading. It is considered that 70% LL is below the daily loads, thus avoiding fatigue to occur due to post-buckling of the skins.

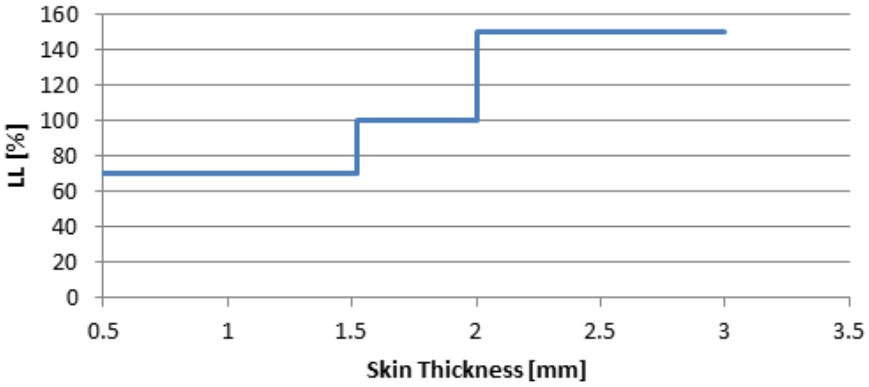


**Figure 4.3:** Post-buckling point as a function of skin thickness.

The conditions for the post-buckling envelope also have implications on the load cases presented in Section 1.3. The post-buckling limits shown in Figure 4.3 for skins up to 2 mm are for two reduced load cases. These are the maximum and minimum Hinge Moment (HM) load cases where the enforced hinge displacements have been omitted to capture the effect of air load alone. In cases where the rudder is damaged skin pockets with a thickness below 2 mm may buckle at any point as long as the strain in the skin is below the allowable strain level. In all situations the substructure; ribs, front spar and skin area from the front spar to the leading edge must remain stable until UL.

Determining the strains in a post-buckled situation is only possible by a non-linear Finite Element (FE) analysis but the buckling load can be found easily and with good accuracy by

performing a linear buckling analysis such a SOL 105, which is an Eigenvalue analysis, in NASTRAN. There was no time to perform a non-linear analysis in this study, but the strains were found to be low (below 1600 $\mu\epsilon$) for the post-buckling skins, so that the assumption can be made that the strains will not exceed the allowable. To account for variation in stiffness and inaccuracies in the linear buckling analysis a knock down of 10% is used on all the results. This has been included in all the values presented in this report.

### 4.2.2 Multi-rib Rudder Sizing Flow

Starting from the C/PPS reference rudder the laminates were changed from C/PPS to the nearest thickness in C/PEKK with the exception of the minimum thickness which was chosen to be 1.52 mm as is the basis for MR11. The results of these load cases showed that some ribs could be removed. One rib in the region between hinges 6 and 7 was removed and the rib pitch was made constant for simplicity. These variations showed that modifications to the substructure do not effect the global behaviour of the rudder and are mostly limited to adjacent bays. The configuration of MR11 was defined first as shown in Figure 4.2 where 2 ribs have been removed between hinges 6 and 7 and 1 rib in the area between hinges 5 and 6. In the development of MR9 one rib was again added in each of these regions, as can be seen in Figure 4.1, to compensate for the lower skin thickness. It is noted that the starting point of the spar was taken to be 12 layers, which had the same cross-sectional bending stiffness (EI) as a 6 layer fabric spar used in the upper part of the C/PPS reference rudder.

When the substructure configuration was determined, the sizing was initiated according to the flowchart of Figure 4.4. The minimum thickness requirements in all regions shown in Figure 2.1 were applied and the full skin area was set to the minimum thickness corresponding to its concept. First the rudder was sized using only a linear buckling analysis (SOL105) for the reduced minimum and maximum HM load cases to ensure that the lightest post-buckling skin design is achieved. The results of the SOL105 analysis were conditioned by an in-house developed EXCEL tool of Fokker Aerostructures. This tool identified the critical load case and corresponding RF for each property region of the Finte Element Model (FEM). The thickness of each skin region of part was increased if the Reserve Factor (RF) was too low. The XML files were updated and CAD2FEM was run again to update the FEM.

Then the linear buckling analysis for the full set of load cases is performed to ensure stability of the substructure and thick skins. In these iterations the ribs and spar mostly required to be thickened to meet stability requirements. Each linear buckling analysis for a single load case required approximately 5 minutes on a 2.66 GHz processor desktop and approximately 10 iterations were required to size each rudder concept. Lastly a linear direct stiffness analysis (SOL 101) was run to determine the strains, deformation and interface loads. The strain allowable was never driving the sizing and is thus not shown in Figure 4.4. A non-linear analysis is still required to verify the assumptions that the strains remain below the allowables in the post-buckled state.

### 4.2.3 Substructure Laminates

For the ribs and spar a ply library available at Fokker Aerostructures, shown in Table 4.1, was used for simplicity. The laminates designed either for the spar or rib are named after

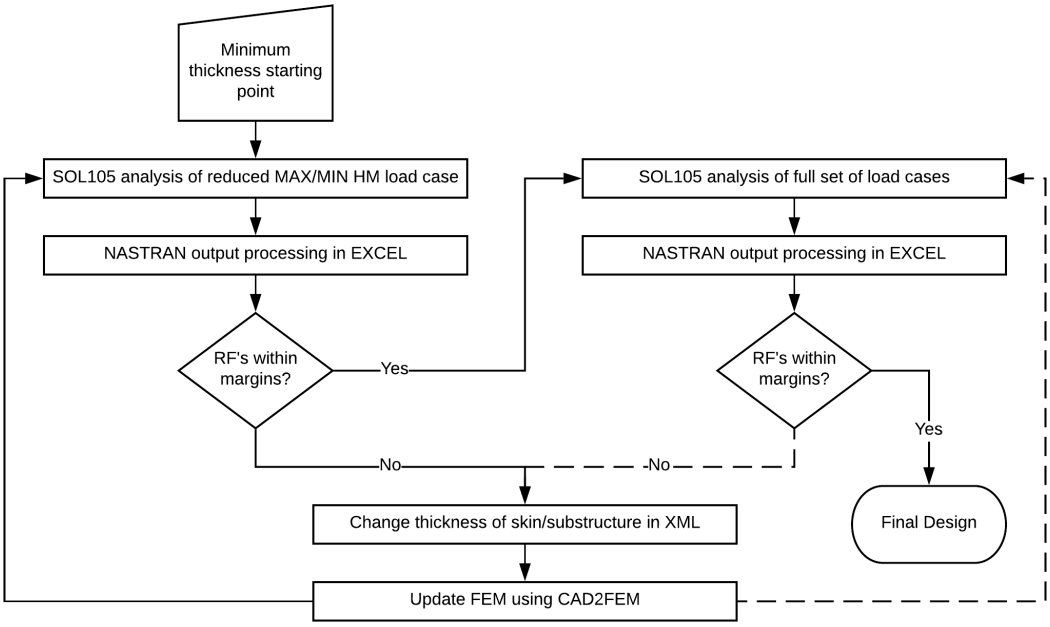


**Figure 4.4:** Sizing flow of the multi-rib rudders.

the part to which they are intended to be applied and the number of layers they contain. RIB_8 for example is a rib laminate consisting of 8 layers. It is noted that in the FEM the 0°direction for the ribs is in chord-wise direction of the rudder while the 0°direction for the spar is in span-wise direction. In both MR9 and MR11 spar laminates were used for ribs because the loads were higher than initially expected. The substructure laminates were not optimized because it was beyond the required level of detail for the trade-off, but should be considered in a detailed design phase.

### 4.2.4 Skin Laminates

The ply libraries for the skins of MR9 and MR11 are shown in Figures 4.5 and 4.6 respectively. As common in composite laminate design Fokker Aerostructures requires laminates to be symmetric and balanced. For improved impact damage resistance the difference in orientation between adjacent plies is set to 45°. An exception is made for thin laminates where this is not possible to achieve and not necessary due to the high flexibility of thin laminates which is beneficial for impact damage resistance. The thinnest possible balanced and symmetric laminate with the C/PEKK tape is 7 layers or 0.966 mm and, while not used in either MR9 or MR11, is the starting point for both ply libraries.

In Figures 4.5 and 4.6 the laminates are build-up from right to left with the 7 layer laminate as a starting point. It is noted that the MR11 skin library was adapted from a previous study performed at Fokker Aerostructures. On the far right a special laminate is shown used to achieve the required minimum thickness at the Trailing Edge (TE) to meet the lightning strike damage requirement described in Section 2.1. In these TE laminates some plies are laid parallel to the skin edge to improve the Buy-to-Fly ratio (BtF) and layup speed.

**Table 4.1:** Laminate names and layup used for the substructure.

| Laminate | Thickness [mm] | Layup |
|---|---|---|
| *Ribs* | | |
| Rib_8 | 1.10 | $[45/0/-45/90]_s$ |
| Rib_12 | 1.66 | $[45/-45/0/-45/90/45]_s$ |
| Rib_14 | 1.93 | $[45/-45/0/-45/90/45/0]_s$ |
| *Spar* | | |
| Spar_12 | 1.66 | $[45/-45/90/45/0/-45]_s$ |
| Spar_14 | 1.93 | $[45/0/-45/90/45/0/-45]_s$ |
| Spar_18 | 2.48 | $[45/0/-45/90/45/0/-45/90/-45/$ $45/90/-45/0/45/90/-45/0/45]$ |
| Spar_20 | 2.76 | $[45/0/-45/90/45/0/-45/90/0/-45/$ $0/45/90/-45/0/45/90/-45/0/45]$ |
| Spar_22 | 3.04 | $[45/0/-45/90/45/0/-45/90/45/0/-45]_s$ |

Characteristic to both libraries is that consecutive laminates utilize the same ply definition of the thinner laminates and add layers to increase the thickness.

Stability is the main driver for the skin sizing, requiring a skin with a high buckling load. Adding ± 45°plies on the outer sides of a laminate is the most efficient way to improve the buckling load. This is especially the case in laminate NMA_11 in Figure 4.6 and less so in Skin_9 in Figure 4.5. The thickest laminates are used in the area around the actuator brackets to ensure sufficient bearing strength as the brackets are fastened to the skin using bolts. Predominately 0°plies are used as these can be placed most efficiently. The fibres lay perpendicular to the main loading direction and it is assumed that this does not significantly affect the stress concentration factor compared to the C/PPS fabric reference and the equal bearing thickness assumptions will hold. It is also noted that the TE laminate of MR9 has 4 layers on each side with almost the same orientation (-8.3°and 0°) and while not in disagreement with the lamination rules, care must be taken to analyse this section in a detailed design to verify its use.

While both ply libraries appeared to perform equivalently on component level, the library used for MR11 and shown in Figure 4.6 appears to yield a more simple skin ply definition. The details such as the weld interface padding discussed in Section 4.2.5 are simpler and may enable a faster layup time.

### 4.2.5 Weld Interface Skin Padding

As discussed in Section 2.1 a minimum thickness requirement is in place for the skin at the weld interface to the ribs. This is 1.8 mm and thicker than the required skin thickness from the sizing. In MR11 this means that the 11 layer laminate must be increased to a 13 layer laminate, as shown in Figure 4.6, at the weld interface. This is done by placing two 4 tows (10 mm wide each) wide plies in 90°(cord-wise) direction along the rib flange interface. The rib flange widths are 25 mm and the 40 mm wide interface should provide sufficient assembly tolerance. Increasing the thickness of the 9 layer base laminate in concept MR9 requires more effort. The patches have been found to result in a significant weight increase of the skins and are included in the weight and cost estimation.

| | Skin_32 | Skin_26 | Skin_20 | Skin_18 | Skin_16 | Skin_14 | Skin_10 | Skin_9 | Skin_7 | Skin_13_TE |
|---|---|---|---|---|---|---|---|---|---|---|
| Layers | 32 | 26 | 20 | 18 | 16 | 14 | 10 | 9 | 7 | 13_TE |
| Thickness | 4.416 | 3.588 | 2.76 | 2.484 | 2.208 | 1.932 | 1.38 | 1.242 | 0.966 | 1.794 |
| Layer ID 10 | 45 | 45 | 45 | 45 | 45 | 45 | 45 | 45 | 45 | 45 |
| 20 | 90 | 90 | 90 | 90 | 90 | | | | | |
| 30 | -45 | -45 | -45 | -45 | -45 | -45 | | | | -8.3 |
| 40 | 0 | 0 | 0 | 0 | 0 | 0 | 0 | 0 | 0 | 0 |
| 50 | 0 | 0 | 0 | 0 | 0 | 0 | 0 | 0 | | 0 |
| 60 | 45 | 45 | | | | | | | | |
| 70 | 0 | 0 | | | | | | | | |
| 80 | 0 | | | | | | | | | |
| 90 | -45 | -45 | | | | | | | | |
| 100 | 0 | 0 | 0 | | | | | | | |
| 110 | 0 | | | | | | | | | |
| 120 | 45 | 45 | 45 | 45 | 45 | 45 | | | | -8.3 |
| 130 | 0 | 0 | 0 | 0 | | | | | | |
| 140 | 0 | | | | | | | | | |
| 150 | -45 | -45 | -45 | -45 | -45 | -45 | -45 | -45 | -45 | -45 |
| 160 | 90 | 90 | 90 | 90 | 90 | 90 | 90 | 90 | 90 | 90 |
| 170 | 90 | 90 | 90 | 90 | 90 | 90 | 90 | | | |
| 180 | -45 | -45 | -45 | -45 | -45 | -45 | -45 | -45 | -45 | -45 |
| 190 | 0 | | | | | | | | | |
| 200 | 0 | 0 | 0 | 0 | | | | | | |
| 210 | 45 | 45 | 45 | 45 | 45 | 45 | | | | -8.3 |
| 220 | 0 | | | | | | | | | |
| 230 | 0 | 0 | 0 | | | | | | | |
| 240 | -45 | -45 | | | | | | | | |
| 250 | 0 | | | | | | | | | |
| 260 | 0 | 0 | | | | | | | | |
| 270 | 45 | 45 | | | | | | | | |
| 280 | 0 | 0 | 0 | 0 | 0 | 0 | 0 | 0 | | 0 |
| 290 | 0 | 0 | 0 | 0 | 0 | 0 | 0 | 0 | 0 | 0 |
| 300 | -45 | -45 | -45 | -45 | -45 | -45 | | | | -8.3 |
| 310 | 90 | 90 | 90 | 90 | 90 | | | | | |
| 320 | 45 | 45 | 45 | 45 | 45 | 45 | 45 | 45 | 45 | 45 |

**Figure 4.5:** Ply library used for concept MR9 based on a 1.24 mm starting point.

Inspection of the MR9 ply library in Figure 4.5 shows that the first laminate that meets the minimum weld interface requirement is Skin_14 with a thickness of 1.93 mm. Thus 5 plies must be added locally and this must be done sequentially as only 2 plies may be added or dropped at a point. The weld patch build-up sequence for MR9 is shown in Figure 4.7. The weld interface is indicated by the gray bar in Figure 4.7 and the 5 additional plies that must be added to the 9 layer skin are sketched in different colours. The minimum tow length of the AFP end-effector is 100 mm and is accounted for in the design of the patch.

The 4 $\pm$ 45°plies are dropped in pairs to ensure the patch is always balanced at the expense of symmetry. In the middle a single ply is added in 90°direction to create the Skin_14 laminate, but this means that the patch outside of the blue area violates the "10% rule" of the lamination rules [9]. If needed, this can be fixed by extending the blue zone to include the other plies. The inner $\pm$ 45°plies consist of 100 mm long tows which have a 70.7 mm width when measured cord-wise. The outer most plies are 110 mm long (90.7 mm cord-wise length) to provide a 10 mm ply drop distance on each side. Measured from the weld interface the patch is also approximately 91 mm long in cord-wise direction, which must be taken into

| | NMA_31 | NMA_23 | NMA_17 | NMA_15 | NMA_13 | NMA_11 | NMA_7 | NMA_13_TE |
|---|---|---|---|---|---|---|---|---|
| Layers | 31 | 23 | 17 | 15 | 13 | 11 | 7 | 13_TE |
| Thickness | 4.278 | 3.174 | 2.346 | 2.07 | 1.794 | 1.518 | 0.966 | 1.794 |
| Layer ID 10 | 45 | 45 | 45 | 45 | 45 | 45 | 45 | 45 |
| 20 | 90 | 90 | 90 | 90 | 90 | | | -8.3 |
| 30 | -45 | -45 | -45 | -45 | -45 | -45 | | -45 |
| 40 | 0 | 0 | 0 | 0 | 0 | 0 | 0 | 0 |
| 50 | 0 | | | | | | | |
| 60 | 45 | 45 | | | | | | |
| 70 | 0 | 0 | | | | | | |
| 80 | 0 | | | | | | | |
| 90 | -45 | -45 | | | | | | |
| 100 | 0 | 0 | 0 | | | | | |
| 110 | 0 | | | | | | | |
| 120 | 45 | 45 | 45 | 45 | 45 | 45 | | 45 |
| 130 | 0 | 0 | 0 | 0 | | | | |
| 140 | 0 | | | | | | | |
| 150 | -45 | -45 | -45 | -45 | -45 | -45 | -45 | -45 |
| 160 | 90 | 90 | 90 | 90 | 90 | 90 | 90 | 90 |
| 170 | -45 | -45 | -45 | -45 | -45 | -45 | -45 | -45 |
| 180 | 0 | | | | | | | |
| 190 | 0 | 0 | 0 | 0 | | | | |
| 200 | 45 | 45 | 45 | 45 | 45 | 45 | | 45 |
| 210 | 0 | | | | | | | |
| 220 | 0 | 0 | 0 | | | | | |
| 230 | -45 | -45 | | | | | | |
| 240 | 0 | | | | | | | |
| 250 | 0 | 0 | | | | | | |
| 260 | 45 | 45 | | | | | | |
| 270 | 0 | | | | | | | |
| 280 | 0 | 0 | 0 | 0 | 0 | 0 | 0 | 0 |
| 290 | -45 | -45 | -45 | -45 | -45 | -45 | | -45 |
| 300 | 90 | 90 | 90 | 90 | 90 | | | -8.3 |
| 310 | 45 | 45 | 45 | 45 | 45 | 45 | 45 | 45 |

**Figure 4.6:** Ply library used for concept MR11 based on a 1.52 mm starting point.

account in the detailed design where these region may interfere with the TE laminate.

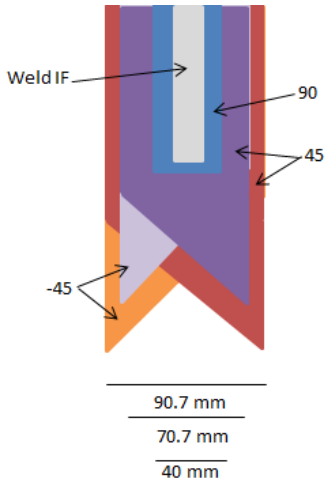


**Figure 4.7:** Sketch of weld interface layup for the MR9 skin.

## 4.3 Sizing Results

### 4.3.1 MR9 Analysis Results

#### Configuration overview

The thickness distribution of the skin is shown in Figure 4.8. Some thickening of the skin is required near the hinge-actuator assembly where interface loads are introduced into the rudder. The section between hinges 6 and 7 required a 10 layer skin. Adding a rib in this area might be a more weight-efficient option, but this option was not investigated. From a cost point of view, adding a rib is considered less cost effective. It is noted that due to the definition of the ply book, the area above hinge 7 has a 14 layer laminate instead of the required 13. The local thickening of the rib weld interfaces are conservatively not modelled in PATRAN and are therefore not shown in Figure 4.8.

The thickness distribution of the substructure is shown in Figure 4.9. The front spar required thickening near the actuator brackets. It was found that the actuator 3 jam case (see Section 1.3 was driving. Due to the induced torsion and bending the lower section of the spar also required thickening. This resulted in a significantly larger thickness than required for the other load cases. The ribs in this area also required thicker laminates.

It is noted that the actuator jam load case can also occur at actuators 1 and 2 and thus all these ribs were thickened to be conservative. It is however possible that this might not be required if the load case would be applied to the other actuators. In the condensed load case selection defined in Section 1.3 it was found that the actuator 3 load case was the most severe and thus representative for the other two jam cases. All the other ribs were modelled with a 1.1 mm, 8 layer laminate which proved to be sufficient. The rib webs are flat without any stiffeners or lightening holes.

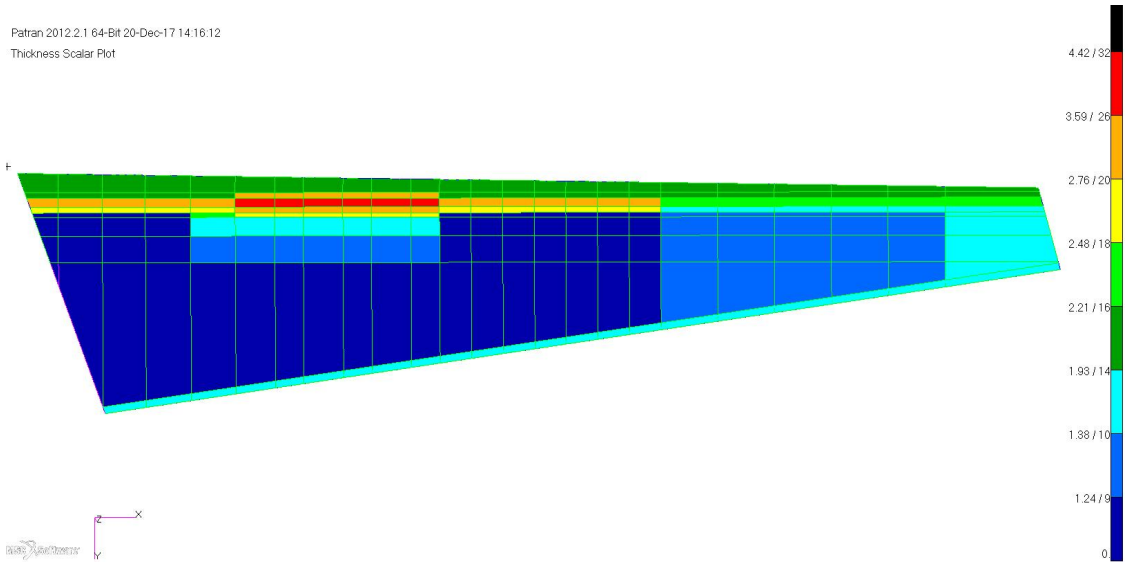


**Figure 4.8:** Skin thickness distribution of concept MR9, in mm / number of layers.

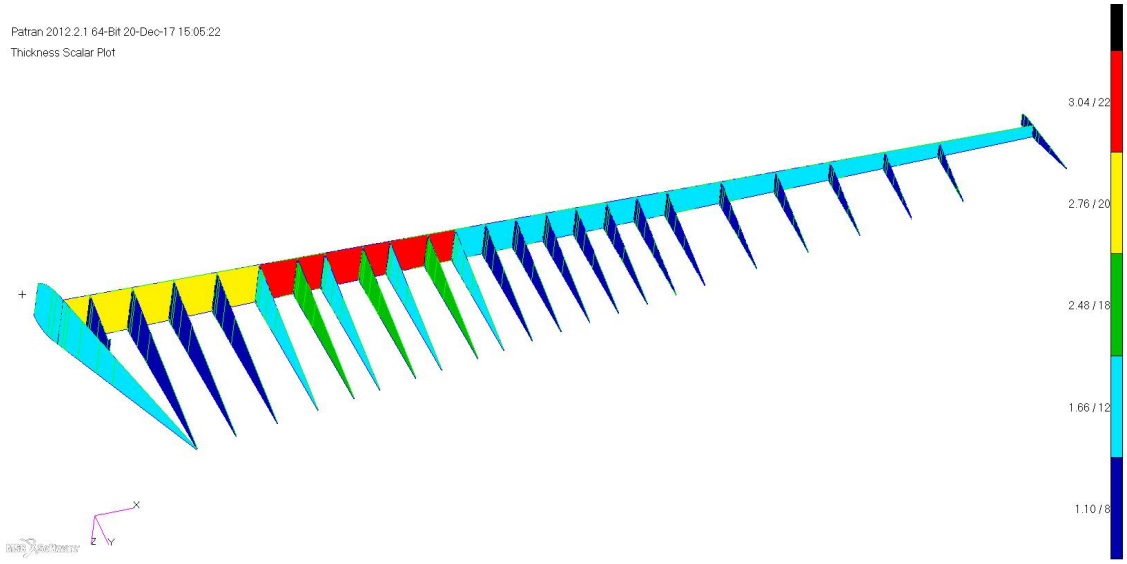


**Figure 4.9:** Substructure thickness distribution of concept MR9, in mm / number of layers.

### Static Analysis

The strains were computed using a linear static analysis in NASTRAN (SOL101). The maximum and minimum principal strains were plotted, where the maximum or minimum strain value of either the upper or lower side of an element were used. No (aerodynamic) limits on the allowed displacements or 'pillowing' are given and therefore are not considered. The pillowing effect is observed due to the aerodynamic load and is increased due compression loads induced by the enforced displacements of the rudder and can be seen in Figure 4.10 and Figure 4.11. The deformation in Figure 4.10 is for the maximum hinge moment case and shows relatively small deformations and enforced displacements. Figure 4.11) and Figure 4.12 on the other hand are deformation plots for load case 3, the most severe case, where high torsion and bending is observed.

Fringe plots of the strains for the actuator 3 jam load case are shown in Figure 4.13 and Figure 4.14 for the entire rudder and the substructure respectively. This is the load case with the highest strains, yet all strains remain well below +/- 3500 $\mu\epsilon$. The only exception is observed at the Multi-Point Constraint (MPC) used to model the load introduction at actuator 3. In this case a 7 kN actuator load is introduced into the structure through a single line of nodes which causes excessively high strains in the order of 10000 $\mu\epsilon$. This is however not realistic and is ignored as these peaks are caused by the modelling approach. The other load cases show lower strains and are thus not shown here.

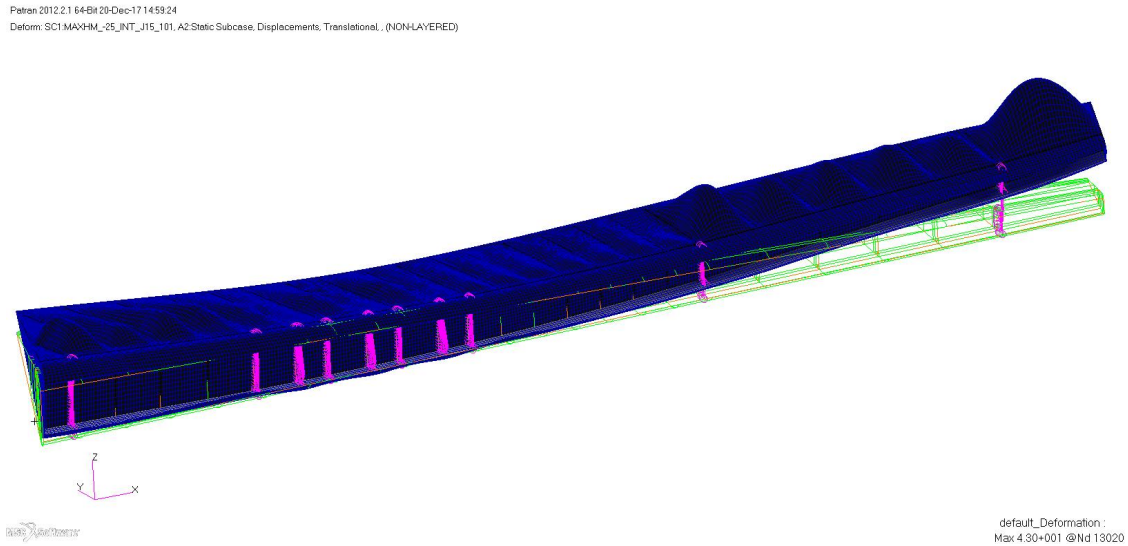


**Figure 4.10:** Deformation with enforced displacements for Maximum Hinge moment load case.

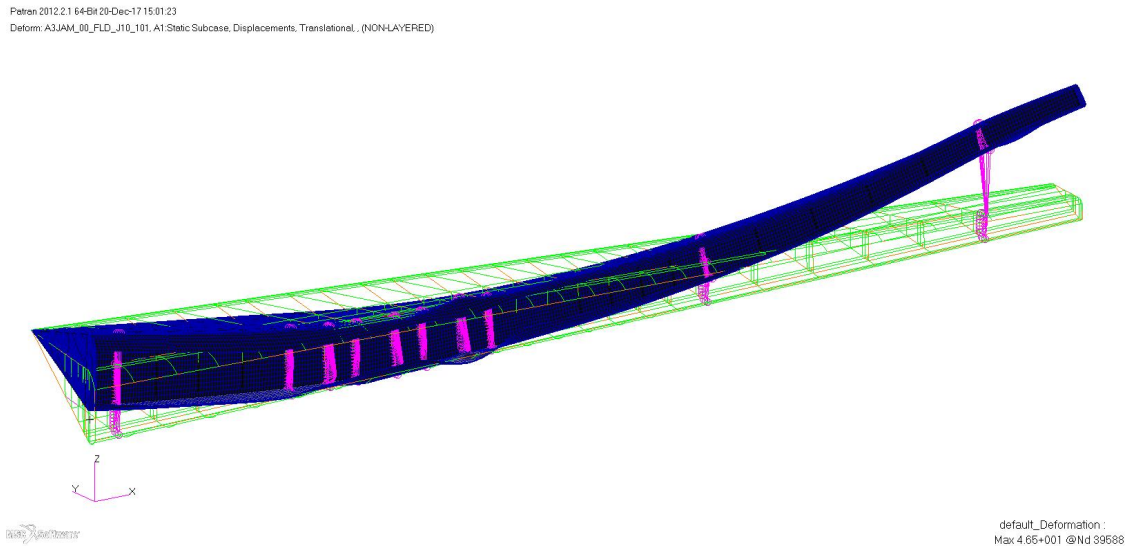


**Figure 4.11:** Deformation with enforced displacement for actuator 3 jam load case (front view).

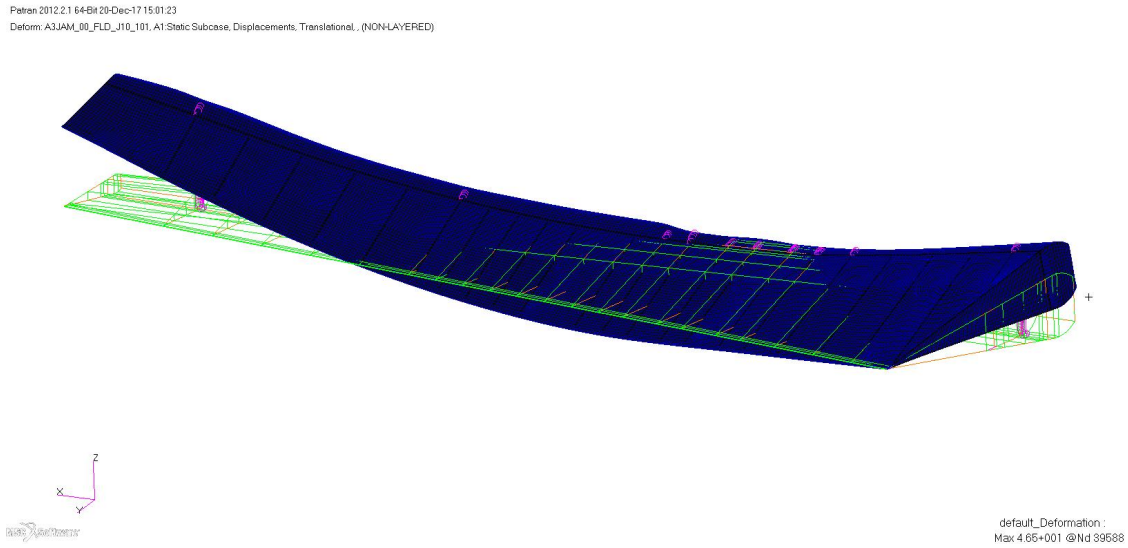


**Figure 4.12:** Deformation with enforced displacement for actuator 3 jam load case (back view).

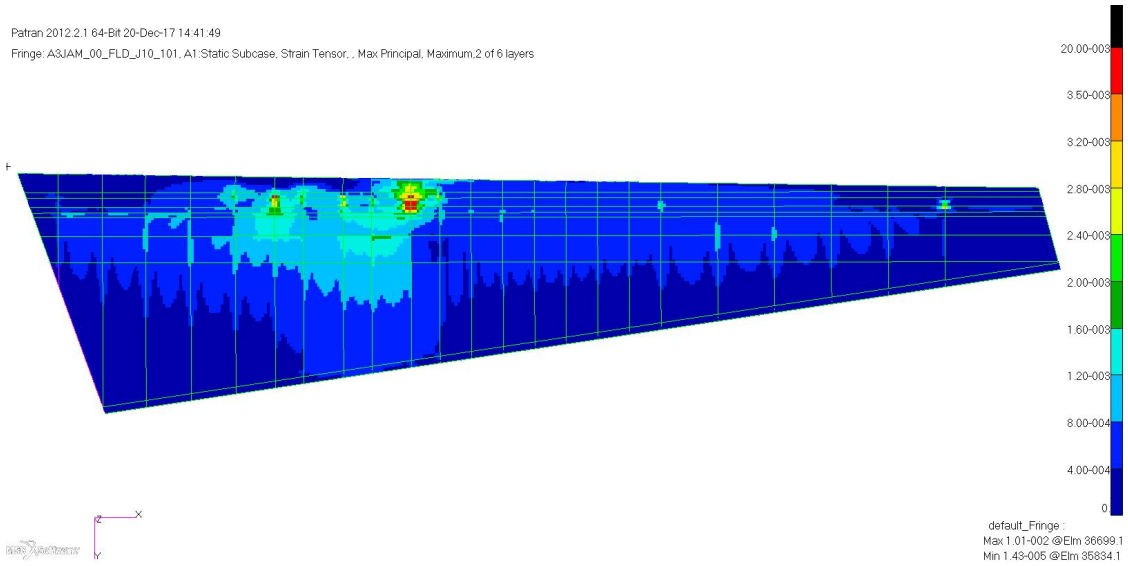


**Figure 4.13:** Maximum Principal strains for actuator 3 jam load case (Full rudder).

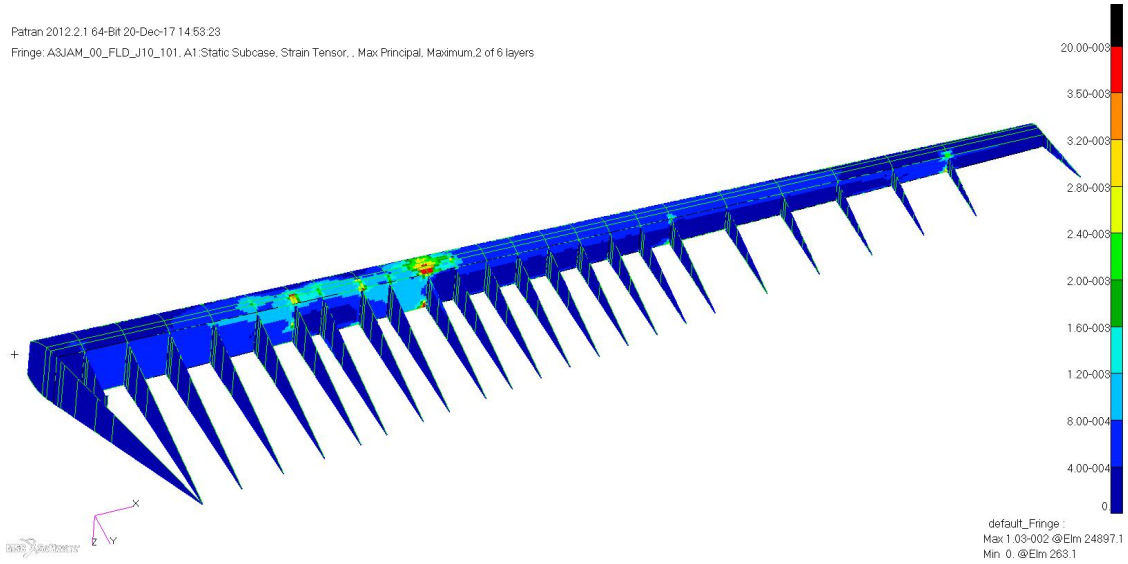


**Figure 4.14:** Maximum Principal strains for actuator 3 jam load case (substructure).

### Stability Analysis

The main driver in the sizing of the rudder is the stability of the skins and the substructure. The critical buckling point for each Eigenmode below UL for the intact cases and LL for the failure case was computed. The buckling point is expressed by a RF, the applied load divided by the buckling load and is thus a fraction.

In the final configuration buckling still occurs below the specified 0.70 LL minimum in two cases. The two lowest Eigenmodes of the reduced maximum and minimum HM load cases are shown in Figure 4.15 and Figure 4.16. It is believed that the skins in these bays can be stabilized by including the weld interface patches and re-pitching of the ribs in case of Figure 4.15 and Figure 4.16. The minimum RF in the area between hinge 6 and 7 ranges from 0.666 to 1.09 where a steady 0.70 is desired. It is believed that the 90 mm wide weld interface patches shown in Figure 4.7 are sufficient to increase the buckling load to the required 0.70 LL. Additionally a re-pitching of the ribs is also an option due to the high RF's in adjacent bays, which implies a larger rib pitch there is acceptable.

The lowest RF for the intact load cases in the substructure is 1.58 LL, including a 10% Knock-Down Factor (KDF) as explained in Section 4.2.1, is the front spar between hinge 5 and 6 due to load case 5 (in-plane bending). The lowest RF of all the non post-buckling skin sections and substructure of all failure cases is that of hinge rib 5, which is 1.05 LL, including a 10% KDF, and is due to load case 4 (ground gust case).

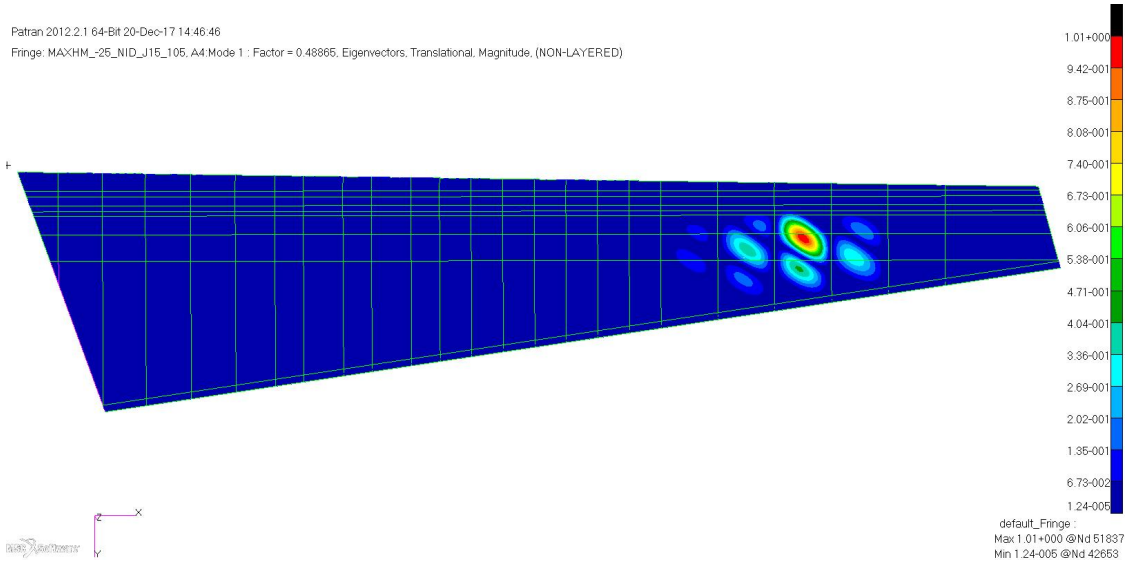


**Figure 4.15:** Fringe plot of linear buckling analysis of max. Hinge Moment load case, RF after LL & KDF = 0.666.

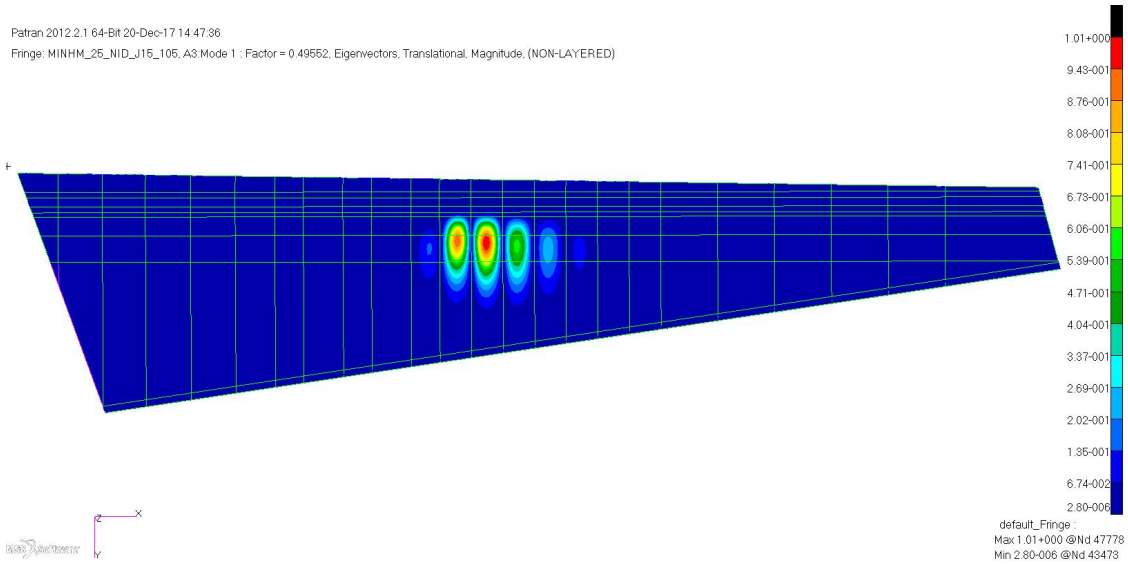


**Figure 4.16:** Fringe plot of linear buckling analysis of min. Hinge Moment load case, RF after LL & KDF = 0.675.

### 4.3.2 MR11 Analysis Results

The general discussion of the results of concept MR9 in the previous Section also applies to concept MR11. Due to the higher stiffness of the skins less thickness variation is observed in the skin compared to the 9 ply minimum concept. On the other hand the enforced displacements induce higher loads as was observed in the interface load analysis for the maximum and minimum hinge moment. This leads to local thickening of parts in the substructure compared to concept MR9.

#### Configuration overview

The skins required very little thickening from the minimum 11 ply thickness starting point. All the thicker areas behind the front spar flange (indicated by the partly red strip in Figure 4.17) is to account for the required drop-off zones. Only three skin patches behind hinge 2 required thickening. The substructure is shown in Figure 4.18, where it is noted that the spar in this model only has 2 thickness zones instead of 4 in concept MR9. All the ribs between hinge 2 and hinge 5 with the actuators in between are thicker than in concept MR9. This is due to the higher induced loads caused by increased stiffness. It is noted that the bottom closure rib is now 12 layers, where 14 layers might be more efficient from a manufacturing perspective. There are now 4 different rib laminates, while the C/PPS reference and concept MR9 only use 3 different rib laminates.

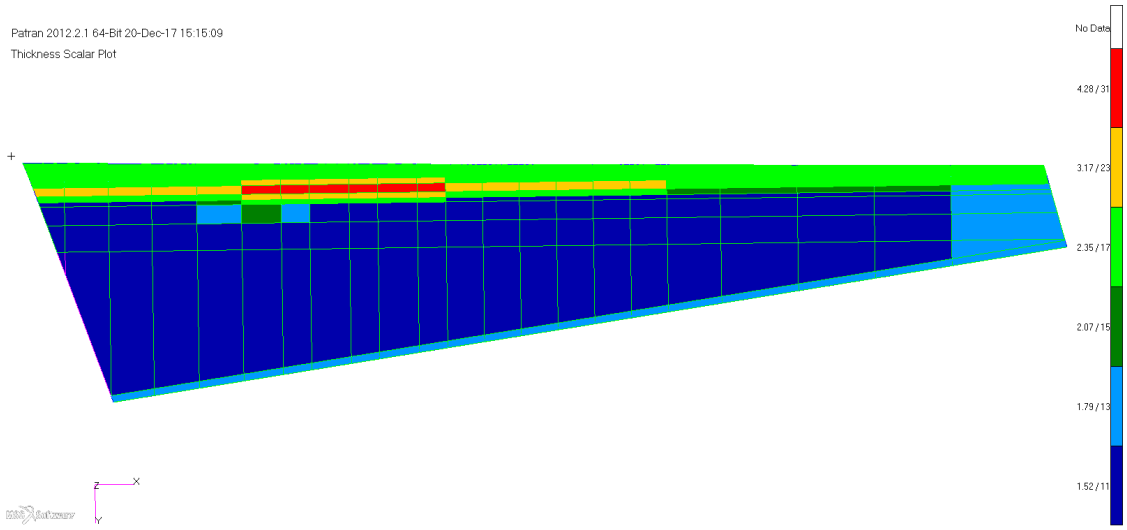


**Figure 4.17:** Skin thickness distribution of concept MR11, in mm / number of layers.

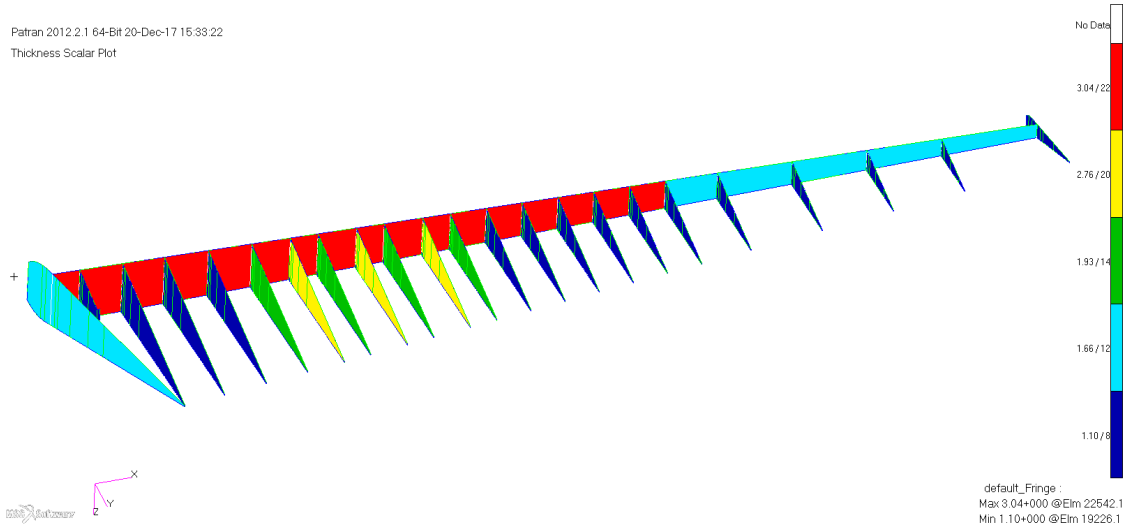


**Figure 4.18:** Substructure thickness distribution of concept MR11, in mm / number of layers.

### Static Analysis

The displacement for the maximum HM load case and actuator 3 jam load case are shown in Figure 4.19 and Figure 4.20 respectively. The total displacement of the skins due to pillowing is lower compared to concept MR9 because of the stiffer skins. The majority of the rudder deflection is however caused by the enforced displacements at the Vertical Tail Plane (VTP).

The strains are also very small in concept MR11 and reach high values at the MPC's. This is shown for the actuator 3 jam load case for the complete rudder and the substructure in Figure 4.21 and Figure 4.22 for the full rudder and the substructure respectively.

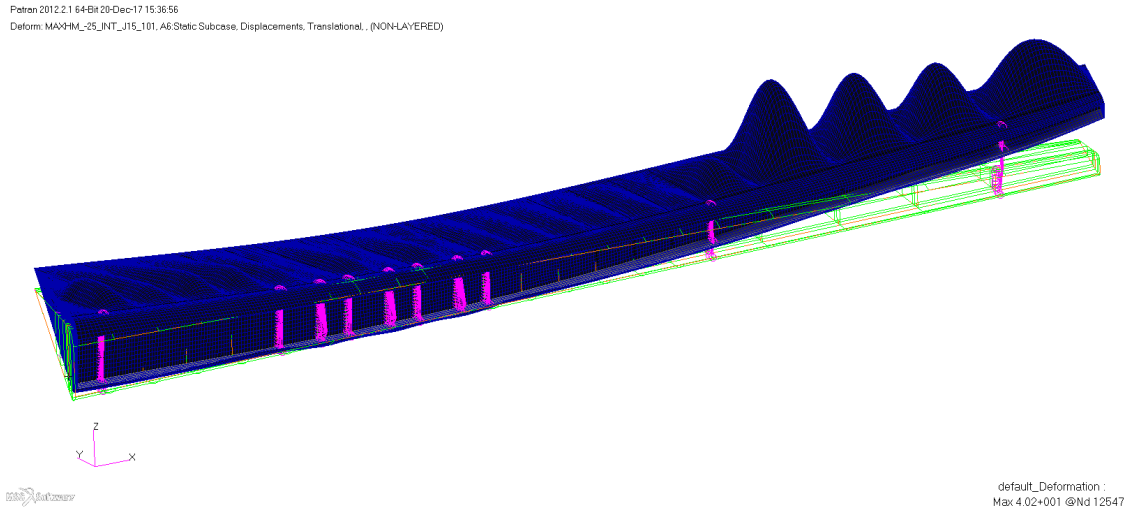


**Figure 4.19:** Deformation with enforced hinge displacements for maximum Hinge Moment load case.

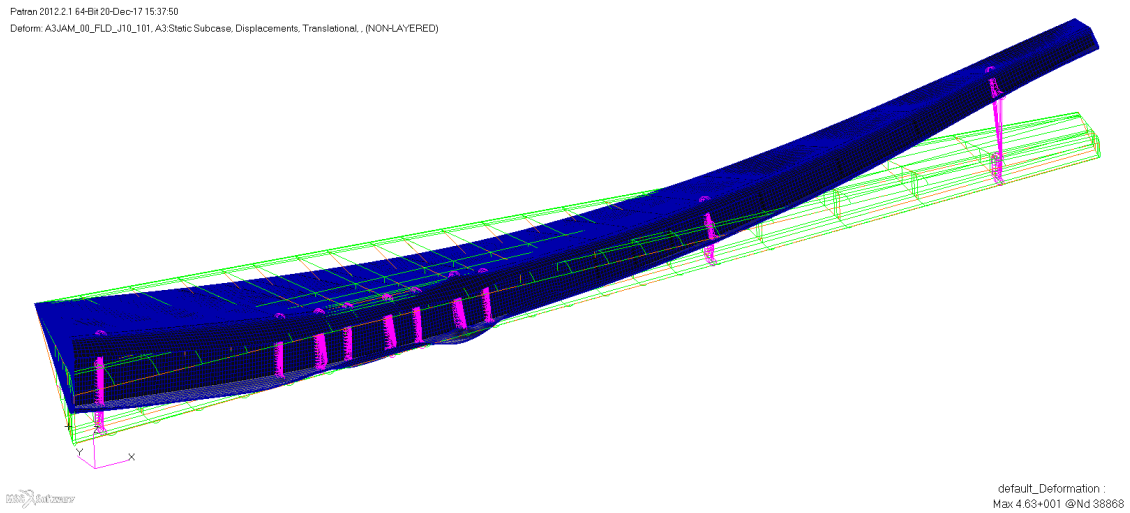


**Figure 4.20:** Deformation with enforced displacements for actuator 3 jam load case.

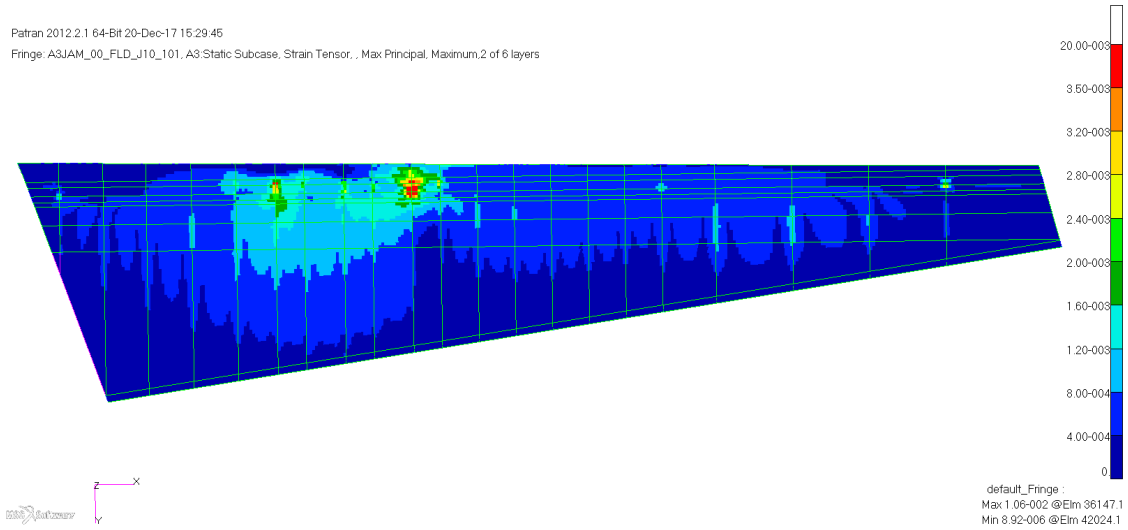


**Figure 4.21:** Maximum principal strains for actuator 3 jam load case (full rudder).

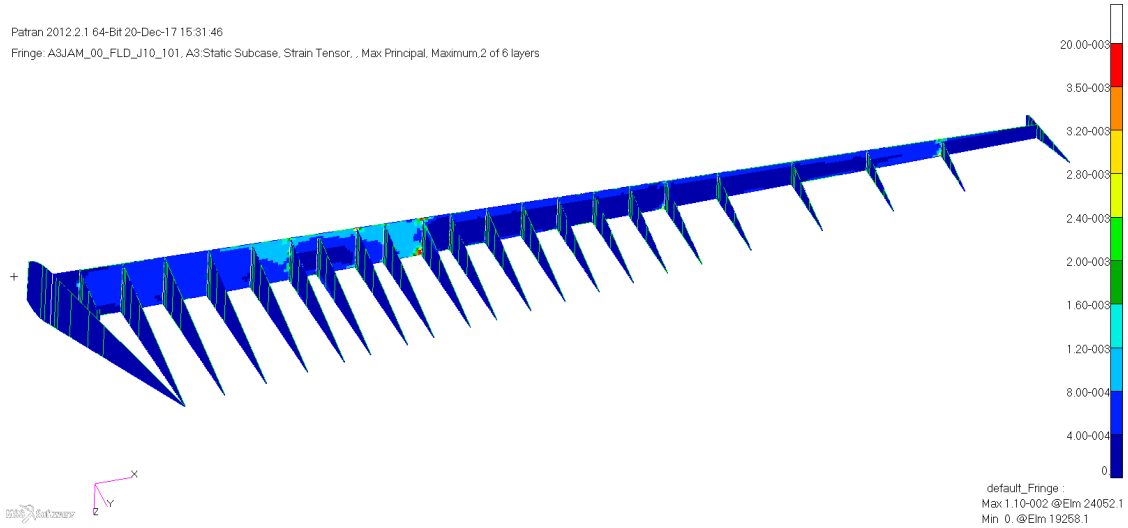


**Figure 4.22:** Maximum principal strains for actuator 3 jam load case (substructure).

### Stability Analysis

The sizing of the skins that are allowed to post-buckle, where only the maximum and minimum HM cases are applied without enforced hinge displacements result in two Eigenmodes with buckling below 0.70 LL. These are shown in Figure 4.23 and Figure 4.24. These premature buckles occur in the same load case and are mode 1 and mode 2. The RF's are 0.674 and 0.698 LL for mode 1 and 2 respectively. The bays adjacent to the prematurely bucking bays have RF's of 1.28 and 1.49 LL. In case of concept MR11 the weld interface patches are more narrow as this consist of 40 mm 90°plies and are not expected to improve the buckling load significantly. An estimate of the required change in rib pitch was made using an approximate analytical shear buckling equation from [9] given as Equation 4.1.

$$N_{xycrit} = \pm \frac{9\pi^4 b}{32a^3}\left(D_{11} + 2\left(D_{12} + 2D_{66}\right)\frac{a^2}{b^2} + D_{22}\frac{a^4}{b^4}\right) \tag{4.1}$$

In Equation 4.1 $a$ is the bay width (span direction), $b$ the bay length (chord direction) and the D terms are those of the ABD matrix of the 11 ply laminate. Equation 4.1 was applied for the bay geometry of mode 1 and the relative buckling load $N_{xycrit}$ was plotted as a function of the bay width $a$. The results were normalized with respect to the modelled width of 530.5 mm with an RF of 0.674 LL and is shown in Figure 4.25. It can be seen that a small shift of the rib position of 15 mm would be sufficient to increase the RF with a few percent. It is judged feasible considering the high RF's in adjacent bays where the buckling RF exceeds 1.0 LL.

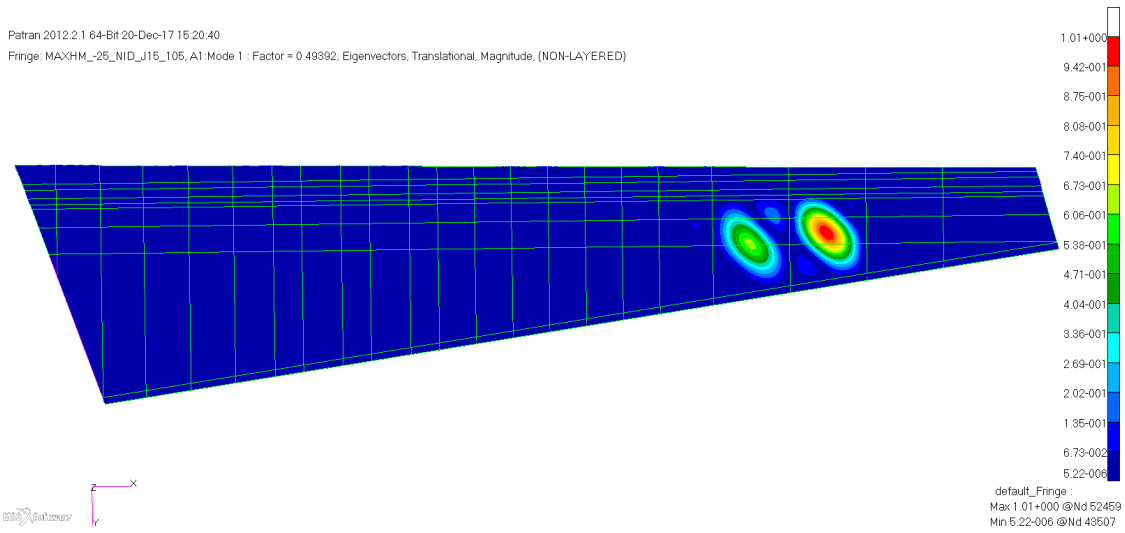


**Figure 4.23:** Fringe plot of linear buckling analysis of max. hinge moment load case, RF after LL correction and KDF = 0.674.

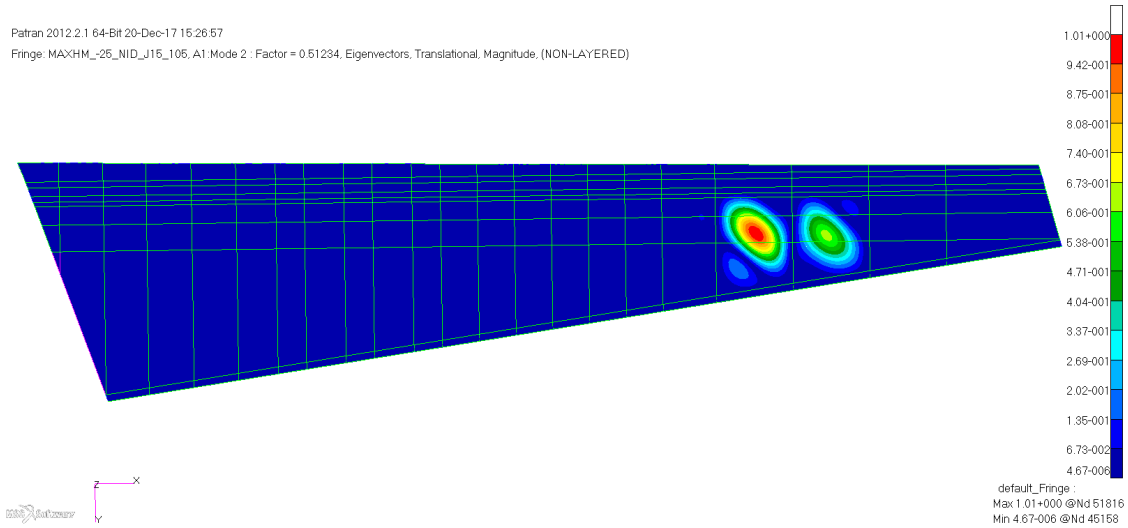


**Figure 4.24:** Fringe plot of linear buckling analysis of max. hinge moment load case, RF after LL correction and KDF = 0.668.

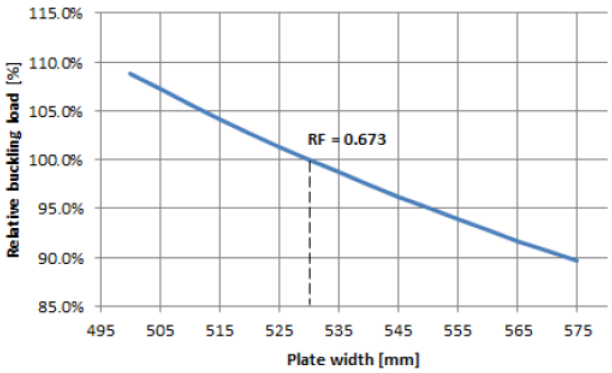


**Figure 4.25:** Normalized buckling load using approximate equation for the buckle of mode 1.

### 4.3.3 Interface Loads

For the trade-off it is assumed that the actuator and hinge brackets for MR9 and MR11 are equal to the C/PPS reference rudder. The brackets are machined aluminium parts and contribute significantly to the rudder cost. If these brackets must be modified for MR9 and MR11, then the cost of these parts shall also change. As the brackets are modelled coarsely a simple method to assess the effects on the brackets is to compare the interface loads at the MPC's. The rudder can rotate around the hinge line and is rotationally constrained by the actuators along their line of action. The rudder is constrained in span-wise direction at hinge 6 only.

The maximum resultant interface loads are shown as a fraction of the interface loads of the C/PPS reference in Table 4.2. Only the hinge interface loads of all load cases of MR9 were compared. The actuator bracket loads are driven by the hinge moment which is equal for all concepts. In Table 4.2 the hinge brackets are noted by 'H' number of the respective bracket as shown in Figure 4.1. It is noted the bracket positions are identical for all concepts in this

**Table 4.2:** Interface loads expressed as a fraction of the C/PPS reference rudder for the max. and min. HM load cases.

| Bracket | Δ MR9 |
|---|---|
| H1 | 61% |
| H2 | 11% |
| H3 | -8.0% |
| H4 | -11% |
| H5 | 36% |
| H6 | -26% |
| H7 | 25% |

study. The bracket loads show a variation that indicates a redistribution of loads compared to the original.

The most highly loaded hinge brackets are 2 - 5 where on average the loads are higher due to the 36% load increase at hinge 5. The difference in resultant at hinge brackets 6 and 7 is relatively large, but in the order of a few kN in absolute terms. A large increase is observed at hinge bracket 1 which is 10 kN and would probably require some redesign. In a detailed design phase the interface loads should be considered to optimize the bracket positions with respect to cost and weight, this is however beyond the scope of the trade-off. Using identical brackets for all multi-rib is considered a reasonable assumption as the total change in cost and weight for all brackets is expected to be limited.

## 4.4 Manufacturing and Assembly

The envisioned C/PEKK part manufacturing concepts are described in Section 2.4. This section presents a discussion of the specific manufacturing aspects and envisioned assembly method of the C/PEKK rudder. So far the discussion was limited to the Computer Aided Design (CAD) model of the multi-rib rudder where non-structural details have been neglected. Many details however are relevant cost drivers and in some cases influenced the design.

### 4.4.1 Thermoplastic Welding

Welding of the ribs, spars and skins is done by dedicated tooling at Fokker Aerostructures as shown in Figure 4.26. Induction welding is currently utilized for joining the C/PPS movables such as rudders and elevators. The welding process is highly automated as the induction coil is mounted on the a robotic arm and moves along the weld lines. The ribs and spar are fixed in the jig and the tools exert a pressure against the flanges and skins to improve the weld quality and eliminate small gaps between the flanges and skins. Grooves are made in the jig to provide access for the induction coil and the welded joints of the multi-rib rudder are indicated in Figure 3.3. The rib to spar-web joint is not welded because it is not possible to apply pressure to the flange from inside the torsion box, thus blind fasteners are used.

The induction process for welding C/PPS fabric is well understood and industrialized. Currently it is unknown if welding of C/PEKK Uni-Directional (UD) tape is feasible and conduction welding is under development as an alternative welding method of UD tape. The

Technology Readiness Level (TRL) of conduction welding is currently 2 or 3 and no cost data or detailed process parameters are known. Thermoplastic (TP) Welding is considered an enabler for the current post-buckling multi-rib concept and development of conduction welding is ongoing. For the trade-off it is assumed that either conduction- or induction -welding suitable for C/PEKK UD tape shall be developed with similar tooling and cost. In the current study the cost of C/PPS induction welding is assumed for the C/PEKK rudder.


**Figure 4.26:** TP welding station for a movable at Fokker Aerostructures. (Courtesy of Kranendonk b.v.)

### 4.4.2 Accessories and Bracket Installation

The non-structural accessories and bracket installation are discussed in this section. The hinge and actuator brackets of the NSA rudder have not been modelled accurately, but will be comparable to those of the Airbus A320 which is similar in size and requirements. A picture of the brackets, front spar and leading edge of the A320 rudder is shown in Figure 4.27. The hinge line is indicated by the orange line and the three actuator brackets are marked. The A320 rudder is a monocoque construction with sandwich skins and differs in some aspects to the multi-rib.

Unlike the A320 rudder the bracket shall be directly fastened to the skin and cut-outs in the spar flanges shall be made to enable this. This will allow the front spar to be welded to the skin without interference due to the brackets. Liquid shim is used to fill any gaps between the brackets and wing box. It is noted that no shim is used between welded parts as is done in fastened joints as shown in Figure 4.27. It is also noted that the joint connecting the brackets to the skin as indicated by the white arrows in Figure 4.27 are not sized and the bearing area of the skin is chosen to be equal to the C/PPS reference rudder.

The most significant accessories are shown in Figure 4.28. These are the tip cap, static dischargers, bonding jumpers and hoisting nuts (not shown in Figure). Copper wire mesh, sealant and primer are included in the cost and weight estimation. The boding jumpers, tip cap, static dischargers and copper wire mesh are part of the lightening strike protection

provisions of the aircraft. The bonding jumpers create and conductive path from the rudder to the vertical tail plane and are connected to the metallic brackets shown in Figure 4.28.

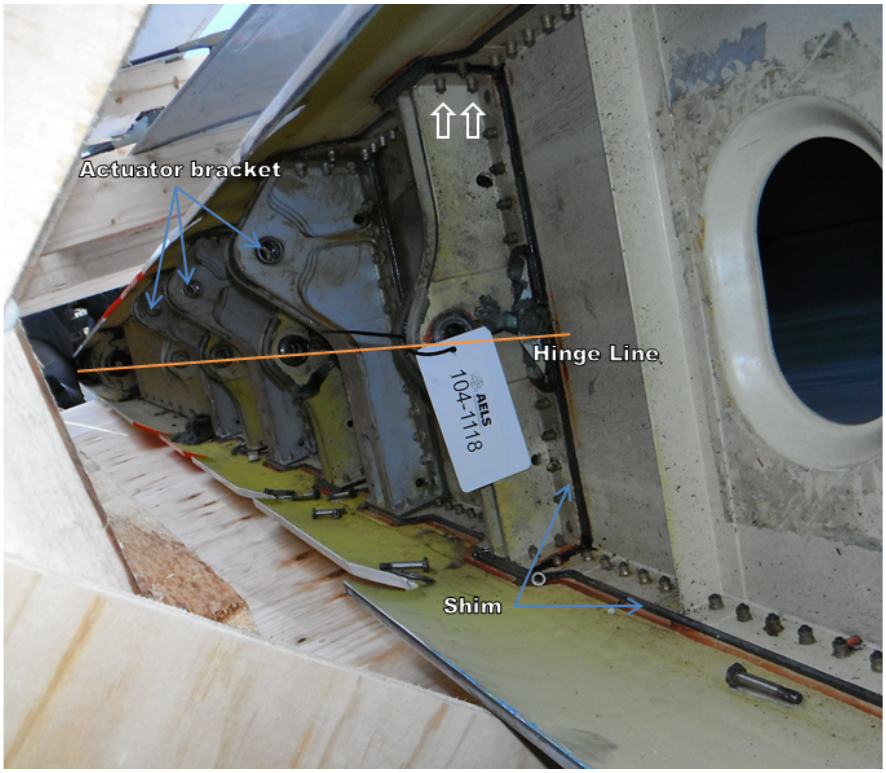


**Figure 4.27:** Hinge line and bracket layout of the Airbus A320 rudder.

### 4.4.3 Fasteners

The number of fasteners is minimized by welding most joints and fasteners for damage tolerance are placed at weld ends as shown in Figure 3.3. The fastener type and locations have been chosen to be equal to the C/PPS reference, but the joints in the FEM were inspected to ensure the load did not exceed the allowable stress. The joints are not modelled explicitly in the FEM and the parts are connected by tying the mesh. The free body forces were plotted for the parts such as shown for actuator 3 rib of MR11 in Figure 4.29. The allowable nodal force is estimated by estimating the element length and flange width. The shear loads were found to be well below the allowable and only the peel forces in some ribs were found to be too high.

The ribs near the actuators showed excessive high peel loads in the area behind the spar. In most cases the fasteners are sufficient to carry the loads but in some ribs such as actuator rib 3 shown in Figure 4.29 nodal forces in the order of 6 kN were observed. This is almost 1.5 times the pull-through strength of the countersunk fasteners used in that area. The high nodal loads are attributed to the course modelling of the brackets and are expected to be much lower when the full brackets are modelled. To remain conservative 3 fasteners with a 6.66 mm diameter are used at the rib-skin weld ends near the front spar. This is only done for the ribs between hinges 2 and 5 where the actuators are located.

**Figure 4.28:** Non-structural detail of the A320 rudder.

The total number of fasteners were calculated in an Excel sheet and included in the Product Breakdown Structure (PBS) for reference. To improve the weight estimation the required grip length of every fastener was determined based on the part thickness in that area. The rib-spar connection cannot be welded and must be fastened. In this joint the loads also appeared to be low and thus a fastener pitch of 8D (8 times the fastener diameter) was selected, which is the largest pitch for which no inter-rivet buckling analysis must be performed according to Fokker handbooks and is considered to be conservative [10].

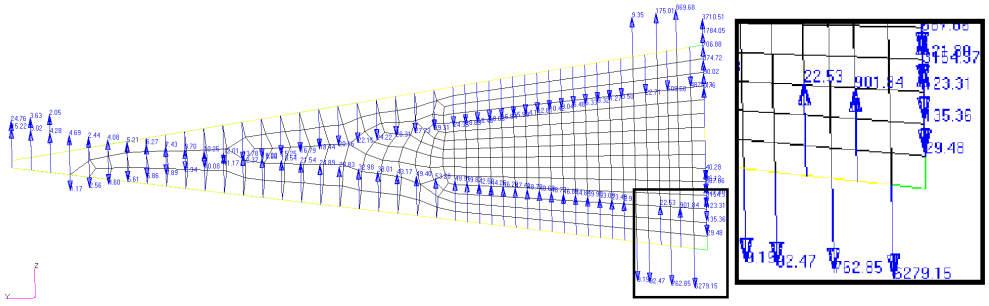


**Figure 4.29:** free body forces of MR11 actuator 3 rib.

## 4.5 Concept Discussion

The C/PEKK multi-rib concepts were found to have similar weight despite the 20% difference in skin thickness. The total weight difference is approximately 200 g as shall be shown in

Chapter 6. The additional weight of the weld patches is 2 kg for MR9 while this is just 0.4 kg for MR11. Combined with the simpler skin definition and lower number of ribs MR11 is taken as a baseline for the C/PEKK multi-rib rudder. The redesign is judged to have been done with sufficient level of detail to allow a trade-off with the C/PPS reference, yet some items remain open for further studies and are discussed in this section.

The course modelling of the actuator brackets results in high local stresses. A more detailed modelling is required to better analyse the stresses and strains at the load introduction points. This will also allow a proper sizing of the brackets, fasteners and skin connecting the brackets. A realistic load introduction shall also improve the accuracy of the observed peel stresses at the ribs. If the peel stresses remain high, radius blocks might be required to improve the load path adding to the cost of the rudder.

A non-linear analysis is needed to compute the strains in the post-buckled state of the rudder to verify that these remain below the allowables. A full non-linear analysis shall also allow any premature buckling of the substructure to be detected. The latter can be caused be a redistribution of the internal loads in the rudder due to buckling of the skin. Modelling of the weld patch for both concepts, especially for MR9, is advised to better understand the effect of these patches on the behaviour and the possibility to reduce the number of ribs should be investigated.

# Chapter 5

# The Grid-stiffened Rudder

## 5.1 Grid-stiffened Skin Parametrization

The selection of Concept 3b in Chapter 3 led to a search for a suitable stiffening method as this was not yet clearly defined in the concept. The sketch of concept 3b on the right side of Figure 3.6 shows three different stiffening methods. Using Short Fibre (SF) reinforced Carbon fibre PolyEtherKetoneKetone (C/PEKK) conventional stiffeners, a gird or an optimized shape could be used to stiffen the skin. In the master thesis study of de Gelder performed at Fokker Aerostructures a cost and weight estimate was made for a stiffener stiffened skin and showed that both cost and weight would increase significantly [11]. As no topology optimization software was available at Fokker Aerostructures, the use of non-structured geometries was also not feasible. Thus the use of grid stiffening was selected as a baseline for this concept. In this Section the theory of Grid-Stiffened (GS) panels is reviewed and the selected modelling approach is discussed.

### 5.1.1 Introduction to Grid-Stiffened Panels

The application, manufacturing and modelling of grid-stiffened panels are discussed in the Literature Study and a brief introduction shall be given in this Section [5]. An interesting overview of the application of grid-stiffening, mainly by the Russian industry, is also given by Vasiliev et al. [1]. GS shells have mainly been applied to launchers due to their high specific buckling load and cylindrical shape allowing manufacturing by filament winding as shown in Figure 5.1. GS shells have been used since the 1950's for machined aluminium structures and then in the 1980's using composite material in combination with hand layup. With the advent of automated manufacturing Automated Fiber Placement (AFP) and filament winding have been applied to manufacture GS skins cost effectively.

Grid stiffening offers much more design freedom than conventional stiffening, but also shows different failure modes and design requirements. Optimization and structural analysis cannot be done with classical methods and suitable alternatives must be used. Two general

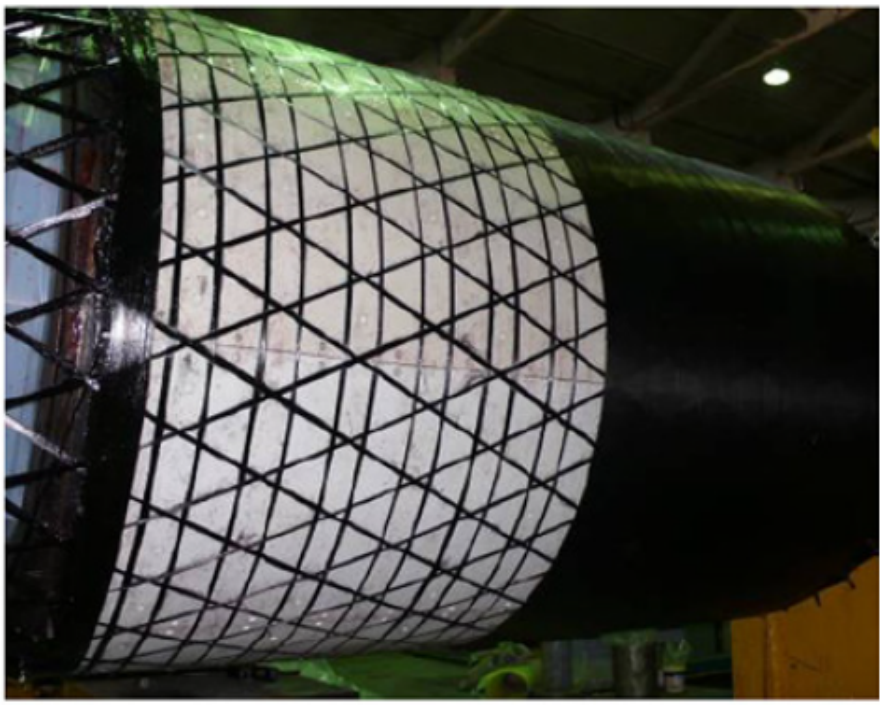

**Figure 5.1:** An example of a launcher section designed and build at the CRISM with fully wound stiffeners and partially wound skin. [1].

methods exist to analyse GS shells as explained by Shroff]; The discrete method and the smeared-stiffness method [12]. The discrete method practically means the creation of Finte Element Model (FEM) of the full grid to accurately capture the stress and strain distribution throughout the structure. While the generation of such a FEM has been automated, optimization requires an update of the model and is computationally expensive. The smeared-stiffness method is simple and (mostly) analytic, but is only suitable for modelling the global behaviour of the panel.

In this study the analysis was limited to the smeared-stiffness model due to time constraints. For a trade-off on conceptual level an initial weight and cost estimate is sufficient. Local failure modes were not considered with the exception of an estimate of the strains in the outer fibre of the stiffeners as discussed in Section 5.4. The grid configurations were chosen conservatively based on engineering judgement to reduce the risk of local failure modes to occur in the design. This judgement however must be checked by the creation of a discrete FEM of the rudder.

### 5.1.2 Smeared-stiffness Modelling Approach

The smeared-stiffness approach used in this study was formulated by Xu et al. and appears to correlate well with Finite Element (FE) results [2]. The method of Xu was implemented in Python and the basic principles are explained in this section. The biggest challenge in the analysis of GS shell is the shift in the neutral plane of the shell-grid combination. When this 'skin-stiffener' interaction analysed using conventional smeared-stiffness methods the stiffness of the structure is usually overestimated.

### Xu's smeared-stiffness theory

The method of Xu can be broken down into 3 steps to reduce a grid-stiffened shell to an equivalent stiffness orthotropic plate and are sketched in Figure 5.2. Starting from a single skin-stiffener combination the moment of inertia of the stiffener is computed by shifting the neutral plane of the stiffener with the skin contiguous to it, this is done to account for the skin-stiffener interaction. It is noted that the stiffener is assumed to be effective only in its axis. The second step is to smear the stiffeners over the unit cell to obtain an orthotropic plate that models the stiffeners and to compute the equivalent neutral plane of the skin and smeared stiffeners. The neutral planes of the skin and smeared stiffeners are indicated by the dashed lines in Figure 5.2 while the neutral plane of the combination is indicated by the solid line.

The properties of the equivalent shell are provided in an ABD matrix which is the sum of the ABD matrix of the smeared stiffener and that of the skin. The latter however is defined about its own neutral plane and must be corrected for the shift in neutral plane position of the skin-shell combination. This is not required for the stiffener because a correction is applied in step 2. The smeared stiffener and skin can be considered to be sub-laminates and the ABD matrix of the skin is corrected for the shift in neutral plane according to equation 5.1 from Mallick [13]. The system of Equations 5.1 transform the entries of the ABD matrix in the laminate axis in terms of a parallel axis, denoted by an apostrophe ('), shifted by a distance $d$.

$$\begin{aligned} A'_{ij} &= A_{ij} \\ B'_{ij} &= B_{ij} + dA_{ij} \\ D'_{ij} &= D_{ij} + 2dB_{ij} + d^2 A_{ij} \end{aligned} \tag{5.1}$$

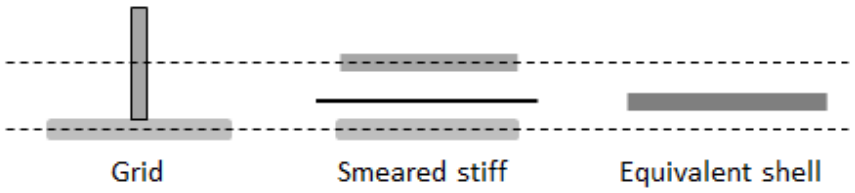


**Figure 5.2:** Main steps in the smeared-stiffness modelling approach of Xu.

Xu's method is based on a parametric definition of a unit cell shown in Figure 5.3 where all the stiffeners have the same height but varying thickness. Xu defines 6 different stiffeners out of which a unit cell may consist. The unit cell is rectangular with stiffeners along the border, orthogonally centred along the sides or angled. The stiffener angle is a function of the unit cell length (x-direction) and width (y-direction) denoted by $a_0$ and $b_0$ in Figure 5.3 respectively. The thickness of the stiffeners is expressed in a vector $\mathbf{s} = [s_1, s_2, s_3, s_4, s_5, s_6]$ where $s_i$ is a fraction of the selected stiffener reference thickness $t_{st}$. In this study the thickness of stiffeners 1 and 2 is taken equal to prevent any shear-extension coupling behaviour and thus the vector $\mathbf{s}$ was modified to only have 5 elements.

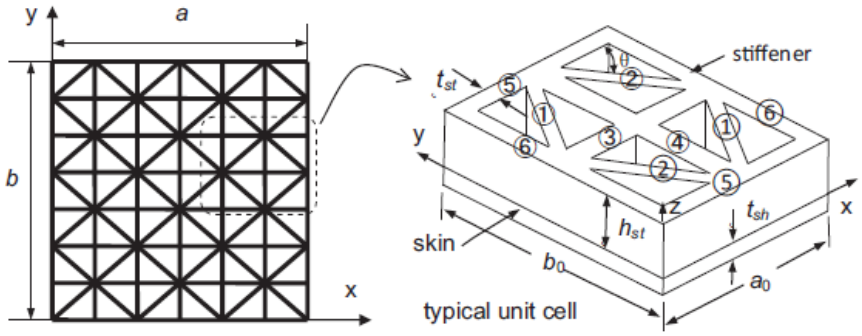


**Figure 5.3:** Parametric unit cell definition of Xu [2].

### Smeared-Stiffness theory implementation

The implementation of Xu's method was done in a single Python script broken down in 8 steps shown in the block diagram in Figure 5.4. The nomenclature of the input variables is given in Table 5.1 where the notation of Xu's paper has been adapted. First the unit cell geometry is defined where the stiffener angle is computed using the outer dimensions (step 1). The skin properties are computed using classical laminate theory, where the skin thickness and equivalent membrane modulus are also computed (step 2). In step 3 the stiffener volumes are computed using the vector **s**, stiffener height and computed stiffener lengths. The skin stiffener interaction (with the skin contiguous to the stiffener) is captured by computing the neutral plane position of the combination $h_0$ and corresponding inertia terms $A_1 - A_3$. Step 5 is the smearing of the stiffener properties over the unit cell area by computing the ABD matrix of the smeared stiffeners $ABD_{st}$ and a weighed equivalent membrane stiffness $A11_{st}$ and $A22_{st}$.

Step 7 is a key step where all inputs from the previous steps, indicated by the dashed lines, are merged to calculate the neutral plane of the skin-stiffener combination $h_{z0av}$ (shown by black line in Figure 5.2). The accuracy of Xu's method is attributed to the proper definition and calculation of the inputs for this step. Step 8 is the application of the correction for the neutral plane shift of the skin laminate using Equation 5.1. Step 6 contains calculations not directly related to Xu's method but additional operations to compute the smeared weight of the unit cell used for the weight estimation of the GS skin. Only the volume of the skin $V_{sh}$ is required for Xu's method.

The implemented code was verified and then validated. First a unit check of the code was done and intermediate results manually checked. Second an example panel from the paper of Xu was in-putted into the code and the results were compared. For the uni-axially loaded panels the buckling load was computed with simplified buckling equations from Kassapoglou [9]. These obtained Eigenvalues were within 9% difference from those presented in the paper of Xu. The difference is attributed to the method used to compute the critical buckling Eigenvalue. As not stiffness values were given, a direct comparison of the smeared-stiffness approach was not possible.

**Table 5.1:** List of input variables for the smeared-stiffness code.

| *Symbol* | *Unit* | *Definition* | *Description* |
|---|---|---|---|
| | | **Unit Cell Geometry** | |
| **s** | [-] | Stiff. Thickness ratios | Thickness of each rib w.r.t. reference |
| $t_{st}$ | [mm] | Stiff. ref. thickness | |
| $t_{sh}$ | [mm] | Skin thickness | Governed by the layup |
| $h_{st}$ | [mm] | Stiffener height | |
| $a_0/b_0$ | [mm] | Unit cell length / width | |
| | | **Material Properties** | |
| $E_{11}$ | [MPa] | Longitudinal modulus | For the skin |
| $E_{22}$ | [MPa] | Transverse modulus | For the skin |
| $G$ | [MPa] | Shear modulus | For the skin |
| $\nu$ | [-] | Poisson's ratio | For the skin |
| $E_{st}$ | [MPa] | Stiff. axial modulus | Membrane modulus of stiffener |
| $LU_{sh}$ | [-] | Skin layup | |
| $\rho_{st}$ | $[g/cm^3]$ | density | Stiffener material |
| $\rho_{sh}$ | $[kg/m^3]$ | density | Skin material |

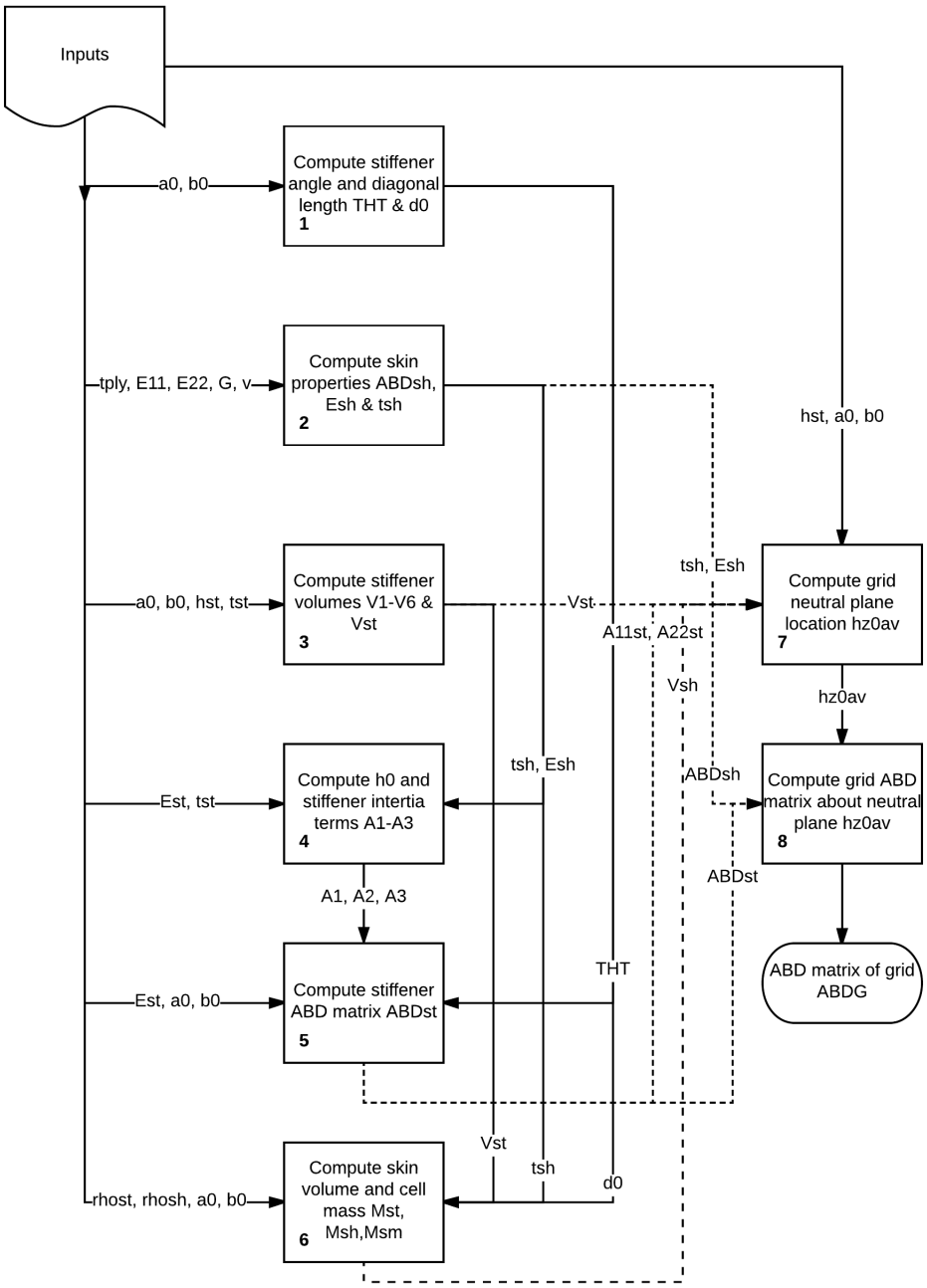


**Figure 5.4:** Block diagram of Python implementation of Xu's method.

## 5.2 Grid Configuration Selection

Using the developed smeared-stiffness model of Xu as explained in the previous Section a parametric study was performed to understand the effects of certain design parameters on the smeared weight and stiffness of the unit cell. A selection for the parameters was made to limit the amount of work, this was possible using knowledge of the behaviour and requirements of the multi-rib rudder. In the parametric study the use of continuous fibre C/PEKK for the stiffeners was investigated to provide an alternative in case the weight of the SF stiffener grids would be too high. The SF stiffeners however proved to be suitable for the application and the modulus of the stiffeners did not affect the behaviour of investigated parameters but only the total values for stiffness and smeared weight. Thus the results of the parametric study for continuous fibre stiffeners shall not be presented in this document. Following the parametric study a set of unit cell configurations were sized using representative loads.

### 5.2.1 Parametric Study of Unit-cell Characteristics

Three different grid configurations, shown in Figure 5.5, were studied where unit cell size, stiffener height and thickness were varied. The chosen configurations are representative for the spectrum of configurations that can be made using Xu's method. An important limitation in the parametric study is that all the stiffeners were chosen to have an equal thickness. The stiffeners inside the unit cell (1,2,3,4 as indicated in Figure 5.3) have the reference thickness $t_{st}$ while the stiffeners at the border have half the reference thickness. When the unit cells are assembled, the stiffeners at the border are merged and the full thickness is retrieved. The effect of varying the skin layup was also investigated by comparing two examples.

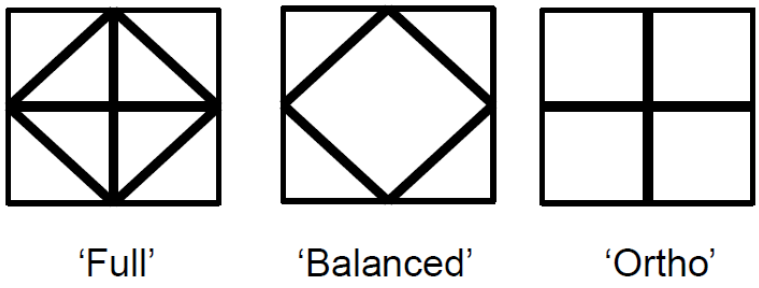


**Figure 5.5:** Sketch of the three studied grid configurations.

The smeared weight $[kg/m^2]$ of a unit cell is computed by the code and given as an output, the stiffness however is outputted as an ABD matrix and must be conditioned so that the stiffness can be assessed using a single numeric value rather than a matrix. Using the knowledge that the rudder is a lightly loaded structure and stability driven the required skin stiffness is estimated by comparing it to existing monocoque construction rudders of which data was available at Fokker Aerostructures. It was judged that a GS skin rudder would not be commercially attractive if the weight would be more than 15% greater than the multi-rib rudder. Based on the cost and weight results the allowable smeared weight of a GS skin was estimated so that a certain cost or weight of the complete rudder would be achieved. For this the cost of a 'stripped' rudder where the skin thickness was reduced the minimum requirements of Section 2.1 and to 1 mm elsewhere. All the ribs except for those between

hinge 2 and 5 as shown in Figure 4.2 were also removed. Three smeared weight benchmarks were then defined; one for which the total cost would be 15% less than the multi-rib based on an assumed price per kg for the skin, one for which the weight would be equal to the multi-rib rudder and the last for a smeared-weight resulting in a 15% weight increase w.r.t. the multi-rib.

The stiffness benchmarks are based on a weighed summation of the D terms of the ABD matrix, called the equivalent stiffness, which is derived from analytical buckling equations and shown in Equation 5.2 [9]. The factors multiplying the D terms are exact for square panels and apply for a large class of load cases including compression and shear. For this reason the unit cells were always made square in the parametric study, while it is noted that general rectangular unit cells should be considered to enable an optimized GS skin design. Three stiffness benchmarks are defined using the available information at Fokker Aerostructures on sandwich construction skin panels. These benchmarks are only used as an order of magnitude reference as the requirements for design of sandwich panels vary significantly from those for a GS skin.

$$D_e = D_{11} + 2D_{12} + 4D_{66} + D_{22} \tag{5.2}$$

One design cure generated in the parametric study is shown in Figure 5.6 where three sub plots can be seen. The header of the plots explains the configuration; 'Grid B' stands for the 'Balanced' stiffener configuration shown in the middle of Figure 5.5, The skin thickness is indicated by $t_{sh}$ in number of plies, 'ab' refers to the unit cell length and width (always taken to be square) and 'mat' is a code for the used material which is SF compound in this example. The stiffener height was varied from 10 mm to 50 mm which were judged to be suitable ranges from both manufacturing and local stability considerations. The stiffener thickness were taken to be 2, 3, 5 and 8 mm which was also based on manufacturing considerations and is discussed in more detail in Section 5.5. In the upper plot the smeared weight is plotted v.s. the stiffener height for the four selected stiffener thickness. The middle plot shows the equivalent stiffness $D_e$ v.s. the stiffener height and the bottom plot shows the equivalent stiffness v.s. smeared weight. The dashed lines are the smeared weight and equivalent stiffness benchmarks, while it is noted that the equivalent stiffness benchmarks shown in the figures in this document are those derived in Section 5.2.2 for improved clarity as the initial benchmarks were one order of magnitude off by the actual required stiffens.

Th plot in Figure 5.6 is the basis for the selected configuration used and is thus shown here, but more plots are shown in Appendix A to support the conclusions presented here. An ideal configuration should have a low smeared weight and high stiffness which in Figure 5.6 would be to the left of the vertical dashed lines in terms of smeared weight and up to the upper most horizontal dashed line in terms of equivalent stiffness.

- The smeared weight was found to increase linearly as a function of stiffener height as the stiffener volume increases linearly.
- For the selected stiffener pitch, which is implicitly controlled by the unit cell size, the smeared weight quickly exceeds the benchmarks when the stiffener thickness exceeds 5 mm.
- The stiffener height can stay below 35 mm to meet the largest equivalent stiffness benchmark for almost all unit cell geometries.

- The most weight efficient configurations have thin and high (slender) stiffeners.
- The benchmarks can be met for the selected configurations and SF material.
- Increasing the skin thickness from 7 (0.996 mm) to 9 (1.24 mm) increases the weight significantly without a significant change in equivalent stiffness for the same stiffener height.

A final note is made with respect to the equivalent stiffens benchmark given in Equation 5.2. It is specific to buckling problems where a high torsional stiffness, expressed in the $D_{66}$ term, is desired for a high buckling resistance. This term is increased most by the diagonal stiffeners and due to (the lack of) this the orthogonal stiffeners (Ortho in Figure 5.5) perform poorly for this application. For the same reason the efficiency of the 'Full' configuration is lower compared to the 'Balanced' configuration. The performance however is limited by local failure modes of the stiffeners and the skin between stiffeners which were not considered in this study. Varying the stiffener thickness is also an option that could be used improve the efficiency of the configuration but this too was not investigated.

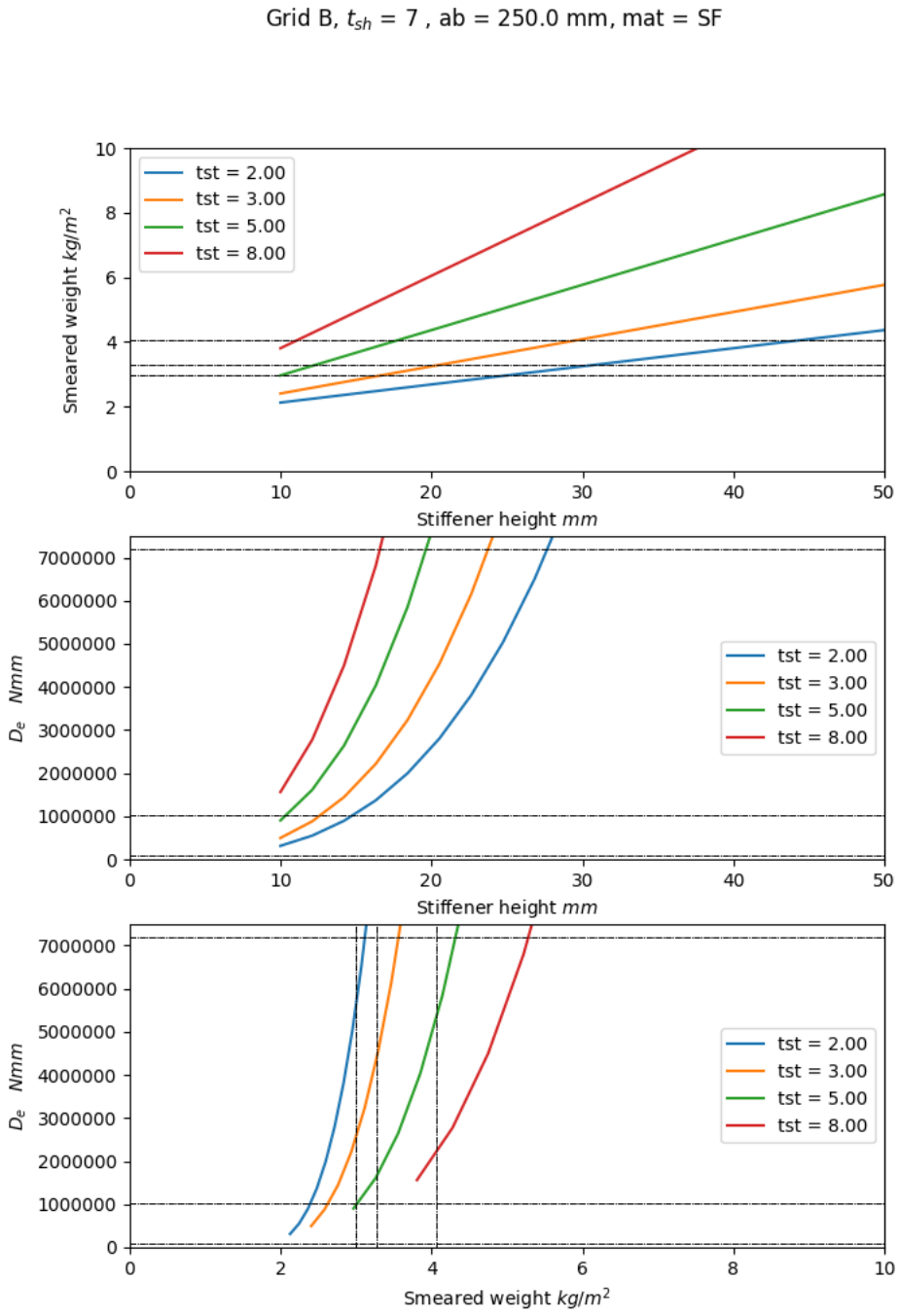


**Figure 5.6:** Design curve from the parametric study for one configuration.

### 5.2.2 Representative Panel Sizing

While the parametric study was performed with stiffness based benchmark data and provided an insightful characterisation of the configuration parameters of a unit cell, no load based assessment was available on the actual required stiffness for the Next Signle Aisle aircraft (NSA) rudder. Using the available data at Fokker Aerostructures a representative panel shown in Figure 5.7 was created along with a set of realistic load cases for the NSA rudder. This panel was used to create the equivalent stiffness benchmark values used in Figure 5.6 and the figures in Appendix A. The representative panel was simplified to a rectangle with constant running loads so that analytical equations could be used to assess the load cases. As the panel was rectangular Equation 5.2 was modified so that the equivalent stiffness would be computed correctly.

Running loads representative for the maximum and minimum Hinge Moment (HM), both averaged and maxima, for the left and right skin were used. The boundary conditions of the panel were assumed to be simply supported to remain conservative and for the same reason tensile loads were neglected so that only shear and compression-shear would be considered. The load cases are shown in Table 5.2 where the loads are shown for the left hand- and right hand -skin, denoted by LHS and RHS respectively and for each load case. The upper rows give the average running loads while the lower rows the worst-case value. Combined compression and shear loads were only observed in the right hand side in the maximum HM load case, where this would also be expected in the minimum HM case. This discrepancy is attributed to the hinge displacements caused by the deformation of the Vertical Tail Plane (VTP) but was not investigated.

In a similar manner 'cut-outs' were made in the large representative panel and the running loads were estimated using the raw data from which the representative panel was derived. The approximate positions of the cut-outs are shown by the orange dashed lines in Figure 5.7. While the panels were smaller, the loads in certain areas such as the lower left cut-out in Figure 5.7 which is located near the front spar (FS), was highly loaded. The middle cut-out was loaded primarily in shear and the upper right cut-out was lightly loaded to provide a lower limit for the benchmark.

The load based equivalent stiffness benchmarks used in Figure 5.6 show that a stiffener thickness between 2 and 5 mm would fall within the smeared weight benchmarks while covering a large range of the required equivalent stiffness. The maximum stiffener height would be

**Table 5.2:** Load cases for the representative panel of Figure 5.7 with constant running loads.

| | LHS | | RHS | |
|---|---|---|---|---|
| Load [N/mm] | min. HM | max. HM | min. HM | max. HM |
| **Average** | | | | |
| $N_x$ | 5.421 | 9.384 | 9.500 | -2.817 |
| $N_{xy}$ | 5.233 | 3.239 | 3.585 | 3.430 |
| | | | | |
| **Worst-case** | | | | |
| $N_x$ | 9.862 | 11.50 | 11.61 | -5.373 |
| $N_{xy}$ | 8.322 | 6.460 | 7.917 | 6.017 |

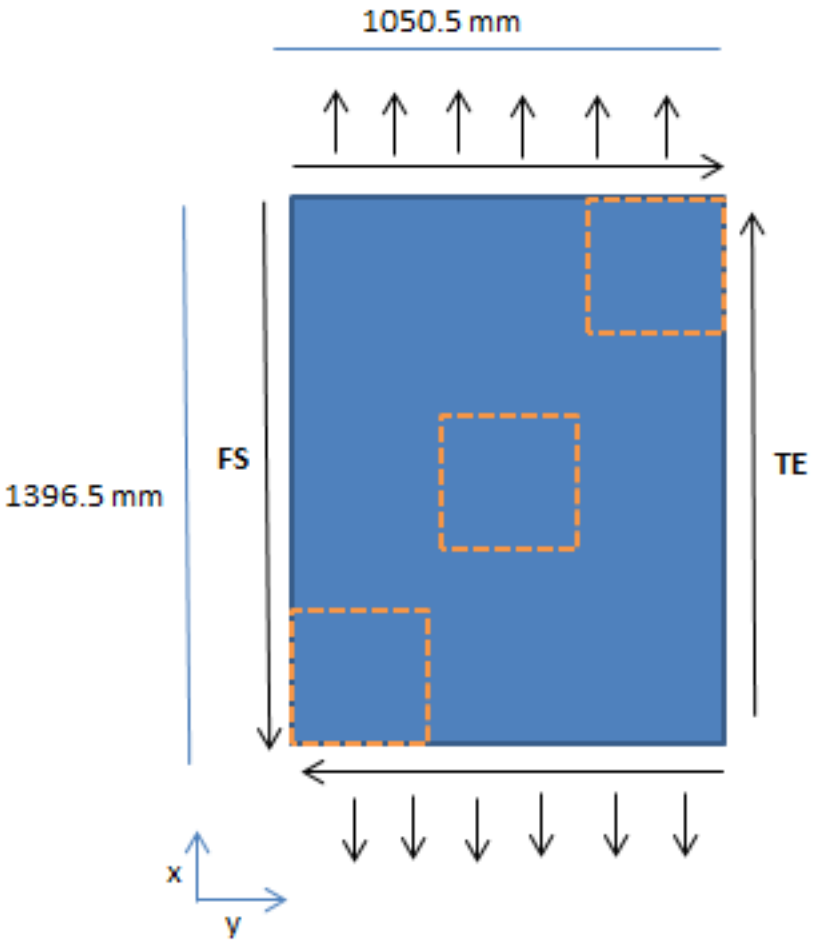


**Figure 5.7:** Dimensions and loads (direction drawn arbitrarily) of the representative panel and sketch of sub cut-outs (dashed orange squares.)

below 25 mm for most thickness and for the lowest benchmark an un-stiffened laminate would be sufficient. As no time was left to perform analysis of local failure modes the decision was made to select a conservative unit cell configuration using engineering judgement to minimize the risk of local failure modes. The unit cell dimension was taken to be 250 mm and the stiffener thickness and maximum height where taken to be 4 mm and 25 mm respectively. The maximum height/thickness ratio of the stiffener would be 5 and was judged to be sufficiently low so that stiffener crippling (local buckling) would not be likely to occur. A 4 mm thickness is also reasonable from a manufacturing perspective as shall be explained in Section 5.5.

When the 'Balanced' grid configuration is taken as a baseline the grid configuration can be modified easily from a manufacturing point of view to create a grid family that covers a larger range of the smeared weight - equivalent stiffness space. The selected grid family is shown in Figure 5.8 where the 'Balanced' configuration can be strengthened by adding the inner stiffeners to create a 'Full' configuration for use in highly loaded areas. In lightly loaded areas the cord-wise stiffeners can be stopped to create the 'Tria' configuration and when only the angled stiffeners are retained the 'Angle' configuration is obtained. As the axial loads are induced by the hinge displacements and a low bending stiffness is beneficial to reduce

the induced loads it would also be interesting to investigate the use of dropping the spanwise stiffener first in the 'Tria' configuration, but there was no time to investigate this. The equivalent stiffness v.s. smeared weight plot for the four configurations are shown in Figure 5.9. It is noted that the layup of the skin is shown in Figure 4.6 as Skin_7.

In Figure 5.9 the benchmarks are indicated for clarity. The smeared weight benchmarks are labelled with 'MR-15%$' the limit to reduce cost with 15% w.r.t. the multi-rib rudder, 'MR' to obtain the same weight as the multi-rib rudder and 'MR + 15%' the limit point where the GS rudder would weigh 15% more than the multi-rib rudder. In a similar fashion for the equivalent stiffness 'min' is the benchmark for the lowest required stiffness, 'H5-6' the maximum required stiffness from the representative panel and 'GV' is the equivalent stiffness of a sandwich skin rudder. A quick FE analysis showed that the properties of the 'GV' sandwich were sufficient to assure stability for the NSA rudder and was thus considered a limit point. The 15 mm and 20 mm high stiffeners cover the required stiffness range while also remaining within the smeared weight limits. The 25 mm high stiffeners are shown for completeness but are, with the exception of the 'Angle' configuration, too stiff for the applied loads.

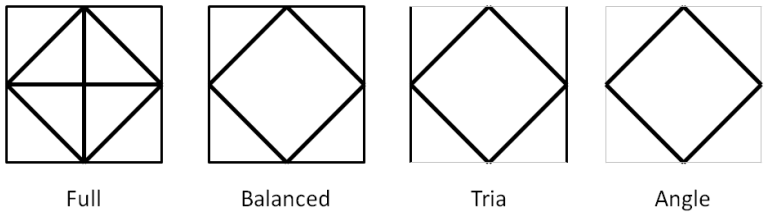


**Figure 5.8:** Selected grid family to be used for the sizing of the GS rudder.

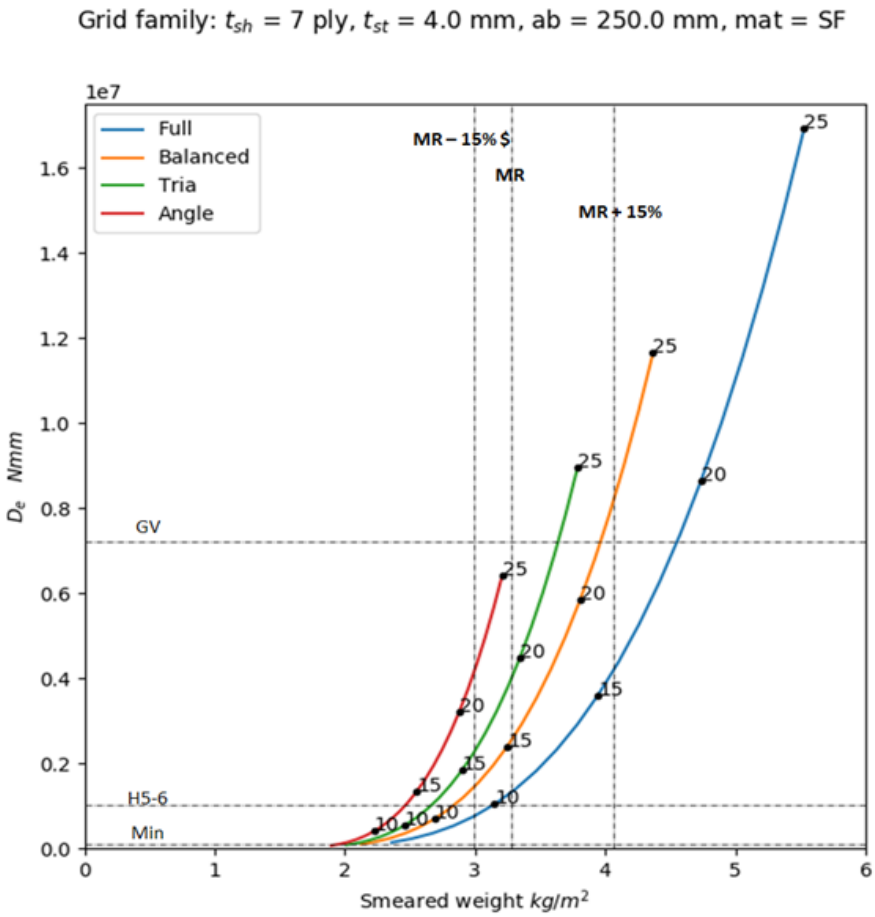


**Figure 5.9:** plot of the equivalent stiffness v.s. smeared weight for the four grid configurations with selected stiffener heights indicated in [mm].

## 5.3 Sizing Methods

With the selected grid family shown in 5.9 the NSA rudder is sized using a modified FEM of concept MR11 from 4. The bottom rib, ribs between hinges 2 and 5 and top rib that models the tip cap are retained while all other ribs are removed. The layup of the spar and remaining ribs are unchanged compared to the layup of MR11. The skin sections from the spar to the Leading Edge (LE) and skin section above hinge 7 are also unchanged due to minimum thickness requirements as specified in Section 2.1. In this Section the method used to size the GS rudder are explained. Unlike the multi-rib concept the GS skin is not to buckle within the load envelope because it is unlikely that the strains in the GS will remain below the allowables.

### 5.3.1 Finite Element Modelling of GS Skin

Modelling the of the smeared stiffness properties of the grids required re-working of the FEM generated in CAD2FEM because it was not designed for composite and isotropic materials. For the FE analysis of the GS skin the ABD matrix computed with Xu's method must

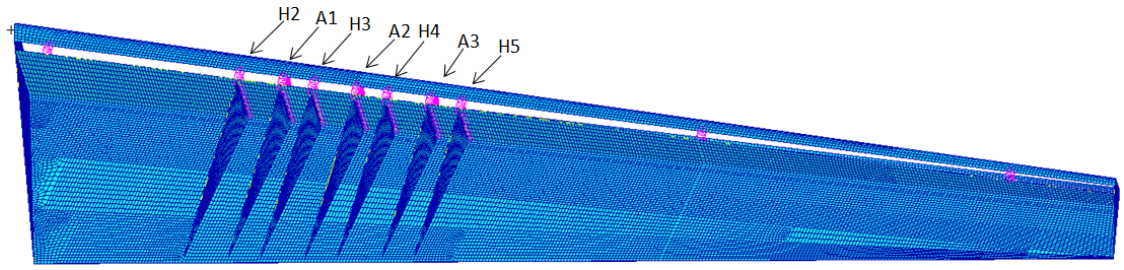


**Figure 5.10:** FEM of the GS skin rudder with labelled brackets between hinges 2 and 5.

be assigned directly to the elements of the model. For this PSHELL elements, which are quadrilateral shell elements, were used in NASTRAN to which anisotropic material properties were assigned using the MAT2 property cards. For each grid configuration two property cards were defined; one for the A matrix (membrane) and one for the D matrix (bending). The B matrix (coupling) was not included because this is neglected in the SOL 105 linear buckling analysis.

The thickness of the PSHELL elements was arbitrarily set to 1 mm, as no equivalent thickness is defined in Xu's method. The shell element is treated as a single ply laminate and from classical lamination theory the stiffness of the laminate is defined by its thickness. Thus a correction factor must be specified in the MAT2 property card that is dependant on the chosen thickness. For a PSHELL thickenss of 1 mm the correction factor is 12, which is a familiar number in the second moment of inertia of a rectangle.

The element type was changed manually for the GS skin regions and the material cards were changed in the NASTRAN bulk data file. Thus the work load to change the grid configuration per region was reduced, but modifications to the boundary region definitions required much work. A total of 30 MAT2 cards were defined for 15 grid configurations, all those indicated by dots in Figure 5.9 with the exception of 'Full' configuration with 20 mm high stiffeners. The sizing was done by selecting one of these configurations for every GS skin property regions.

### 5.3.2 Running Load Analysis

The running loads in the rudder with an un-stiffened 7 layer skin configuration were analysed to divide the skin in regions and to select a starting configuration for the rudder sizing. The loads were relatively constant over large areas and changing the element type in the skin was labour intensive, so the skin was divided into 7 property regions. A linear static analysis, using SOL 101, for the 6 load cases was done for the un-stiffened skin model to analyse the running loads $N_x$, $N_y$ and $N_{xy}$. Simultaneously Equation 4.1 was used to determine the critical running load for every grid configuration. The sides of the panel $a$ and $b$ in Equation 4.1 were taken be the local chord length. By estimating the critical shear load for each grid configuration a selection could be made based on the observed running loads in the un-stiffened 7 layer skin model.

While the span-wise and chord-wise loads were also assessed the initial grid configuration was not based on them. The chord-wise loads were low and not driving, while the span-wise loads are induced by the enforced hinge displacements and thus the stiffness. The actuator 3 jam load case showed the highest loads and fringe plots for $N_x, N_y$ and $N_{xy}$ are shown in Figures

5.11 to 5.13 respectively. The loads are highest near the actuators and near the spar in case of $N_x$ as would be expected. The shear load tends to fan out from the actuator area which is also expected as the air load acts on the entire skin surface.

Based on the shear load distribution of the 6 load cases the region definition for the GS skin was made in Figure 5.14 where the area between hinges 2 and 5 is coloured in red.

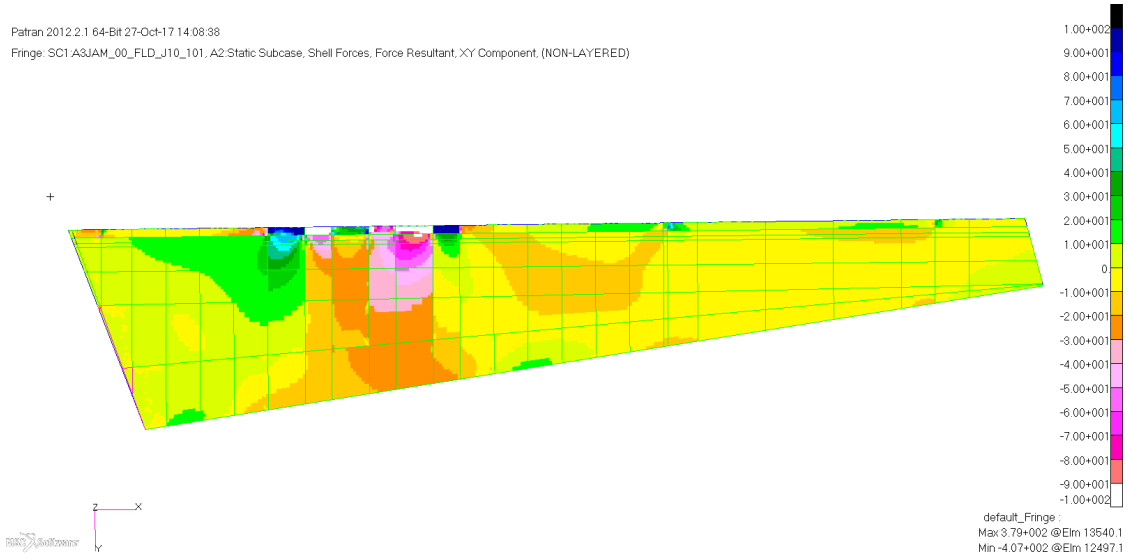


**Figure 5.11:** Running shear load $N_{xy}$ in an un-stiffened skin for load case 3 in [N/mm].

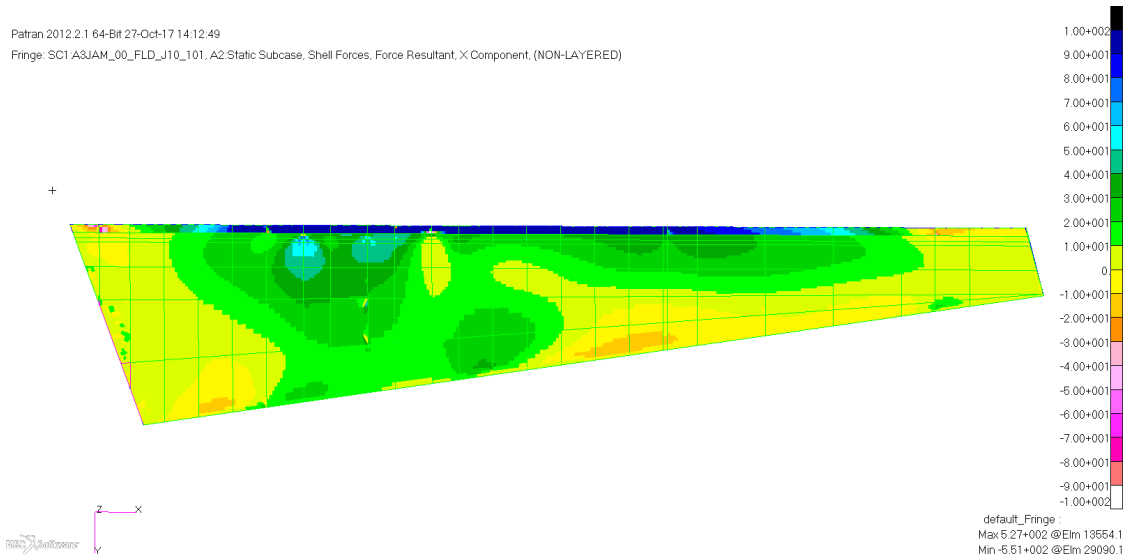


**Figure 5.12:** Running load $N_x$ in an un-stiffened skin for load case 3 in [N/mm].

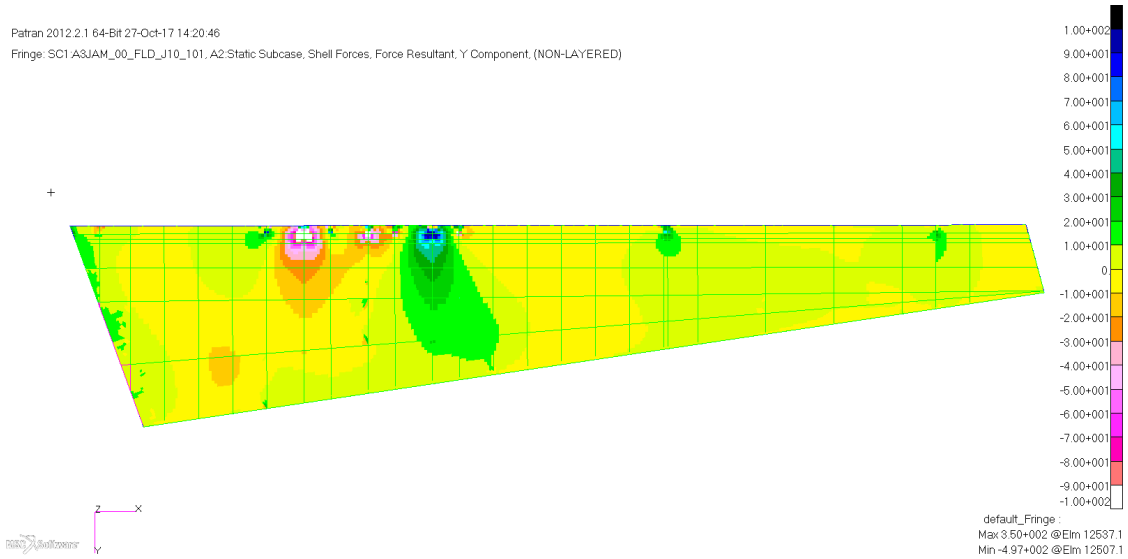


**Figure 5.13:** Running shear load $N_y$ in an un-stiffened skin for load case 3 in [N/mm].

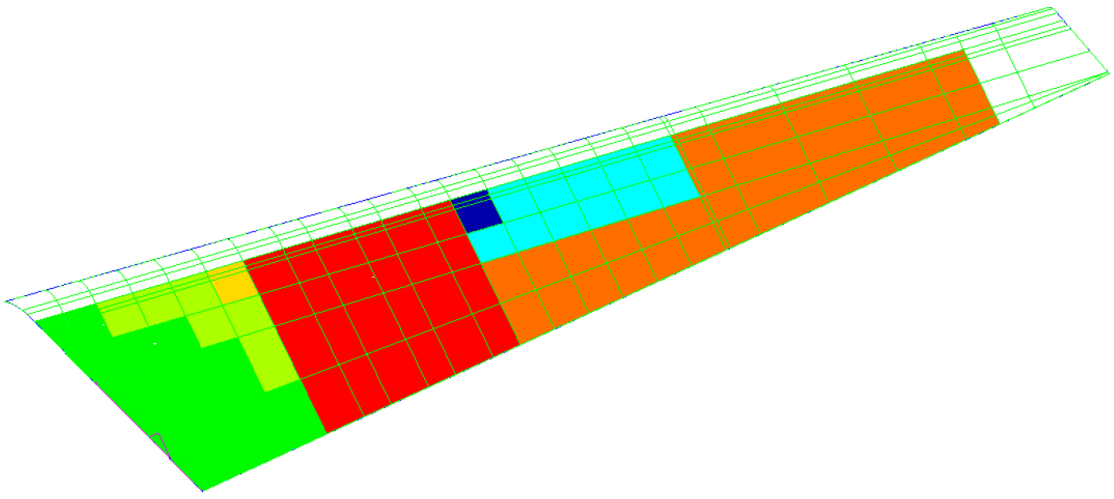

**Figure 5.14:** Property regions for the GS skin, with monolithic laminate sections shown in white.

## 5.4 Sizing Results

### 5.4.1 Final Configuration

The final configuration of the GS skin rudder was obtained after several iterations. Changes were made to the grid configuration but also to the substructure which needed to be thickened. The full set load cases, static and linear buckling, were run for configuration shown in Figures 5.15 to 5.17 which is dubbed 'GS_FEM'. The skin laminates for the monolithic regions are from library 4.6. It is noted that ramp-down regions behind the spar shown in 4.2 are not modelled because these are GS skin areas. In Figure 5.15 the grid configurations, sketched in Figure 5.8, are indicated followed by a number which is the stiffener height.

The skin deformation in the area below section hinge 2 was found to be very large and thus a skin configuration where the entire lower section consisted of 'Tria 20' grids was investigated. A linear and linear buckling analysis was performed for only the actuator 3 jam load case. This showed that the running load increase was limited and stability was maintained. With these considerations this configuration was chosen as the baseline and is called concept 'GS_Baseline'.

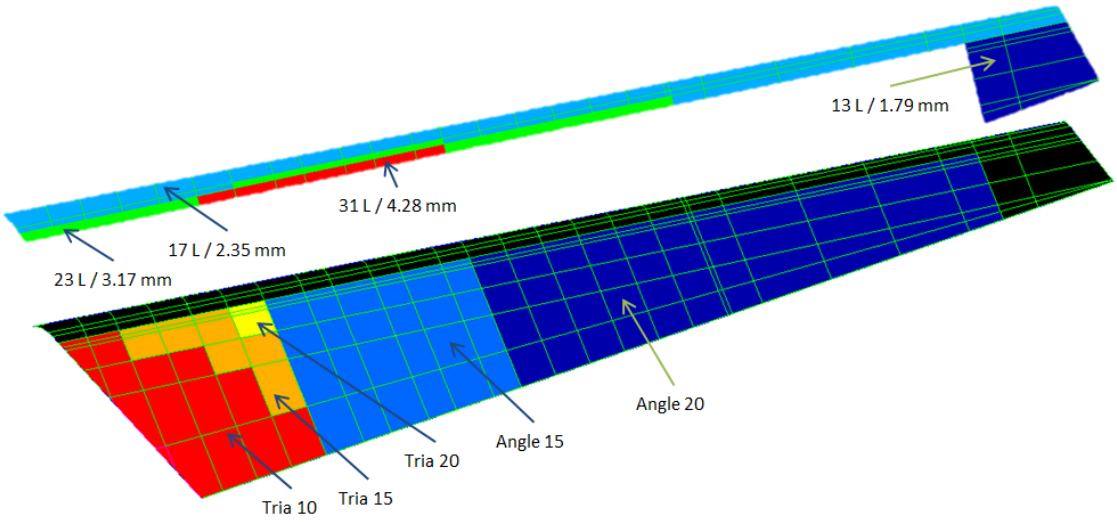


**Figure 5.15:** Layup and grid configuration for GS_FEM, colours of monolithic and grid regions are unrelated.

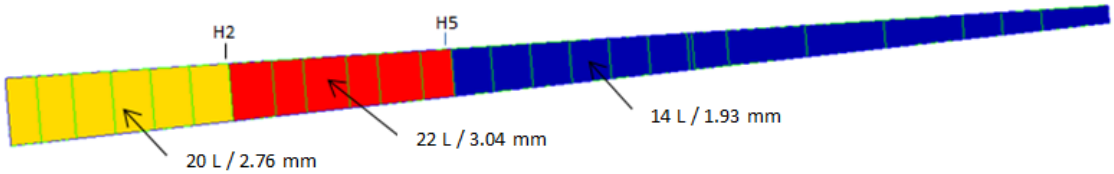


**Figure 5.16:** GS_FEM spar layup using laminates from Table 4.1.

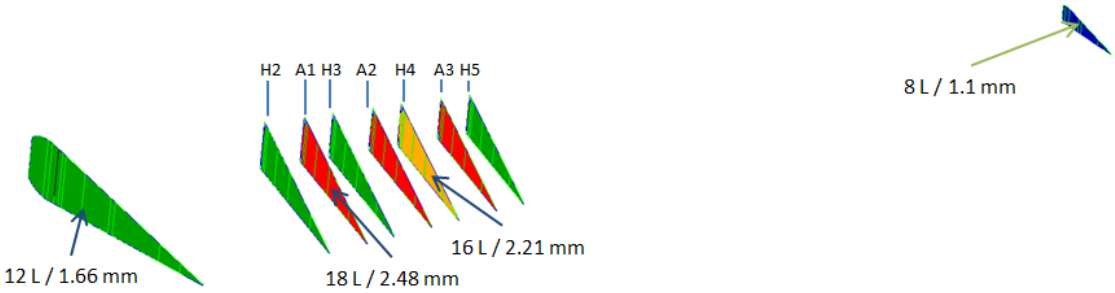


**Figure 5.17:** GS_FEM rib layup using laminates from Table 4.1.

### 5.4.2 Stability Analysis

Similar to the multi-rib rudder concepts

In the linear buckling analysis the first 60 Eigenmodes of each load case were extracted and none showed buckling of the skins. The two Eigen modes with the lowest Reserve Factor (RF) were in the substructure and are shown in Figure 5.18 for the actuator jam load case and Figure 5.19 for the ground gust load case where a 10% knockdown has been applied on the RF's from NASTRAN. The skins did not show any buckling while the highest RF's observed in the analysis were higher than 2. This indicated that the GS skin may be over designed and this is attributed to the large steps in stiffness between the grid configurations shown in Figure 5.9. In a detailed design smaller steps in the stiffener height must be used to reduce the buckling margins and weight.

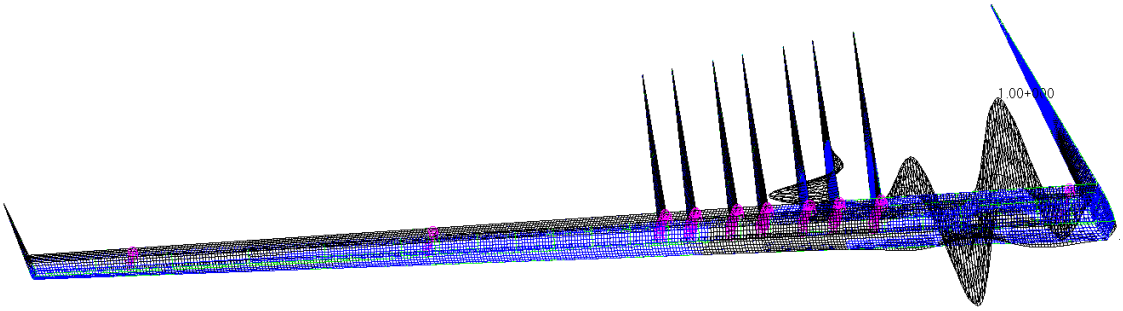

**Figure 5.18:** Shape of the first Eigenmode of actuator 3 load case (damaged), RF = 1.019.

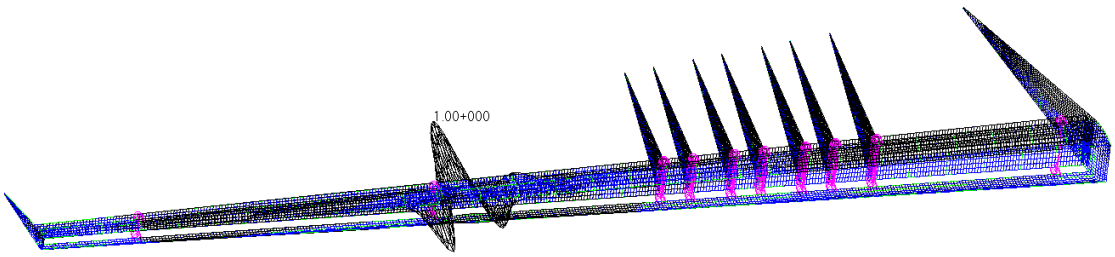


**Figure 5.19:** Shape of first Eigenmode of ground gust load case (damaged), RF = 1.047.

### 5.4.3 Running loads

The running loads of concepts GS_baseline were compared to those of the un-stiffened skin shown in Section 5.3.2. The results were compared to understand the effect the stiffeners on the loads in the rudder. The chord-wise loads remained low and are not shown in this Section. The running shear load shown in Figure 5.20 is very similar to the plot of Figure 5.11 where only some load redistribution has occurred. This is logical as the shear loads are induced by the aerodynamic load which is unchanged. The span-wise running load has in creased as can be seen by comparing the plot for the GS skin in Figure 5.21 and the un-stiffened skin in Figure 5.12. The increased stiffens due to the addition of the grid has caused in increase in the span-wise running loads induced by the enforced hinge displacements as would be expected.

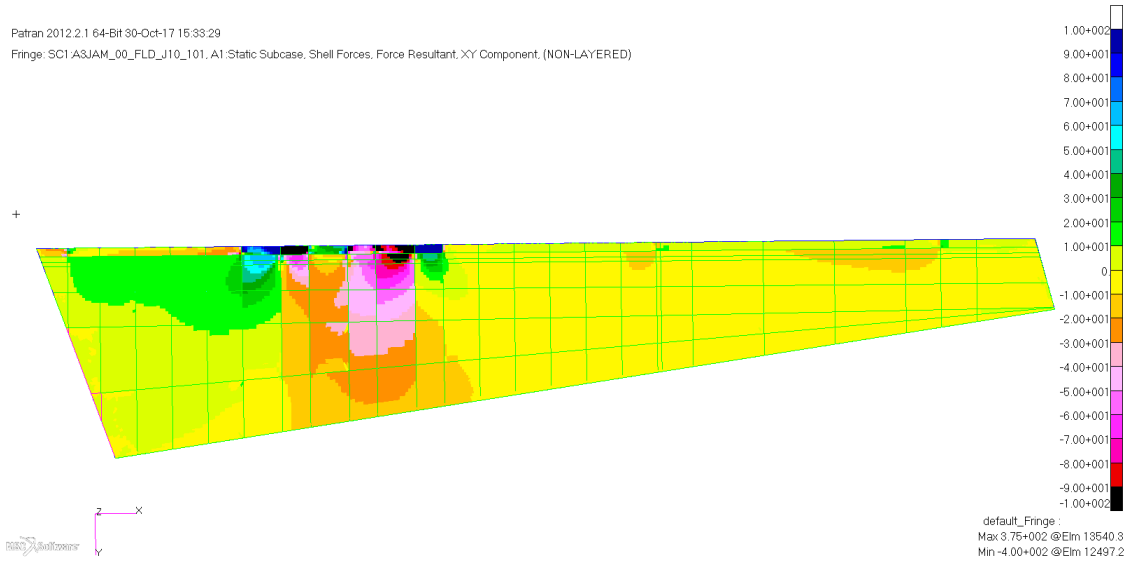


**Figure 5.20:** Running shear load $N_{xy}$ for the actuator 3 jam load case [N/mm].

### 5.4.4 Displacements and Deformations

Despite the stability of skins large deformations were observed in the static analysis. While no aerodynamic requirements were given on the deformation of the skin (called 'pillowing'), the deformation was much larger than in the multi-rib variants. This is due to the lack of ribs and was most pronounced in the area below hinge 2 in configuration GS_FEM as can be seen in Figure 5.22. Differentiating between the deformation due to air load and hinge displacements is difficult and thus the maximum and minimum HM load cases without hinge displacements were run to obtain an indication of the amount of pillowing of the skin. The skin below hinge 2 showed a maximum deformation of 82 mm and while this is under ultimate load, the deformation due to daily loads is estimated to be 20% of the ultimate load and will probably also still too high.

While the maximum deformation is large, the deformation gradient appears to be low indicating that the pillowing is smooth. A smooth deformation is more acceptable from an aerodynamic point of view, but without proper requirements it is not possible to determine if the maximum deformation is the driving requirement for a GS rudder. It is also noted that

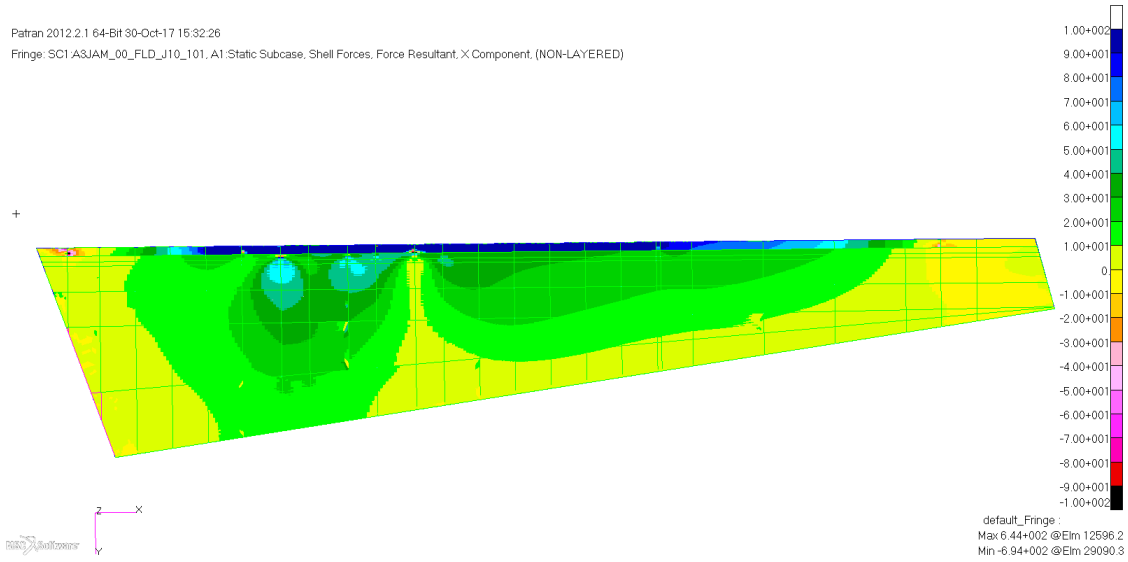


**Figure 5.21:** Running span-wise load $N_x$ for the actuator 3 jam load case [N/mm].

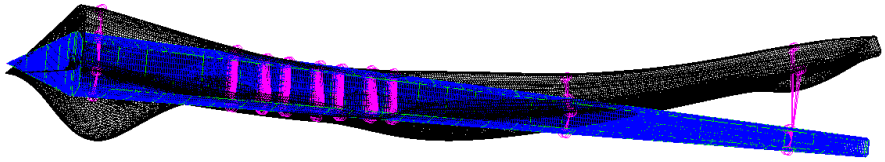

**Figure 5.22:** Deformation of configuration GS_FEM due to actuator 3 jam load case with enforced hinge displacement.

the skin pockets between the stiffeners may also pillow and such behaviour is not captured by the smeared-stiffness modelling used in the analysis.

To assess the impact of increasing the GS skin stiffness on the deformation of the area below hinge 2, configuration GS_Baseline was made. In this configuration the 'Tria 10' and 'Tria 15' grids in Figure 5.15 were changed to 'Tria 20'. Fringe plots of the deformation for configuration GS_FEM and GS_Baseline are shown in Figures 5.23 and 5.24 respectively. The minimum HM load case showed the highest deformation. Changing the grid configuration resulted in a reduction of the maximum deformation from 82 mm to 25 mm in GS_Baseline. The deformation in the other regions of the rudder are unchanged.

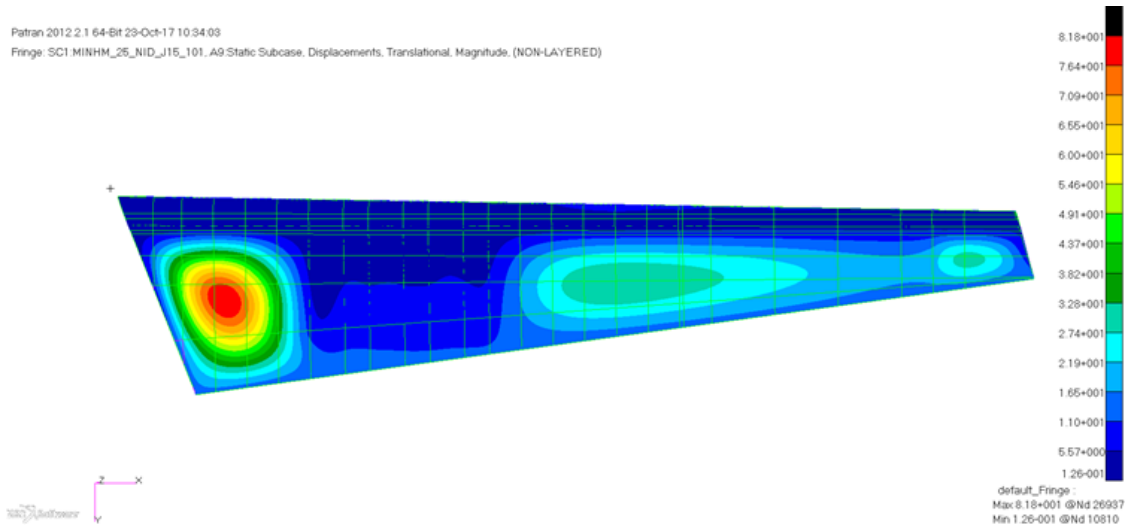


**Figure 5.23:** Fringe plot of deformation of configuration GS_FEM due to air load only of the minimum HM load case.

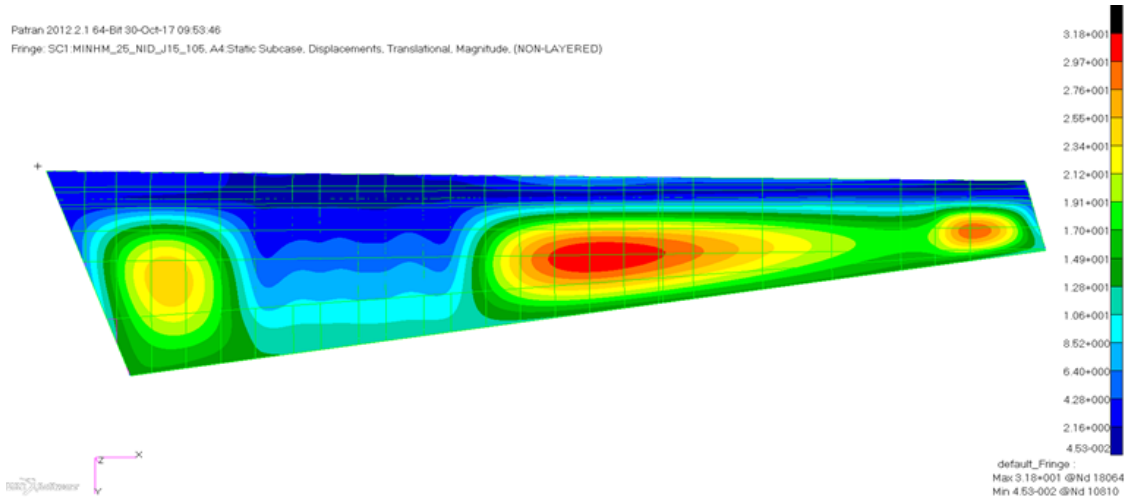


**Figure 5.24:** Fringe plot of deformation of configuration GS_Baseline due to air load only of the minimum HM load case.

### 5.4.5 Interface Loads

The resultant of the interface loads are compared to those of the Carbon fibre PolyPhenylene Sulfide (C/PPS) and and C/PEKK multi-rib concepts. There was no time for a full analysis and thus only the minimum and maximum HM are compared. The resultant loads are only compared with concept MR9 as was done in Section 4.3.3 with the hinge brackets. It was understood from the study of the C/PPS concept that the variation of the actuator bracket interface load is driven by the aerodynamic load and does not vary significantly. Thus the actuator brackets are not included in the analysis and the hinge bracket loads are given in Table 5.3 where they are denoted as H1-H7.

The resultant loads are expressed as a relative difference $\Delta = \frac{GS-X}{X}$ and expressed as a percentage, where GS is configuration GS_FEM and 'X' either MR9 or the C/PPS reference. The largest resultant of the minimum or maximum HM load cases is taken. These cases do not show the highest interface loads but do provide a general insight into the difference in load distribution. Compared to MR9 the loads are always lower except at hinges 4 and 6, which indicates a load redistribution and subsequent concentration at these points. This explains the need for a thicker rib behind hinge 4 (Figure 5.17) and the second lowest Eigenmode of the substructure shown in Figure 5.19. The load distribution in the GS rudder varies from a multi-rib and this must be accounted for in the interface design. Comparison of the differences with the C/PPS reference indicates that the assumption to use the same interface brackets for cost and weight estimation is reasonable in a total sense.

### 5.4.6 Strain and Strength

The largest strains were observed under the actuator 3 jam load case and the maximum and minimum principal strains are shown in Figures 5.25 and 5.26 respectively. The membrane strains are relatively low with, like the multi-rib rudders, with stress concentrations at the bracket which are ignored. The strains in the substructure show a similar behaviour and are not shown. While the membrane strains are low, a simple estimation of the strains at the outer fibre of the stiffeners was made to assess the strength of the GS skin.

The grid is modelled by 1 mm thick shell elements causing the strain on the surface of the shell to be similar to that of the mid-plane. The stiffener height however is 20 mm in most areas and combined with the large deformations as shown in Figure 5.24 for example the strain at the top of the stiffener, called outer fibre strain, is larger than computed by PATRAN. The

**Table 5.3:** Difference in resultant interface load between the GS_FEM and the multi-rib rudders.

| Bracket | Δ MR9 | Δ Reference |
|---|---|---|
| H1 | -25% | 15% |
| H2 | -34% | -60% |
| H3 | -14% | -12% |
| H4 | 55% | 53% |
| H5 | -27% | -1.0% |
| H6 | 20% | -3.0% |
| H7 | -14% | 12% |

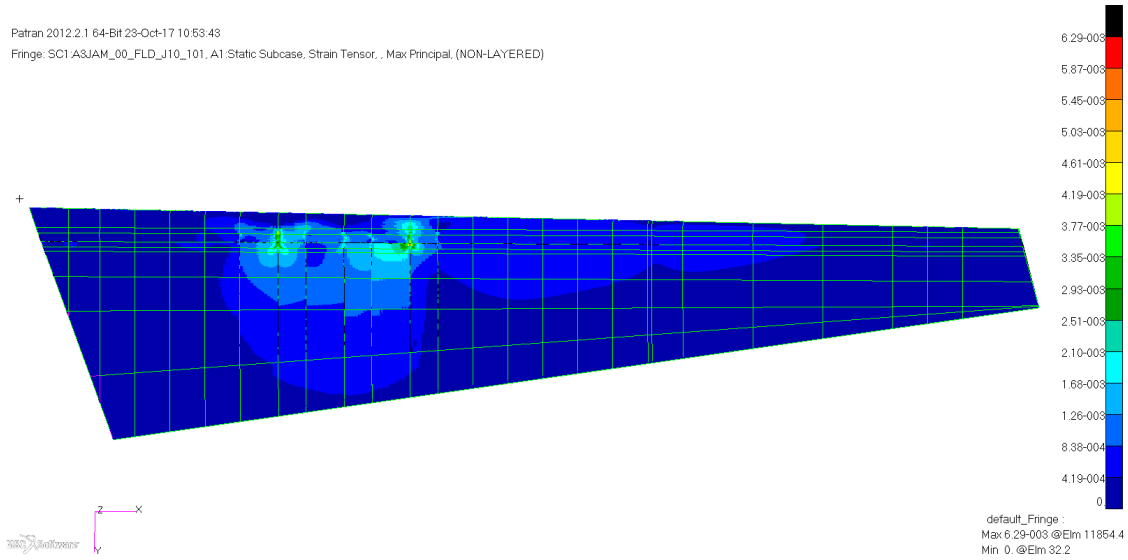


**Figure 5.25:** Maximum principal strain of GS_FEM under actuator 3 jam load case.

outer fibre strain is computed using an estimate of the curvature at the area below hinge 2 for configuration GS_Baseline. The outer strain is given by $\epsilon$ in Equation 5.3 where $\epsilon_0$ is the mid-plane strain, $\kappa$ is the curvature and $z$ the distance from the mid-plane to the top of the stiffener. The relationship between the curvature, mid-plane strain and outer fibre strains are sketched in Figure 5.27 where it is noted that in the figure the radius of curvature $\rho = 1/\kappa$ has been sketched.

$$\epsilon = \epsilon_0 + \kappa z \tag{5.3}$$

The curvature $\kappa$ is estimated using Equation 5.4 where $M$ is the running moment and $EI$ the equivalent smeared bending stiffness per mm of a unit cell. Using the smeared $EI$ is an approximation and thus the limitation of the accuracy of this method. The running moment is extracted from the shell forces and is also an average of the moment through the GS skin.

$$\kappa = \frac{M}{EI} \tag{5.4}$$

Substituting Equation 5.4 into Equation 5.3 and rewriting it to be an expression for the running moment $M$ Equation 5.5 is obtained. In this equation the failure strain $\epsilon_u$ for the SF material from Table 2.1 is used to determine the failure running moment $M_{max}$ for a given mid-plane strain $\epsilon_0$. The equivalent bending stiffness of a unit cell is computed using the properties of the D matrix by $(EI)_x = D_{11} - \frac{D_{12}^2}{D_{22}}$ in x direction and $(EI)_y = D_{22} - \frac{D_{12}^2}{D_{11}}$ in y direction.

$$M_{max} = \frac{EI}{z}(\epsilon_u - \epsilon_0) \tag{5.5}$$

The properties of the grid configurations used in concept GS_FEM are give in Table 5.4. The distance between the outer fibre $z$ is measured from the neutral plane position $z_{0av}$ which is

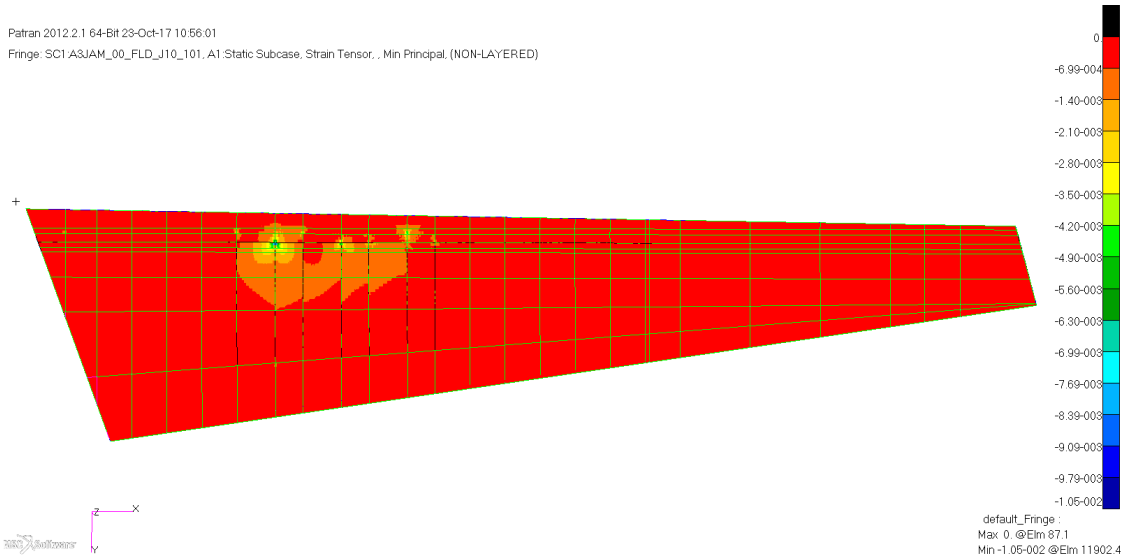


**Figure 5.26:** Minimum principal strain of GS_FEM under actuator 3 jam load case.

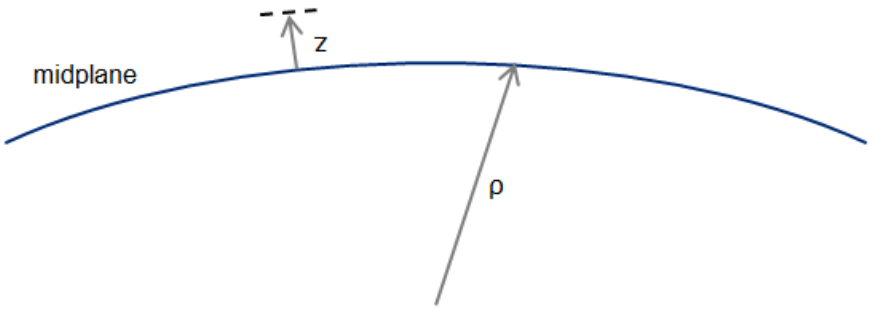


**Figure 5.27:** Sketch of the relation between outer fibre strain, mid-plane strain and curvature.

an output of Xu's method. It is emphasized that in this approach the geometric mid-plane of the shell element coincides with the average neutral plane of the grid. Filling in these values in Equation 5.5 the maximum allowable running moments for the grids used in the areas with highest deformation (GS_FEM) are computed and shown in Table 5.5. The strain allowable for the SF material is 5120 $\mu\epsilon$ and is taken to be the lowest value of compression and tension to be conservative.

The running moment in x and y direction are shown in Figures 5.29 and 5.31 respectively. The areas with the largest deformation as seen in Figure 5.24, have the highest running moment as expected. The strain at the neutral plane in x and y direction is shown in Figures 5.28 and 5.30 respectively. The strains in the area of maximum deformation is approximately 300 $\mu\epsilon$ as can be seein in Figures 5.28 and 5.30. Inspection of Figures 5.29 and 5.31 shows that in some cases the running moment in the skins exceed the computed allowable shown in Table 5.5. The running moment at the root of GS_Baseline appeared to be nearly identical to GS_FEM despite the lower deformation.

The angle grid (Ah20) appears to have a low allowed running moment due to the low bending stiffness and relatively high stiffeners used. In x direction the allowed running moment is

**Table 5.4:** Input properties of grids used in GS_FEM for strength calculation.

| Type | $h_{st}$ [mm] | $z_{0av}$ [mm] | $z$ [mm] | $(EI)_x$ [Nmm$^2$/mm] | $(EI)_y$ [Nmm$^2$/mm] |
|---|---|---|---|---|---|
| Th10 | 10 | 0.72 | 9.28 | 9.73E+04 | 4.74E+4 |
| Th15 | 15 | 1.48 | 13.5 | 3.39E+5 | 1.70E+5 |
| Th20 | 20 | 2.43 | 17.6 | 8.38E+5 | 4.29E+5 |
| Ah15 | 15 | 0.94 | 14.1 | 6.17E+4 | 5.62E+4 |
| Ah20 | 20 | 1.58 | 18.4 | 1.66E+5 | 1.51E+5 |

**Table 5.5:** Allowable running moment for GS_FEM for strains and moments at locations of maximum deformation

| Type | $M_x$ [Nmm/mm] | $M_y$ [Nmm/mm] |
|---|---|---|
| Th10 | 50.47 | 24.62 |
| Th15 | 120.7 | 60.62 |
| Ah20 | 43.51 | 39.45 |

43.51 Nmm/mm while a running moment of 66.7 Nmm/mm is observed in Figure 5.29 in the pillowed areas below hinge 2 and above hinge 5. The running moment is relatively low in the area between the ribs as expected due to be limited deformation of the skin. The solution is to use a slightly stiffer grid to reduce the deformations. It is judged that slightly increasing the grid height will suffice for the current load case. It is noted that a full model of the grid is required to better understand the deformations and moment distribution in the GS skin.

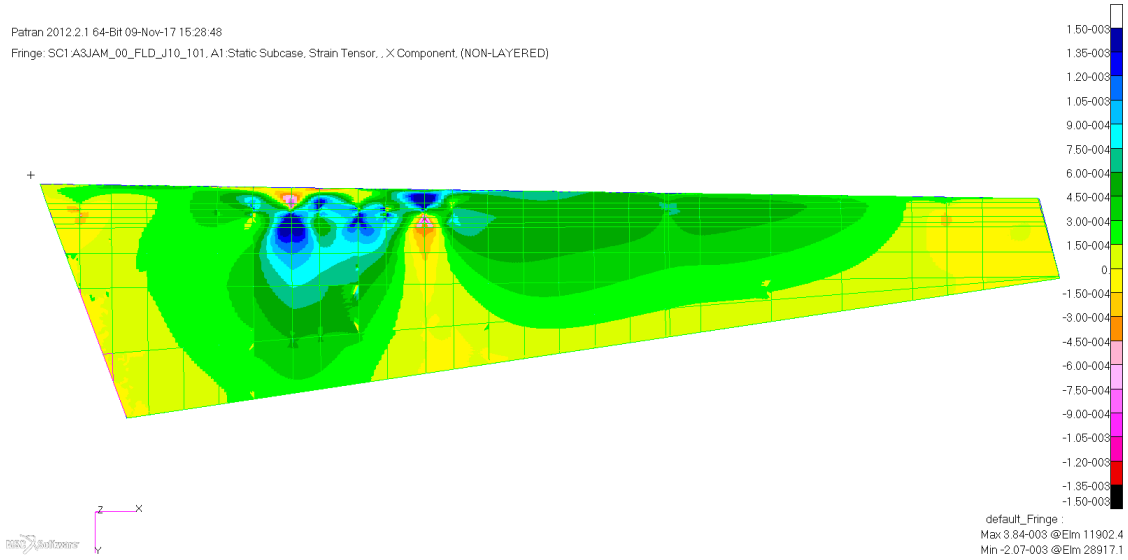


**Figure 5.28:** x component of mid-plane strain under actuator 3 load case.

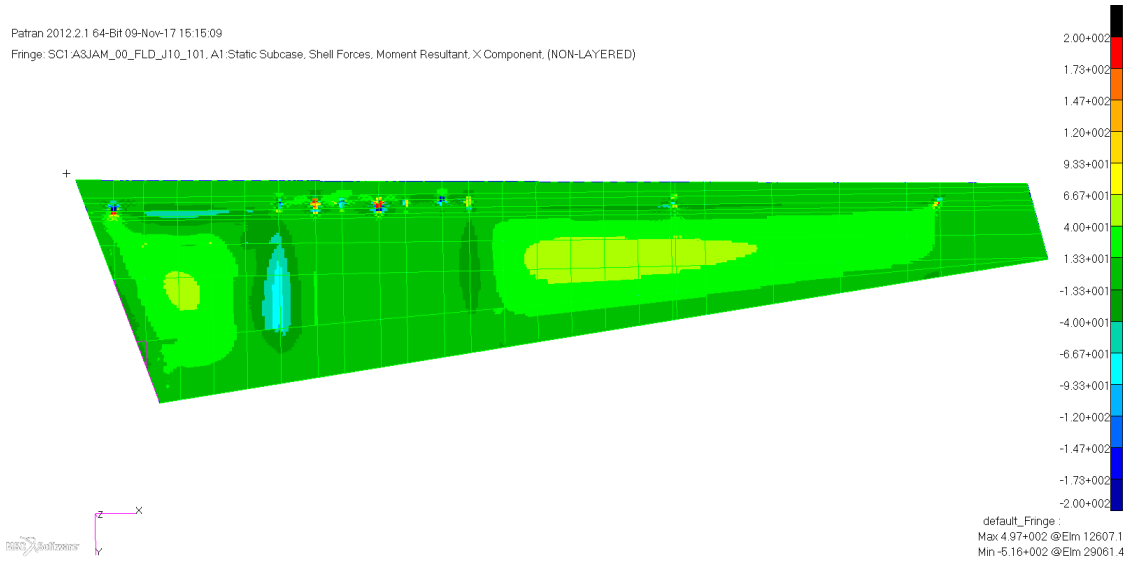


**Figure 5.29:** Running moment in x direction under actuator 3 load case.

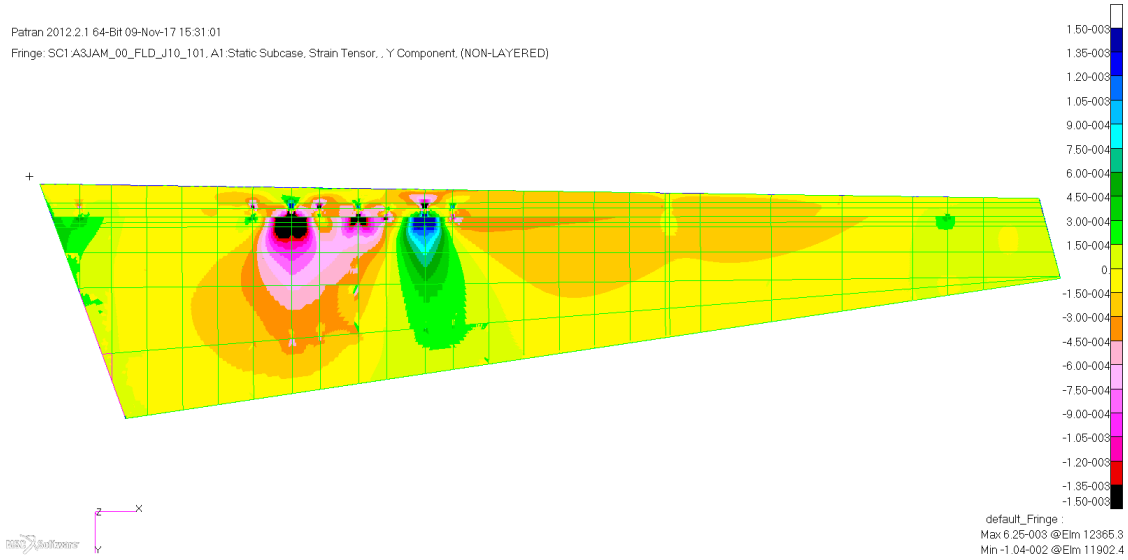


**Figure 5.30:** y component of mid-plane strain under actuator 3 load case.

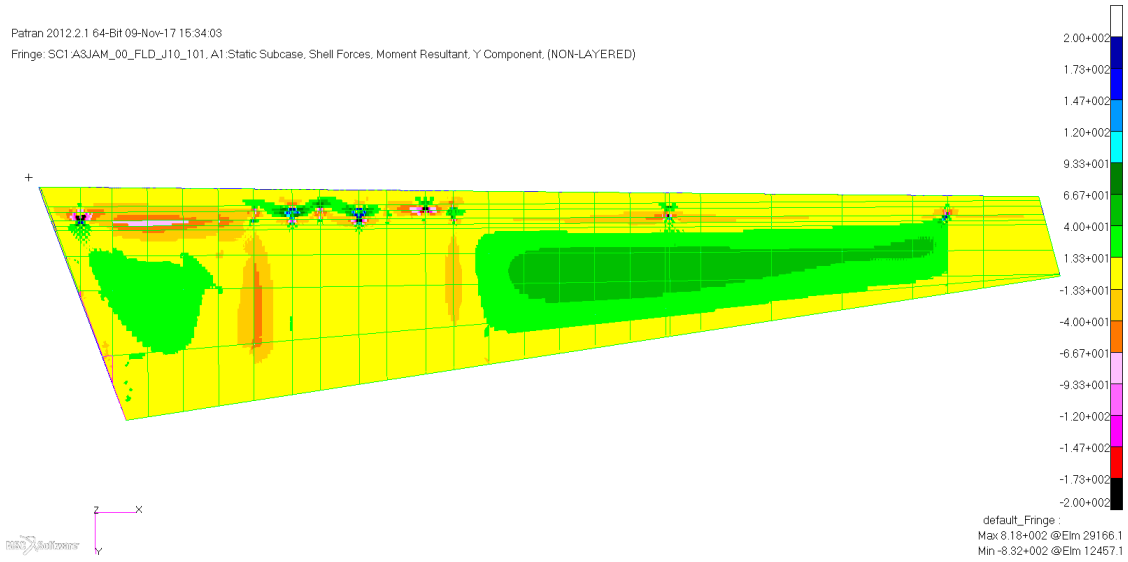


**Figure 5.31:** Running moment in y direction under actuator 3 load case.

## 5.5 Manufacturing and Assembly

The part manufacturing of the GS rudder is identical to that of the C/PEKK multi-rib with the addition of the grid manufacturing. Two processes are available to manufacture the grid; Overmolding and 3D printing. As the grid consists of repetitive unit cells it was initially envisioned to overmold the grid in multiple steps using a limited set of unit cell moulds. This proved to be infeasible as is explained in the next section and the manufacturing concept was modified. There was no time to study 3D printing and thus a trade-off for the manufacturing concept is left as a recommendation. The assembly is similar to the multi-rib rudder as welded ribs are still used, but fastened ribs are also considered and will be discussed.

### 5.5.1 Overmolding

Overmolding is a process where a (SF reinforced) polymer is injection moulded into an insert placed in the mould. The general process steps are shown in Figure 5.33 where a formed insert is placed in a mould which is then closed to inject the polymer. While this process is established for the manufacturing of consumer goods, it is not used in combination with aerospace grade polymers. Recently ThermoPlastic Research Company (TPRC) has researched the application of overmolding using C/PPS and the Victrex SF Carbon fibre PolyEther Ether Ketone (C/PEEK) compound and made a demonstrator shown in Figure 5.34. An artist impression of an overmolded rib web is shown in Figure 5.32, the stiffener dimensions and pitch of the grid are comparable to those of GS_FEM.

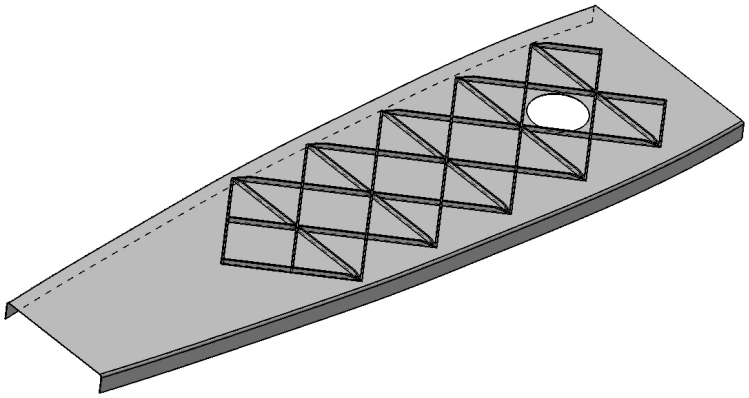

**Figure 5.32:** Artist impression of a grid-stiffened rib web using overmolding.

The injection pressure of the polymer is high and thus closed moulds are used as shown in Figure 5.33. While it is assumed that a single sided mould could be used on a flat surface, overmolding an interlocking grid is not feasible. The adjacent unit cell would be required to deliver this confining pressure, which is unlikely. The manufacturing concept was thus modified to assume the grid would be overmolded onto the skin in sections. A rib would be placed in the gap between two overmolded sections to act as a panel breaker. The size of the overmolded sections would be governed by the size of the overmolding press and tooling cost and it is unlikely that a full skin can be overmolded in a single shot at reasonable cost. A

span-wise section of 1.8 m is assumed to be a maximum and thus the cost estimate was based on overmolding 5 bays.

The substructure must be modified to allow overmolding of multiple bays and an envisioned layout is shown in Figure 5.35. Substructure a is the current configuration where ribs are placed between hinges 2 to 5. By using a stiffer grid near the actuators it could be possible to omit most ribs and to only use 5 ribs spread evenly in span-wise direction to get substructure b in Figure 5.35. A more conservative approach is to keep all the ribs between hinges 2 and 5 and to place additional ribs to create the overmolding bays giving substructure c in Figure 5.35. It is noted that no structural analysis has been performed for rudder concepts with substructure b or c, and these are purely proposed layouts.

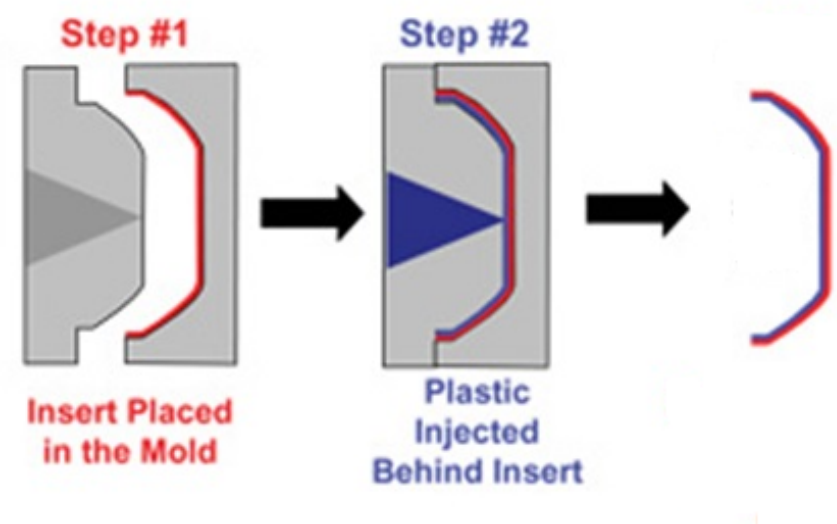


**Figure 5.33:** Overmolding process using a preformed insert. (Modified from Yomura.com)

Some manufacturing aspects visible in the TPRC demonstrator shown in Figure 5.34 which have an impact on the sizing, but have been neglected in the modelling are discussed. To improve the release of the mould the stiffeners have a rake angle (taper) which has an effect on the stiffness of the grid. Transition of grid height and ramp-up of the grid must be sized to control the load path. Care must be taken to design an efficient transition between the monolithic skin near the front spar to the grid stiffened skin in the torsion box. These aspects are relevant in a detailed design and are mentioned for completeness. It is not expected that these have a significant impact on the conclusions of this study.

### 5.5.2 Assembly

Assembly of the rudder follows the same flow as the multi-rib rudder. As the skin may not buckle before the highest loads are reached welding of the ribs to the skins will not add much value. Considering that the baseline design for the GS skin only uses 8 ribs compared to over 20 for the multi-rib rudders, it may be more economic to fasten the ribs. While the recurring cost and weight of the joints is higher, the non-recurring cost would be lower as no welding

**Figure 5.34:** Overmolded grid demonstrator made by TPRC. (Courtesy of JEC composites magazine)

jigs are needed. The spar-skin connection and trailing edge weld are kept in the baseline as these do not require closed box welding and associated tooling.

To facilitate the ribs a local skin thickness must be 1.8 mm for a welded joint and even larger for a fastened joint. The base laminate of a GS skin must be increased from 1 mm to 1.8, which will require a 90 mm wide build-up area as was the case in the interface patch of MR9 sketched in Figure 4.7. This ramp region can be used to smoothly build down the grid while the stiffness of the cross-section is still high due to the thicker skin as sketched in Figure 5.36.

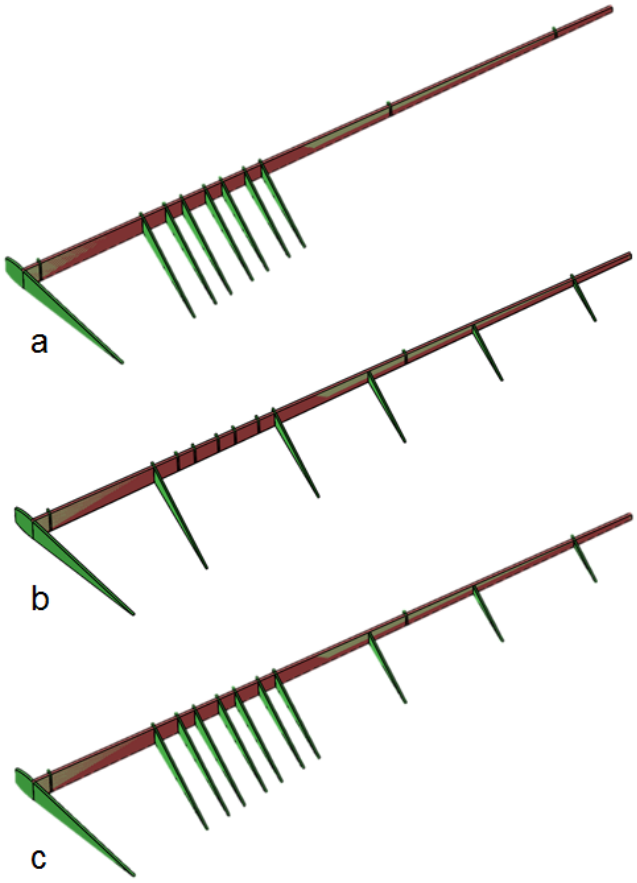


**Figure 5.35:** (a) Baseline rib layout (b) Envisioned 'multi-bay' layout (c) Hybrid layout.

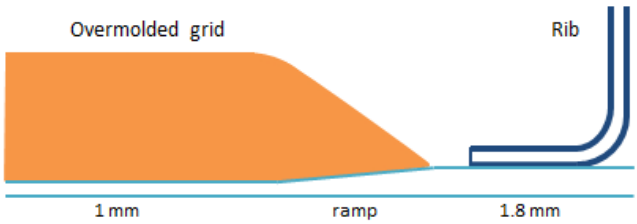


**Figure 5.36:** Sketch of the transition are between a rib and a GS skin (Not to scale).

## 5.6 Concept Discussion

The GS rudder design showed that within the current assumptions application of SF grid stiffening can be feasible. The grid height and stiffener density in the grid is reasonable in terms of weight. As local failure modes have not been studied sufficiently the concepts requires further analysis. The manufacturing concept is not yet mature and also requires more work to better understand the impact on design. It was been shown that a large number of ribs may be omitted including ribs behind hinge brackets 1, 6 and 7 allowing more design freedom.

When local failure modes can be analysed it will be possible to extend the parametric study and to design more optimized grid configurations. These can be subsequently used to further reduce the weight of the grid. More work is also needed to better understand the load distribution between the stiffeners and the skin to allow the design of transition regions. To mature the concept topics like repairability, interface strength and damage tolerance must also be studied.

# Chapter 6

# Weight and Cost Results

Weight and cost are the two most important parameters of the trade-off between the three developed concepts. The results of the weight and cost estimation are presented in this chapter and form the basis for the conclusions in the next chapter. The composite parts of the rudder account for most of the total weight and cost. These parts have been sized in detail to allow an accurate weight and cost estimation. The non-composite parts and accessories account for a significant fraction of the weight and cost, while these are assumed to be equal to the Carbon fibre PolyPhenylene Sulfide (C/PPS) reference the assumptions are also discussed for completeness.

## 6.1 Weight Estimation

An overview of the final weight for the C/PPS reference and the 3 developed concepts is presented in this section. The component weights are shown along with a breakdown of the weight and a sensitivity analysis for the Grid-Stiffened (GS) rudder. The weight of the multi-rib rudders is comparable with the C/PPS reference rudder being the lightest. The baseline GS rudder is heavier than the multi-rib concepts but within the initially specified limit of 15% weight increase w.r.t. the Carbon fibre PolyEtherKetoneKetone (C/PEKK) multi-rib. The total weights are shown in Table 6.1.

**Table 6.1:** Component weight for the 4 rudder concepts.

| **Concept** | **Weight [kg]** |
|---|---|
| C/PPS | 81.6 |
| MR9 | 82.2 |
| MR11 | 82.4 |
| GS-BL | 83.6 |

### 6.1.1 Weight Breakdown

The weight of the rudder is broken down into 7 groups for clarity. The skins, ribs and spar are each considered as individual groups due to their large contribution to the rudder weight. The brackets, including their fasteners, are one group which are assumed equal for all concepts. The fasteners used to assemble the wing box are a separete group (Box Assy) that has a low impact on weight but a significant impact on cost. The two remaining groups are the accessories, such as discussed in Section 4.4.2, and the primer and sealant. The first contains parts that are required for the functionality of the rudder, while the latter is based on the assumption to supply a primed product. The groups are enumerated below for completeness and it is noted that the weight of the 3 last groups is constant for all concepts.

- Skins
- Ribs
- Spar
- Box Assy
- Brackets
- Accessories
- Prim + Seal

The weight of the composite parts is obtained from WIng BOx MODeller (WIBOMOD) and corrected for non-modelled details. These are the weld interface patches and copper wire mesh on the skins and glass fabric patches on the spar. These glass fibre patches are placed at locations of the metallic brackets to prevent galvanic coupling between the carbon fibre and metal. The fastener count is a function of the number of ribs and the weight estimation is improved by accounting for the required grip length of each fastener by considering the local total joint thickness. The breakdown of the weights per group is shown in Figure 6.1. The weight breakdown in Figure 6.1 shows that the component weight is dominated by the skins. The ribs and brackets are second depending on the concept followed by the spar. The weight of the fasteners, accessories and primer and sealant is low.

The skin weight of the C/PPS concept is much lower compared to the other concepts, including MR9 which has the same thickness. This is attributed to two things; first the total weight of all the rib-skin weld interface patch is almost 2 kg per skin in MR9. Second is the 3% higher density of C/PEKK compared to C/PPS which is caused by the larger fibre volume faction. The weight of the ribs is large in the C/PPS concept due to the larger minimum thickness for most ribs and the higher number of ribs. It is noted that the total rib weight for concept MR11 is slightly larger than MR9 despite the fact that the first has two ribs less. This is caused by the thicker actuator and hinge ribs used in MR11 between Hinges 2 till 5 as can be seen by comparing Figures 4.9 and 4.18. The spar weight is comparable for all multi-rib concepts and is largest in GS-BL.

### 6.1.2 Grid Weight Estimation

In the smeared-stiffness approach of the GS-skin no exact definition of the grid was made. The weight of the GS skin is estimated using a smeared-weight approach. This approach

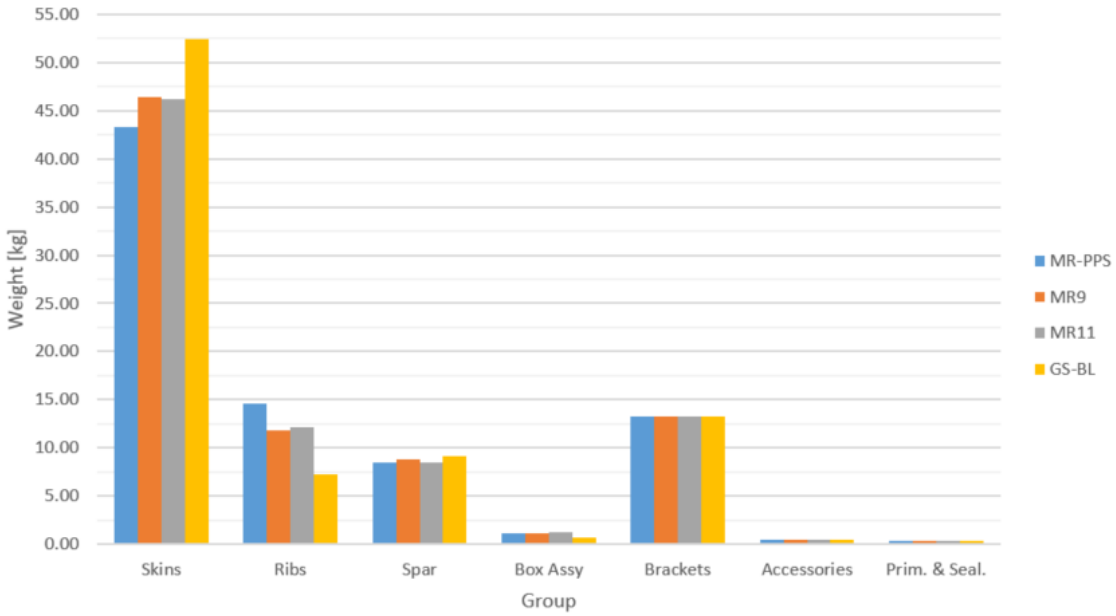


**Figure 6.1:** Weight breakdown of the rudder concepts and the C/PPS reference.

is suitable for a large area but is inaccurate at the borders and transition regions. Three non-modelled details are expected to result in the largest inaccuracy in the weight estimation and were studied in detail for configuration GS-FEM. These are the unit cells directly behind the front spar, the tailing edge and the transition region between grids with different hight. These regions are shown in Figure 6.2 where their location is indicated.

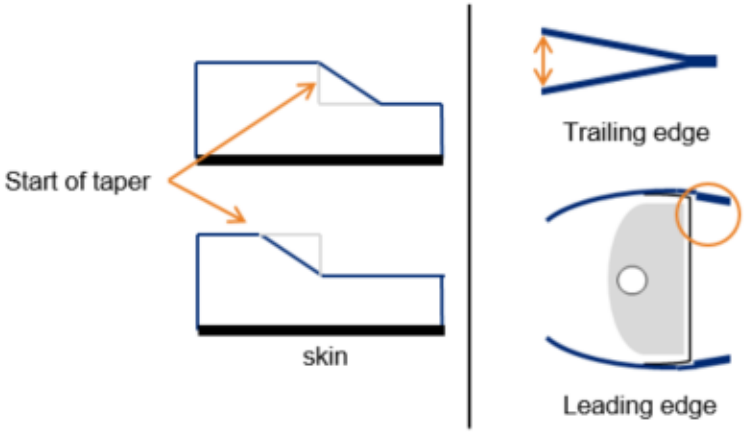


**Figure 6.2:** Non-modelled grid details; Grid height transition (left), Grid height in the trailing edge (upper right) and monolithic to GS transition (lower right)

To prevent jumps in the cross-sectional stiffness of the GS skin and ease the flow during overmolding the grid height must change gradually. Two extreme cases have been sketched on the upper side of Figure 6.2. In the upper sketch the grid is ramped down over the distance of half a unit cell with the next lower height. The sketch on the lower side shows a grib being ramped down in the last higher unit cell. For configuration GS-FEM this results in a weight

difference of 305 gr. per skin and may be an increase or decrease depending on the selected ramp down method.

In the Finte Element Model (FEM) the GS skin was modelled to run until the trailing edge. This is non-physical as there would be no space for the grids. The volume of the wedge at the trailing edge where the total height is lower than 40 mm was estimated. The difference in the modelled grid weight and grid weight that would fit was calculated. The weight of the increased thickness of the trailing edge, to improve lightening strike damage resistance, is not modelled and was also accounted for in the calculation. The total weight reduction is estimated to be 228 gr.

The skin must transition from a thick monolithic laminate to a thin GS skin behind the front spar. Care must be taken to design a good load path and it is expected that this will require additional elements to be added to the grid. The weight increase associated with this provision is estimated to be 305 gr. when the weight of the 'full' grid layout is assumed for the unit cells directly behind the front spar.

The weight variation from these aspects is 500 to 600 gr. in total when the positive or negative contributions are considered separately. The total skin weight of configuration GS-FEM however is 24.89 kg. Thus the total difference is expected to be 3% and is deemed sufficiently accurate for the current level of detail.

### 6.1.3 Weight Sensitivity Analysis

Considering difference in maturity between the the multi-rib and the GS rudder concept a one-to-one comparison on cost and weight would not be justified. There are much more uncertainties in the GS rudder concept that must be investigated before a comparison can be made. This is done by a sensitivity analysis for the GS rudder. Comparable analyses have been performed for the multi-rib rudder concepts at Fokker Aerostructures, but the results shall not be discussed here as it was not part of this thesis study. The weight sensitivity analysis shall provide a measure for the potential weight deviation of concept GS-BL. This will allow a better comparison with the multi-rib concepts.

The weight (and cost) estimation of six GS rudder configurations has been made. While only configurations GS-FEM and GS-BL have been subjected to structural analysis, the other four provide useful insight in the potential weight change in a development phase. The various configurations are listed and described in Table 6.2. The first three configurations are modifications to the grid type using the GS-FEM configuration as a basis. GS-FR is a version of GS-FEM where the ribs have been fastened and GS-9L is a version of GS-FEM where the base thickness is 1.24 mm (9 layers) with the stiffener height modified to keep a constant $D_e$. Configuration GS-MB uses the multi-bay substructure layout and a grid which is constant in span-wise direction to allow the same mould to be used.

**Table 6.2:** Description of the various GS rudder configurations.

| Name | Description |
|---|---|
| GS-FEM | Configuration obtained by sizing for all load cases |
| GS-BL | Baseline configuration with stiffened lower section |
| GS-PESS | Stiff grid configuration to model a pessimistic scenario |
| GS-FR | GS-FEM with the ribs fastened instead of welded |
| GS-9L | GS-FEM with GS skin modified to have a 9 layer base. |
| GS-MB | Configuration based on multi-bay substructure in Figure 5.35 |

## 6.2 Cost Estimation

The cost estimation for all concepts was performed by the cost estimating department of Fokker Aerostructures. The inputs were provided as a Product Breakdown Structure (PBS) in an EXCEL sheet where each line entry contained the relevant cost information for a part of the rudder. As the tools for the cost estimation are proprietary to Fokker Aerostructures and actual cost data has been used, no absolute cost figures shall be presented in this document. A cost breakdown, using groups similar to those in the preceding section, shall be given to show the contribution of each group to the total cost. The cost of the GS configurations defined for the sensitivity analysis is also computed. This will allow to asses the cost impact of certain aspects in the design.

### 6.2.1 Cost Breakdown

Similar to the weight breakdown certain costs were grouped to better analyse the contribution of certain elements to the rudder as a component. The groups are nearly identical to those used to assess the weight with the exception of the 'Primer and sealant' group which now includes 'documentation'. This is a relatively large fraction of the cost which contains the cost for the 'paperwork' to trace the part manufacturing and assembly. This is an overhead cost and equal for all concepts. As the costs are given relatively, the 'Doc. & Prim.' group has a different contribution for each rudder. The breakdown is shown in Figure 6.3 where the bars for each concept add up to 100%.

The first observation is that the cost breakdown of MR9 and MR11 is nearly identical as would be expected. As MR9 has 2 ribs more than MR11, the Ribs group accounts for a slightly larger fraction of the component cost. Compared to the C/PPS reference (MR-PPS) the skins account for a much larger fraction of the component cost. This is due to the costly manual lay-up of the skins and the relatively high Buy-to-Fly ratio (BtF). The ribs of the C/PPS reference on the other hand show lower cost, which is due to the lower material price as compared to C/PEKK. The GS rudder shows a large contribution from the skins, as expected due to the overmolding step. The ribs, and box assembly in lesser degree, have a much lower contribution to the relative cost resulting in the increase of the relative cost of the other groups.

Automated manufacturing results in reduced cost for the skins, but this is not true for the spar. As discussed in Section 2.4 the laser tacking Automated Fiber Placement (AFP) is a time consuming process that requires expensive equipment. In this case manual lay-up

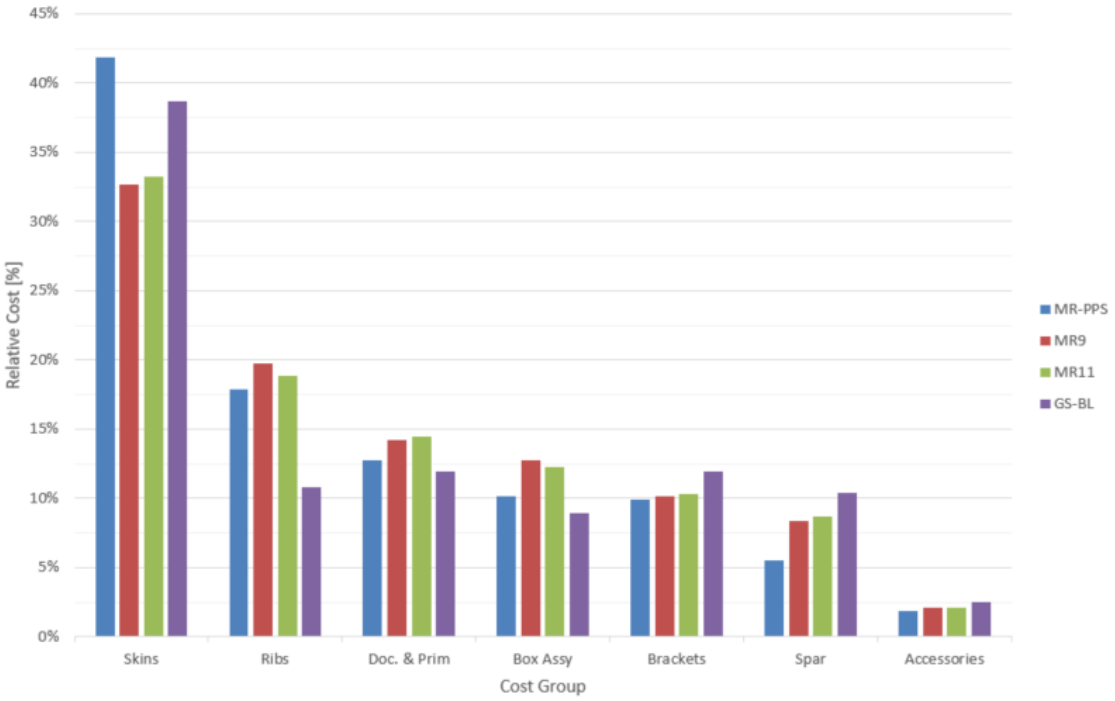


**Figure 6.3:** Breakdown of relative costs per cost group.

appears to be more cost effective due to the use of a fabric composite in the C/PPS reference. Manual lay-up of Uni-Directional (UD) tape is more labour intensive compared to fabric and is not a viable solution.

### 6.2.2 Cost Estimation of Overmolding

The cost estimation of the overmolding step in crude and some notes are made to better explain its validity and impact on the total cost estimation. The material cost of the Short Fibre (SF) compound is based on the cost of a similar compound produced in small quantities. The price of a compound is however also a function of the total volume sold by the supplier and could be reduced in this case if volumes increase sufficiently. The labour cost of the overmolding step was estimated by modifying cost estimates for Resin Transfer Molding (RTM) processes. Doubling the estimated labour cost of the overmolding step will result in an increase of 6% of the total GS rudder cost.

Overmolding shows many similarities to RTM being a closed tool process into which a polymer is injected under high pressure. With the help of the R&D department at Fokker Aerostructures the process times of an envisioned overmolding process were estimated and the RTM cost estimate Cost Estimating Relationships (CER) was modified accordingly. The RTM equipment varies much from that required for overmolding and thus the rates for the equipment shall differ. Due to a lack of accurate data the rates for RTM have been used, this is a limitation in the accuracy of the cost estimate.

## 6.3 Cost-Weight Overview

The cost and weight estimates are combined in a single graph to aid the trade-off between the various concepts. The weight and cost performance are expressed as the relative difference with respect to the C/PPS reference rudder as shown in Figure 6.4. The relative difference for both cost and weight 'R' is calculated according to $R = \frac{PPS-X}{PPS}$ where 'X' is the value of a certain concept and 'PPS' the cost or weight of the C/PPS reference. The cost and weight of a 'stripped' rudder (Strip. 7L) is also shown which represents GS-FEM before sizing and application of the grid. The stripped rudder represents the absolute limit in terms of weight and also cost as long as the material price does not change significantly. This limit is however for a starting point and is not a 'flyable' concept as the strength and stiffness requirements are not met.

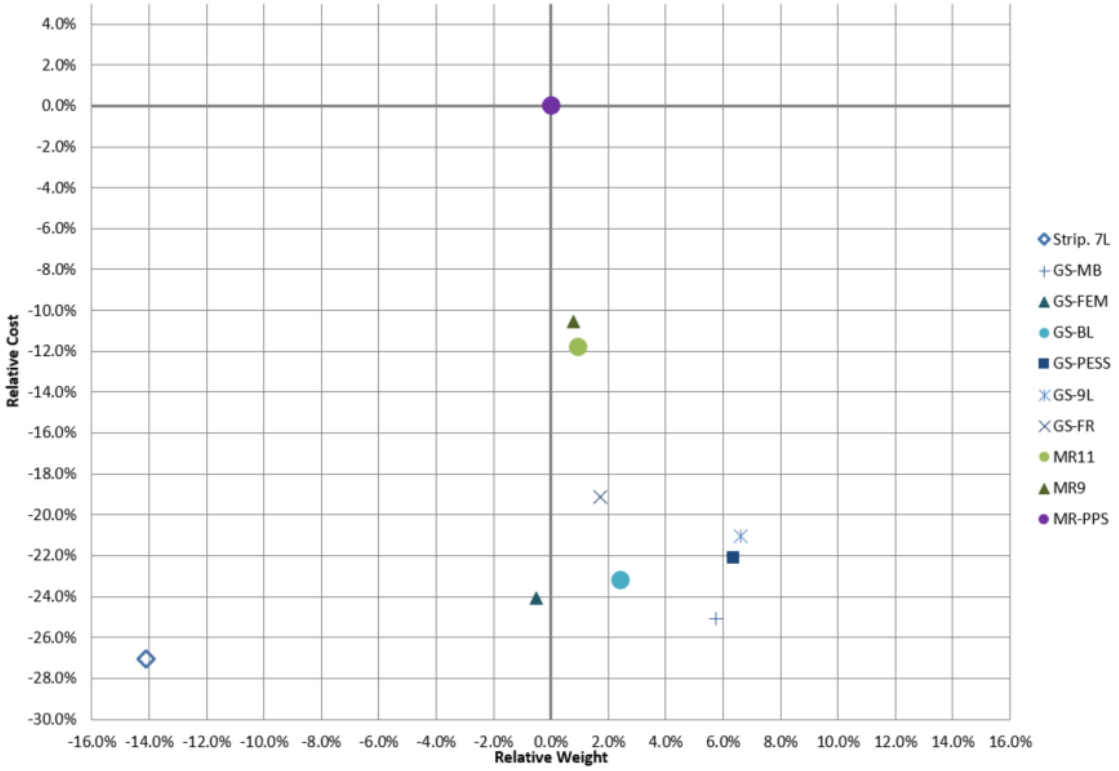


**Figure 6.4:** Relative performance of all rudder concepts w.r.t. the C/PPS reference rudder.

The C/PPS reference rudder is shown at the origin of the graph in Figure 6.4. Positive values are an increase w.r.t. to the reference while negative values indicate a reduction. The selected baseline for each concept is represented by a circle. It can be seen that MR11 shows a near 12% cost reduction while the weight increase is approximately 1% w.r.t. the C/PPS reference. Configuration GS-BL shows a 23% cost reduction at a 2.5% weight increase. The C/PEKK multi-rib concepts show near identical weight performance and only a significant cost reduction w.r.t. to the C/PPS reference.

The GS rudder configurations where only the grid has been varied are indicated with solid markers for clarity. The unfilled markers indicate variations of GS-FEM as explained earlier. Looking at GS-FEM, GS-BL and GS-PESS in Figure 6.4 the cost and weight increase due to

variation of the grid is clearly visible. While the deformation of GS-FEM was judged to be too high, it represents a lower weight limit for the baseline substructure configuration. GS-PESS on the other side is a predicted 'worst-case' scenario where the grid required further stiffening due to local effects. The observed range in both cost and weight is relatively narrow and close the initial cost and weight targets. The cost of GS-BL is 13% lower than that of MR-11 where the initial target was 15%.

The labour cost of overmolding does not vary much as a function of the grid weight. As the material cost is of the SF compound is also relatively low, variation in the overmolded mass does not have a large impact on cost. Increasing the base skin thickness to 1.24 mm (9 layers) does have a large impact on both cost and weight as indicated by GS-9L. This is due to the relatively high added cost for AFP while the grid remains similar compared to GS-FEM. Fastening the ribs increases weight and cost as indicated by GS-FR in Figure 6.4. Welding is a cost effective joining method and in this case necessary to meet the cost reduction targets for the selected substructure.

Cost and weight estimates were made for a theoretical configuration better suited for overmolding. As explained in Section 5.5.1 the ribs can be equidistantly distributed span-wise to create multiple bays. A single tool can be used to overmold the grid, where the cord-wise injection is varied. The cost and weight performance for this concept is indicated by GS-MB in Figure 6.4. The potential cost savings are high because the ribs are smaller, but the weight performance is lower due to the use of a single grid configuration. It is noted that no structural analysis has been performed for this concept and it is only included to estimate the potential for an optimized GS rudder concept.

# Chapter 7

# Conclusions and Recommendation

## 7.1 Conclusion

The research question was broken up into three sub-questions which have been answered in this study. The cost and weight performance of the multi-rib rudder concept was determined by sizing two configurations and estimating cost and weight. Help of experts was used to generate and assess alternative stiffening concepts out of which one was selected. Grid-stiffening using Short Fibre (SF) compound was selected and a rudder concept was developed. Cost and weight for this alternative concept was also determined and the cost and weight performance was compared to the multi-rib configurations and the Carbon fibre PolyPhenylene Sulfide (C/PPS) reference rudder.

### 7.1.1 The C/PEKK multi-rib rudder

Two multi-rib rudder configurations with different minimum thickness, dubbed MR9 and MR11, were designed according to the defined requirements. Concepts MR9 and MR11 proved to have a 1% higher weight than the C/PPS reference and this difference cannot be considered to be significant in a conceptual design phase. The increased stiffness of the Uni-Directional (UD) tape could not be exploited to further reduce weight. Though the UD tape material allowed a reduction of the total number of ribs compared to the C/PPS reference, the 3% higher density of the Carbon fibre PolyEtherKetoneKetone (C/PEKK) material undid most of this weight reduction. The assumption to place one rib behind every hinge and actuator bracket reduces the design space for the substructure. Only an integer number of ribs can be placed between two bracket ribs, resulting in a slight over-design in some cases.

The cost of the C/PEKK rudder concepts is 10% lower than the C/PPS reference. This has two causes; firstly the Buy-to-Fly ratio (BtF) of the Automated Fiber Placement (AFP) process is lower than a fabric and manual layup based process. The difference in BtF approximately offsets the difference in material price, where the price of C/PEKK is higher than C/PPS. The second cause for the cost reduction is the lower labour cost associated with

AFP layup. The recurring cost of the UltraSonic (Us) tacking AFP process is low due to its relative simplicity and high layup speed.

Thermoplastic welding is a key technology for the multi-rib concept, but unlike induction welding of C/PPS conduction welding has not been fully matured for C/PEKK. Press-forming of C/PEKK parts is not implemented for series production and manufacturing process of the C/PEKK spar still shows some uncertainties. While these items are expected to be resolved with relative ease, some development time is required. This translates in a lead time in the development process of a Next Signle Aisle aircraft (NSA) C/PEKK multi-rib rudder.

### 7.1.2 The GS rudder

Several alternative stiffening concepts were created in a multidisciplinary session with experts from Fokker Aerostructures. Continuous carbon fibres are costly and contribute much to the total material price, thus the use of a cheaper material will allow the potential for cost reduction. The weight of the Grid-Stiffened (GS) rudder concept is estimated to be 83.6 kg and recurring cost to be lower than the multi-rib concepts.

Implementation of Xu's smeared-stiffness approach for modelling of the global behaviour of GS panels [2] allowed a parametric study into the stiffness characteristics of a set of grid configurations. It was observed that slender stiffeners are most efficient and that the stiffener pitch, which translates into a unit cell size, is the most effective variable to scale the total stiffness. No SF PEKK based compound with a high stiffness was available and thus the properties a PEEK compound were assumed. The parametric study showed that the stiffness targets could be met with SF stiffeners while remaining within the set weight limits.

The GS rudder was sized with MR11 taken as a starting point after reducing the skin thickness inside the wing box to 1 mm and removing all ribs accept those between hinges 2 and 5.The chosen increments in the stiffener height of the grid proved to be too large to optimize the GS skin. A stable design was obtained, but the deformation of the skin was judged to be too high. As no requirements on the allowed deformation were given the design was not updated.

The grid configurations were chosen conservatively to reduce the risk of local failure modes to occur. This was done using engineering judgement and the assumptions must be verified in future studies. A simplified analysis was made to estimate the strains in the outer fibre of the stiffeners at the locations with the highest deformation. It was found that the selected 'Angle' stiffeners are most probably insufficiently strong, but a slight increase of the height or the use of a 'Tria' grid should provide the required strength.

Overmolding was selected as a manufacturing process for the grid, but some issues remain in the feasibility of the manufacturing concept. The pressure required for overmolding will not allow a continous gird to be overmolded in sections. Thus the tooling required for overmolding will be large and costly and may not be off-set by the envisioned manufacturing rate. As tooling is part of the non-recurring cost which is not considered in this study, the effect of tooling was not quantified.

### 7.1.3 Trade-off Conclusions

Comparing the 3 developed rudder concepts to the C/PPS reference it can be concluded that the multi-rib rudder is the lightest solution with the current assumptions. Further

optimization will allow a limited weight reduction, but this is expected to be equal for both C/PPS and C/PEKK. Cost can be reduced by automation of the manufacturing processes. The improved BtF of tape is an inherent advantage and will leverage cost reduction when material prices reduce. The GS rudder showed that grid-stiffening has a potential to further reduce component cost and part count. The weight of a GS rudder is expected to be 2-5% higher compared to the multi-rib concept. There is no repair concept available for the GS rudder and the analysis is less thorough than that of the multi-rib concepts.

It is concluded that the C/PEKK multi-rib rudder offers the most potential for the near future if all the manufacturing and assembly issues are resolved. The application of grid-stiffening requires more studies, but the outlook is that further cost reduction is feasible. The GS rudder is judged to be a suitable candidate for the long-term future and a potential successor for the multi-rib concept. More study on the detailed behaviour of GS skins is required to determine the potential of the GS rudder more accurately.

## 7.2 Recommendations

In this trade-off study many assumptions have been made that require verification. In the development of the GS rudder limited optimization has been performed due to time constraints leaving opportunity for more studies into its performance. Several elements of the C/PEKK and GS rudder concepts are considered key enablers and require further development to mature the concepts. All recommendations fall under these categories have been defined and are listed separately for the multi-rib and GS rudder.

### 7.2.1 Multi-rib Rudder

**Improved cost estimate of C/PEKK parts** The cost estimation of the C/PEKK parts was made by estimating several process parameters with the aid of experts. These parameters must be checked to reduce the uncertainty in the cost estimation. A simulation of the AFP layup of the skins is recommended. This will allow an accurate calculation of the BtF, weight and process time. The latter can be used to determine the required machine capacity and thus a significant part of the non-recurring cost.

**C/PEKK spar manufacturing** The Technology Readiness Level (TRL) of all spar manufacturing concepts is low and require further development. A trade-off between several manufacturing processes is recommended to identify the optimal process. The selected process should enable thickness steps in the spar as assumed in the current study.

**Closed-box welding of C/PEKK UD tape** Both recurring and non-recurring cost of conduction welding of C/PEKK must be estimated. The assumption that the recurring cost are equal to induction welding of C/PPS must be verified. Limitations such as minimum box height and weld edge quality must also be quantified. If the minimum weld-able box height is larger than that for induction welding the ribs will become shorter cord-wise. The effect on the structure must be checked by performing analysis.

**Skin-rib weld interface patch** In this study the assumption was made that the skin-rib weld interface patches would consist out of laminates defined in the ply-book. This added to much weight and cost in concept MR9 that may be reduced. The use of more simple patches, in terms of layup and weight, should be studied to improve concept MR9.

### 7.2.2 GS rudder

**Local failure mode analysis** To verify the GS rudder design local failure modes must be studied. These include both strength and stability and can be done by building a discrete model of the GS skin. This will allow a verification of the global stability using the smeared-stiffness method. It is also recommended to investigate the development of analytic local strength and stability analysis methods to increase the speed of conceptual design. Building a tool to parametrically construct a discrete Computer Aided Design (CAD) model of a GS skin would be a next step.

**Monolithic to GS skin transition** The transition regions from a GS skin to a (thick) monolithic skin must be analysed and modifications to the grid must be designed if necessary. The load transition must be smooth and no cause excessive shear and peal forces in the stiffener-skin interface. This will also provide more insight in the feasibility and performance of a multi-bay concept.

**Manufacturing process of the grid** In the alternative concept trade-off phase 3D printing of the grid was considered, but later abandoned due to the availability of data on overmolding. The assumption that the grid could be overmolded in sections proved to be incorrect. Thus 3D printing should be investigated again as it can potentially reduce the high tooling cost associated with overmolding. It is recommended to perform a trade-off between overmolding and 3D printing to better understand the differences between the two manufacturing technologies.

**Development of a repair concept** The use of a 1 mm thick skin showed to increase efficiency significantly compared to the countersunk fastener repairable 1.24 mm thickness. A repair method suitable for a GS skin must be developed to meet customer requirements. It is recommended to investigate the use of a bonded or welded repair to omit the need for fasteners.

**Application of Grid-stiffening for other parts** Addition of a grid on a thin laminate, especially using overmolding, can greatly increase stiffness at a slight increase of cost and weight. The application of grid-stiffening on rib-webs and potentially spar-webs should be investigated. In case of rib-webs a single tool could be used for multiple ribs of similar size to reduce the number of required tools.

**Development of a (near)-monocoque rudder** The hinge loads were found to vary significantly between configurations. Placing a rib behind every bracket was not necessary and it is expected that this could also be the case for the brackets between hinges 2 and 5. It is recommended to investigate the development of a full monocoque rudder without any ribs. This would further reduce part count and the need for closed box welding.

# References


[1] V. V. Vasliev. Anisogrid composite lattice structures - development and aerospace applications. *Composite Strucutres*, 94:1117–1127, 2012.

[2] Yuanming XU, Yan Tong, Manqing Liu, and Bajracharya Suman. A new effective smeared stiffener method for global buckling analysis of grid stiffened composite panels. *Composite Structures*, 158:83–91, 2016.

[3] J. Meuzelaar. Xxxx thermoplastic welded rudder - requirements baseline 3. Technical Report OF303XX000-14-0003, GKN Fokker Aerostructures, April 2014.

[4] A.H. van der Laan, T. van den Berg, and L.M. Hootsmans. Integrated multidisciplinary engineering solutions at fokker aerostructrues. In *Challenges in European Aerospace*, number 105. 5th CEAS AIR and SPACE CONFERENCE, 2010.

[5] Salwan al Jaberi. Literature study. Literature study preceding this thesis project, 2017.

[6] R. Curran, S. Raghunathan, and M. Price. Review of aerospace engineering cost modelling: The genetic causal approach. *Progress in Aerospace Sciences*, 40:487–534, 2004.

[7] A.S. Herrmann, P.C. Zahlen, and I. Zuardy. Sandwich structures technology in commercial aviation. In *Sandwich Structures 7:Advancing with Sandwich Structures and Materials*, pages 13–26, 2005.

[8] Andrea I. Marasco, Dennis D.R. Cartié, Ivana K. Partridge, and Amir Resai. Mechanical properties balance in novel z-pinned sandwich panels: Out-of-plane properties. *Composites Part A: applied science and manufacturing*, 37:295–302, 2006.

[9] Christos Kassapoglou. *Design and Analysis of Composite Structures*. John Wiley & Sons Ltd, 2013.

[10] D. van Bergen. Stressing guidelines for the sms elevators & rudder. Technical Report Re-SMS-Tail-0199, GKN Fokker Aerostructures, August 2012.

[11] Vincent de Gelder. Concepts for a large commercial aircraft rudder. diploma thesis, TU Delft, 2015.

[12] Sonell Shroff. *Design, Analysis, Fabrication and Testing of Composite Grid-Stiffened Structures for Fuselage Applications.* PhD thesis, TU Delft, 2014.

[13] P.K. Mallick. *Composites Engineering Handbook.* Taylor & Francis, 1997.

# Appendix A

# Grid Unit Cell Design Curves

## A.1 Parametric Study Design Curves

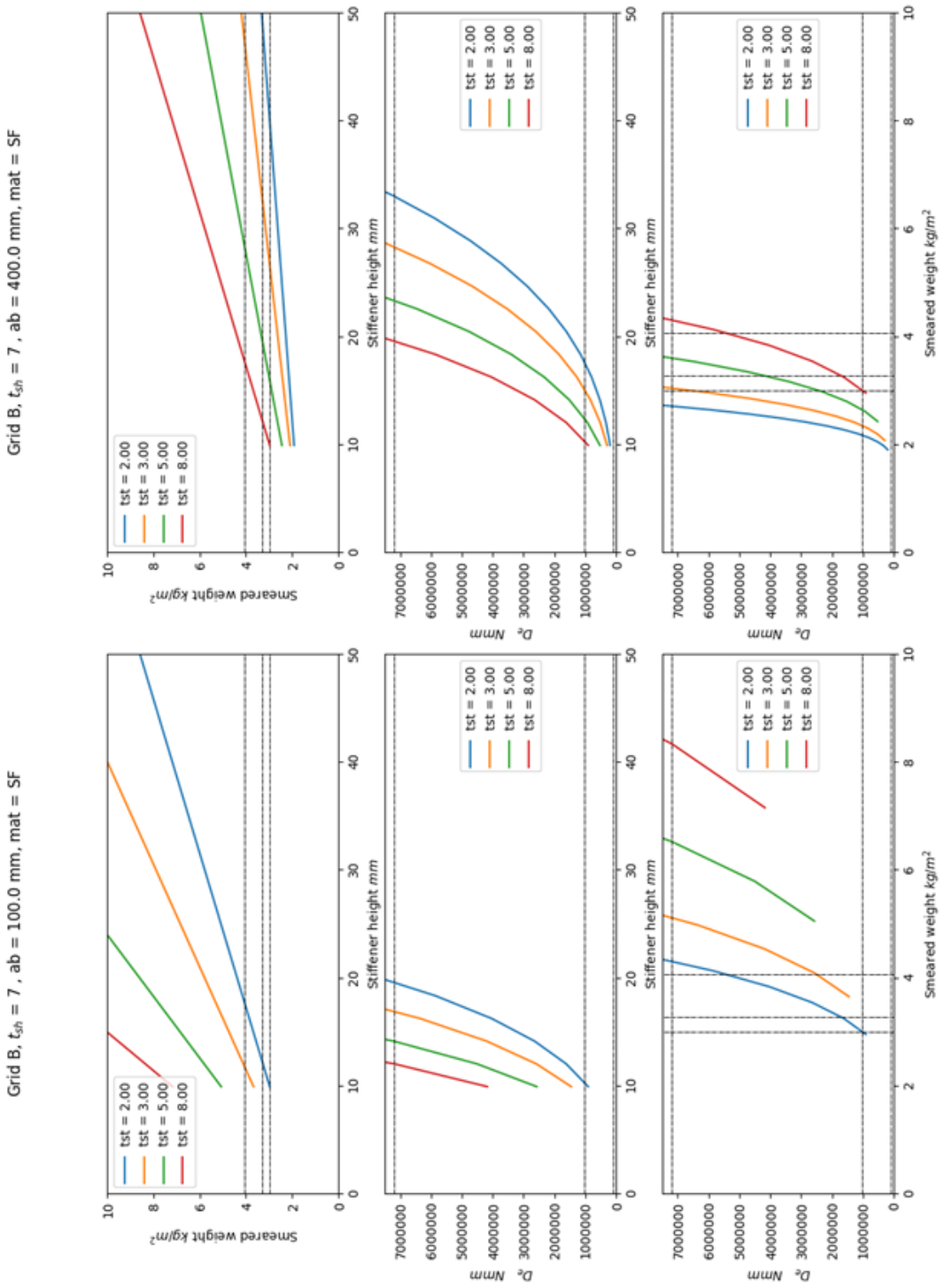


**Figure A.1:** Effect of unit cell size on smeared weight and equivalent stiffness.

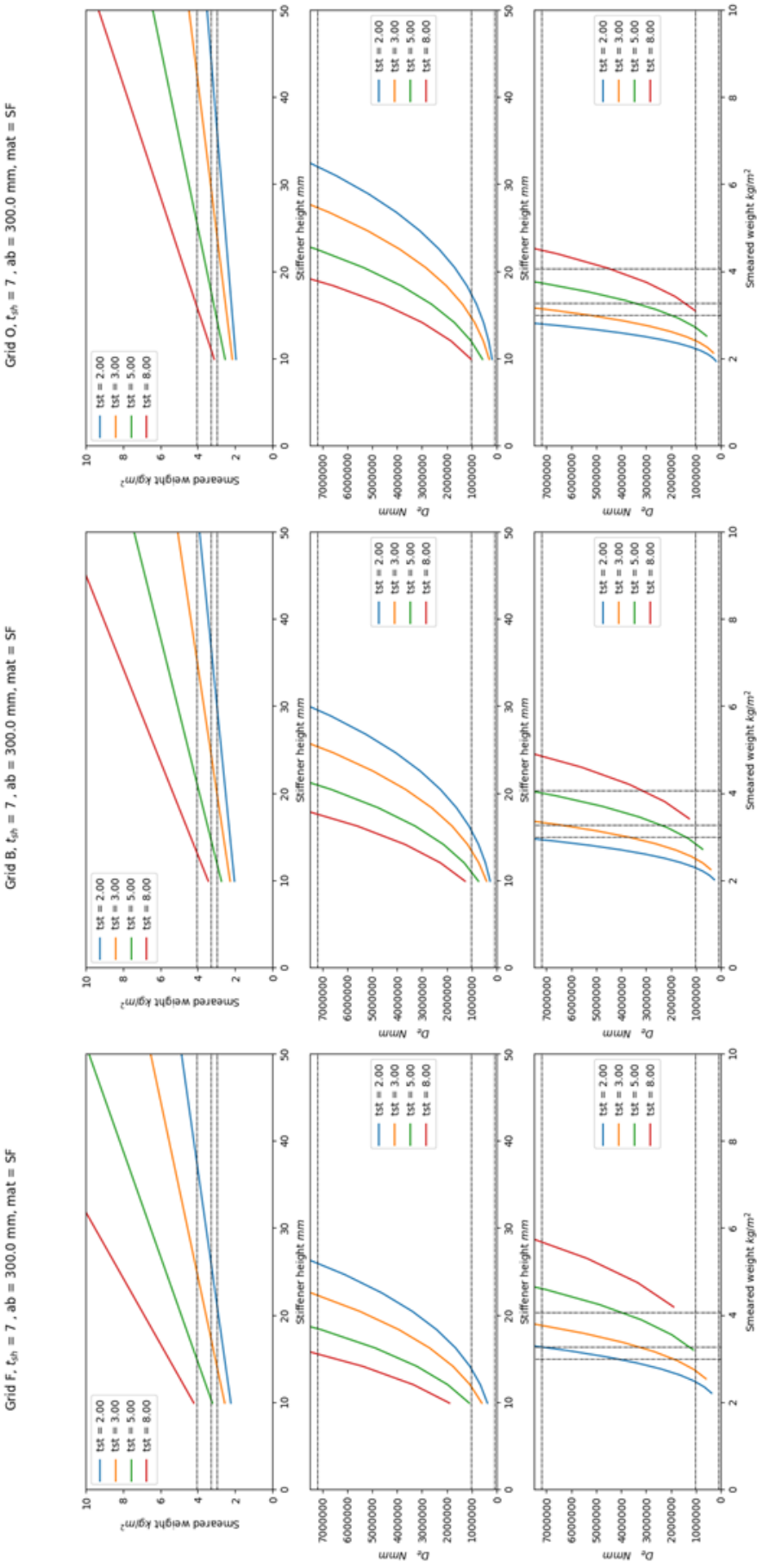


**Figure A.2:** Comparison of 'Ortho', 'Balanced' and 'Full' grid configuration.

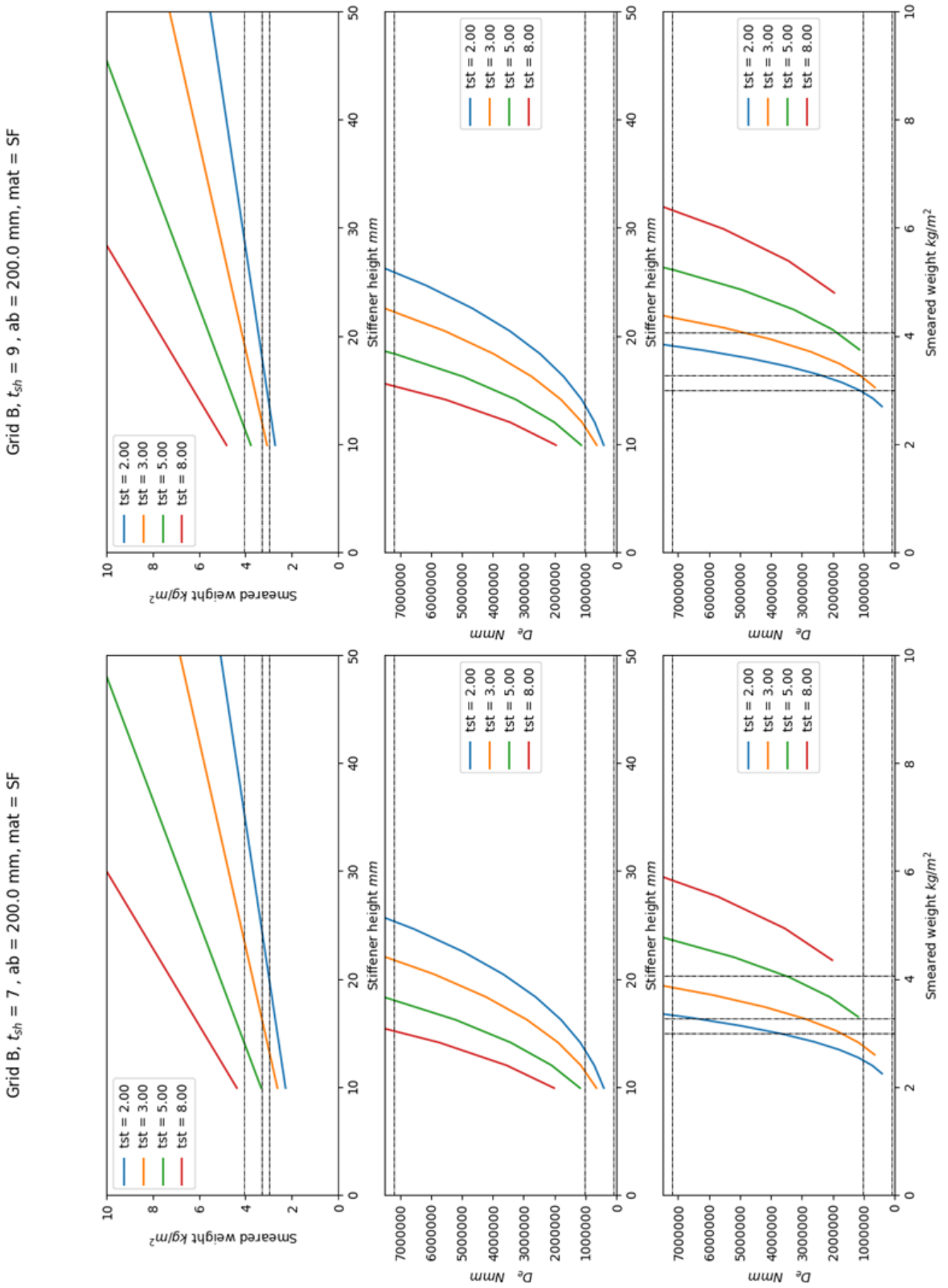


**Figure A.3:** Effect of skin thickness on unit cell smeared weight and equivalent stiffness.